The Cenozoic Magmatism of East Africa: Part II – Rifting of the Mobile Belt

Tyrone O. Rooney

Dept. of Earth and Environmental Sciences, Michigan State University, East Lansing, MI 48823, USA

Abstract

Despite the foundational role East Africa has played in the advancement of our understanding of continental rifting, there remains substantial ambiguity as to how magmatism has evolved during progressive rift development. This contribution is a comparative study that explores the temporal development of magmatism in both rifts, and within the interposing Turkana Depression. Notwithstanding the independent evolution of the Main Ethiopian Rift and Kenya Rift prior to their quaternary linkage, magmatic events within them show remarkable parallelism. Following an initial pulse of basaltic magmatism ca. 20 Ma, more evolved compositions (flood phonolites in Kenya, rhyolites in Ethiopia) dominated the landscape until ca. 12 Ma. From ca. 12 Ma to 9 Ma, a renewed phase of widespread basaltic volcanism (Mid-Miocene Resurgence Phase) impacted the entire region from the Afar margin to Kenya, though activity in the south slightly predates equivalent basaltic events to the north. Following this widespread basaltic event, silicic magmatism again dominated the now nascent rifts until a renewed phase of basaltic activity commenced ca. 4 to 1.6 Ma termed the 'Stratoid Phase'. Following the termination of the Stratoid Phase, the modern expression of volcanism in both rifts has been dominated by central silicic volcanoes. Magmatic activity within the Turkana Depression broadly parallels that in both rifts – basaltic events are evident at ca. 20 Ma, 12 Ma, and 4 Ma, however

Figure 1

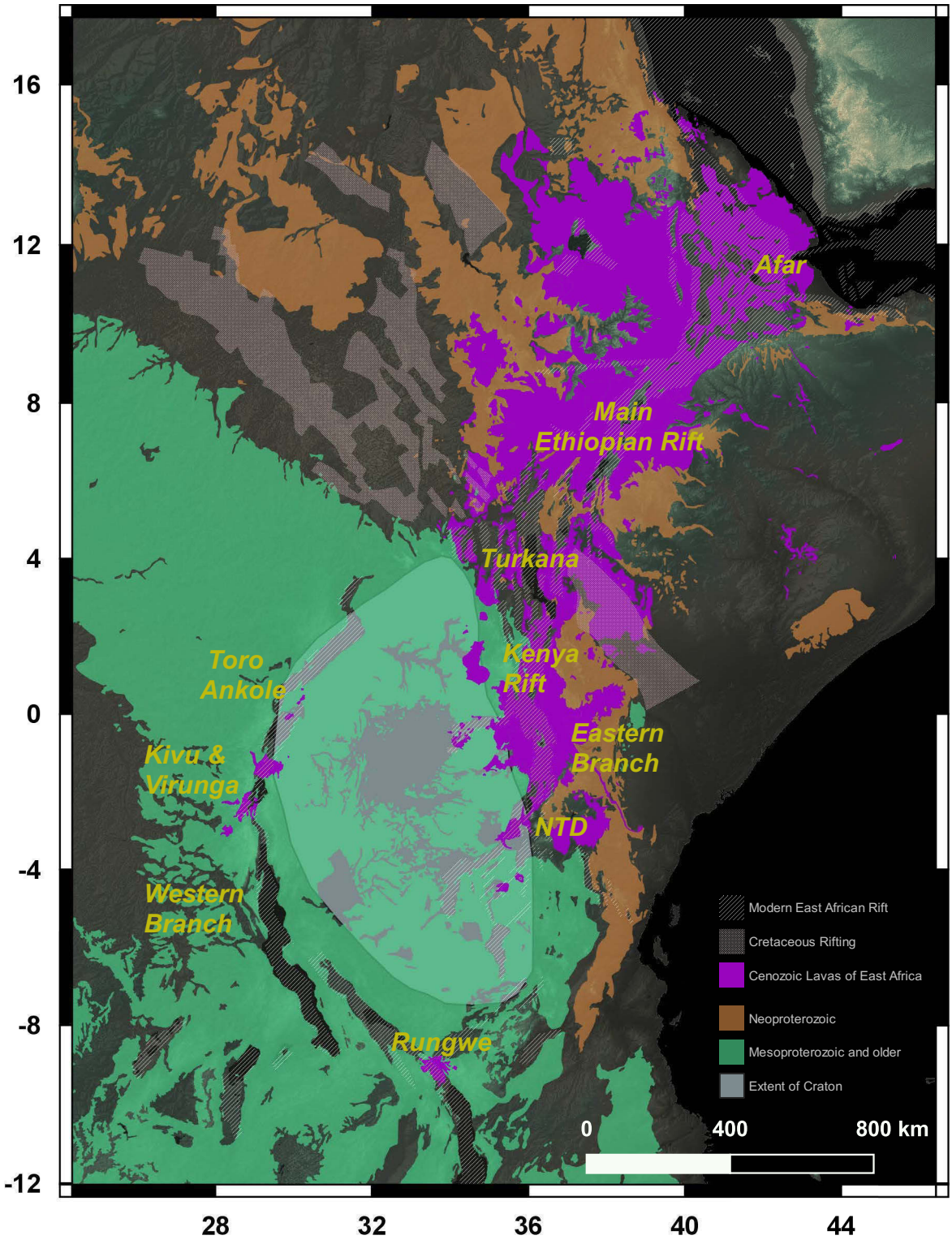
16
12
8
4
0
-4
-8
-12
28
32
36
40
44
Afar
Main
Ethiopian Rift
Turkana
Kenya
Rift
Toro
Ankole
Eastern
Branch
Kivu &
Virunga
NTD
Western
Branch
Rungwe
Modern East African Rift
Cretaceous Rifting
Cenozoic Lavas of East Africa
Neoproterozoic
Mesoproterozoic and older
Extent of Craton
0
400
800 km

Figure 2

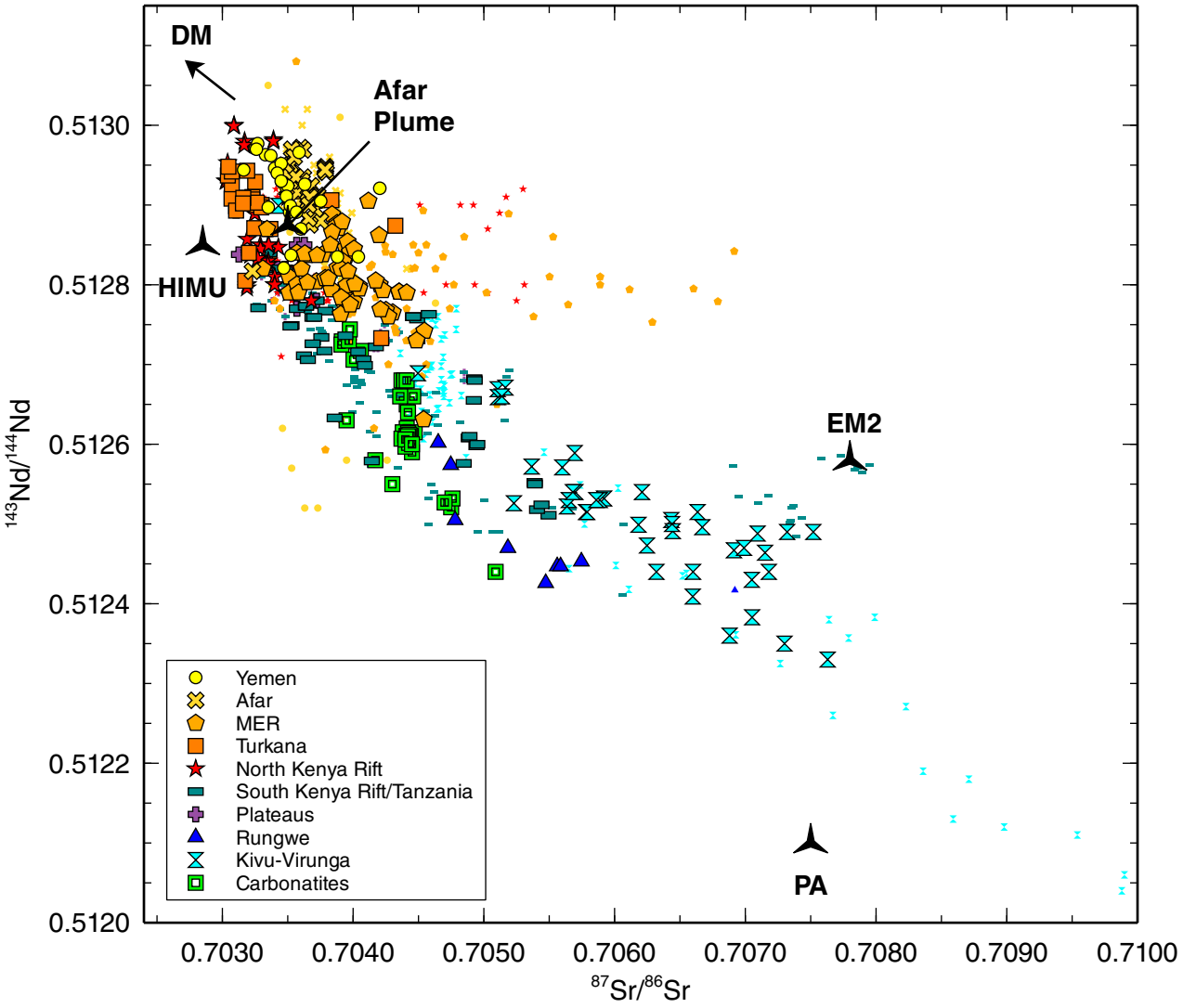
DM
Afar
Plume
HIMU
EM2
PA
Yemen
Afar
MER
Turkana
North Kenya Rift
South Kenya Rift/Tanzania
Plateaus
Rungwe
Kivu-Virunga
Carbonatites
0.5130
0.5128
0.5126
0.5124
0.5122
0.5120
0.7030
0.7040
0.7050
0.7060
0.7070
0.7080
0.7090
0.7100
143Nd/144Nd
87Sr/86Sr

Figure 3

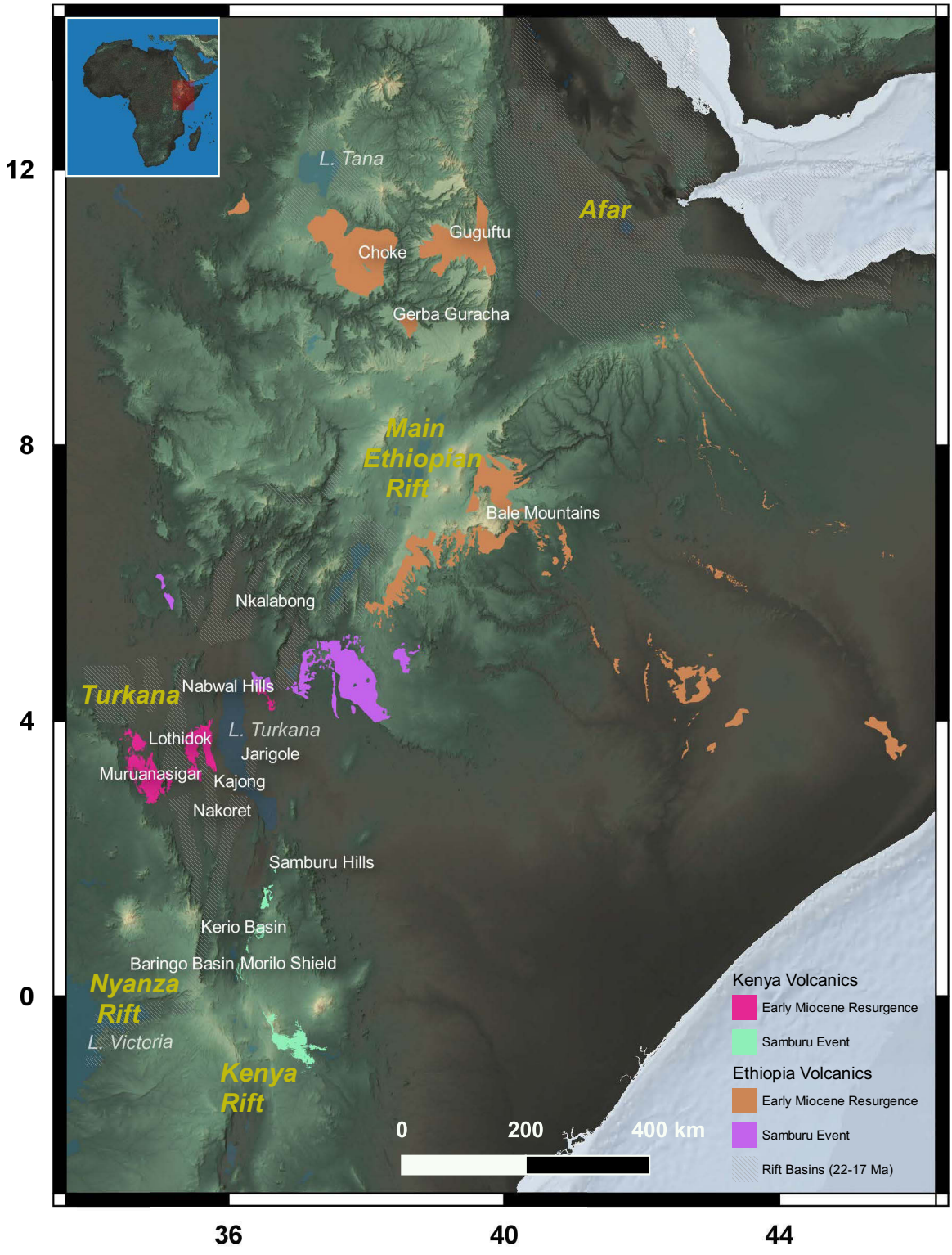
L. Tana
Afar
Guguftu
Choke
Gerba Guracha
Main Ethiopian Rift
Bale Mountains
Nkalabong
Turkana
Nabwal Hills
L. Turkana
Lothidok
Jarigole
Muruanasigar
Kajong
Nakoret
Samburu Hills
Kerio Basin
Baringo Basin
Morilo Shield
Nyanza Rift
L. Victoria
Kenya Rift
0
200
400 km
Kenya Volcanics
Early Miocene Resurgence
Samburu Event
Ethiopia Volcanics
Early Miocene Resurgence
Samburu Event
Rift Basins (22-17 Ma)
12
8
4
0
36
40
44

Figure 4

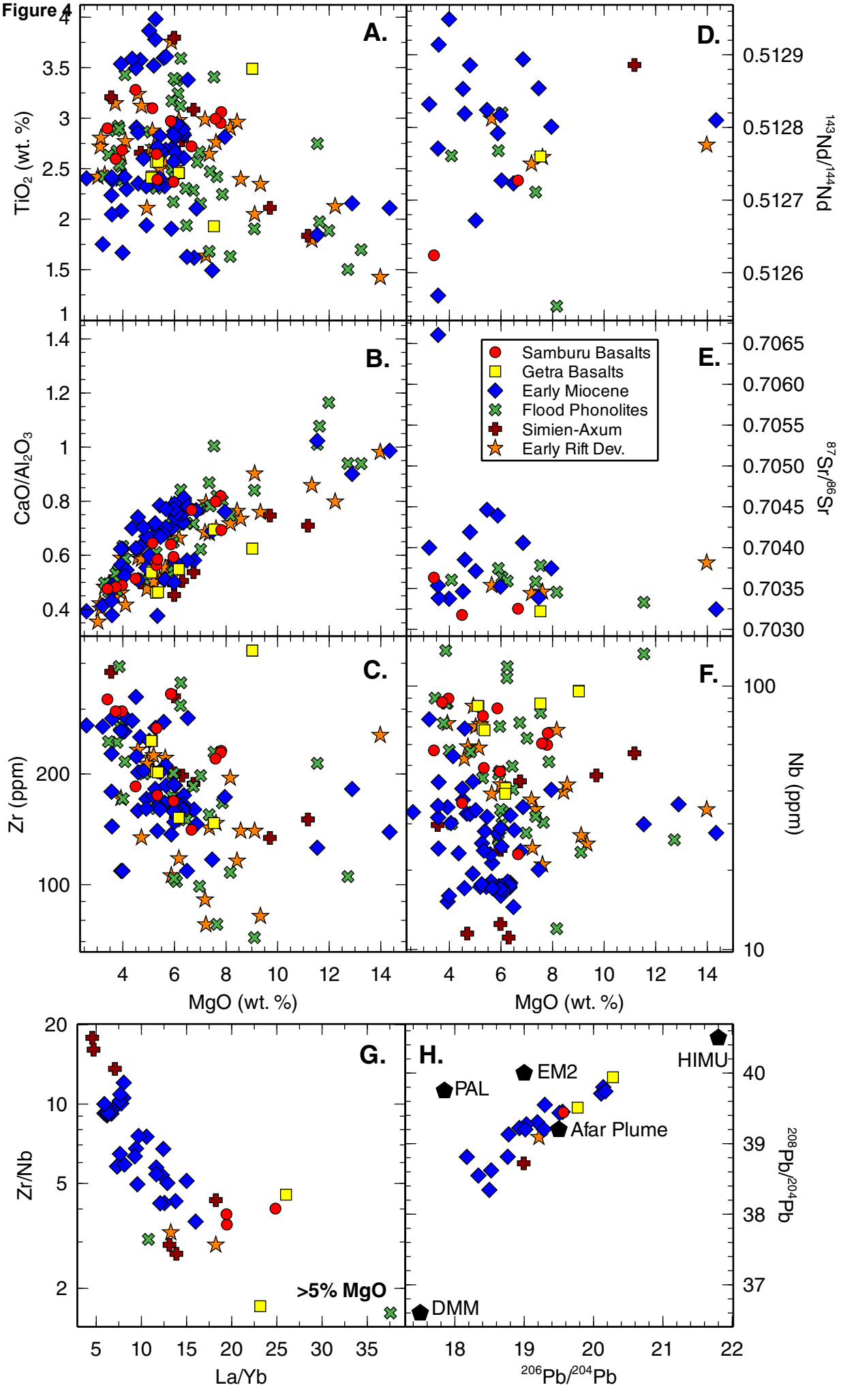
A.
B.
C.
D.
E.
F.
G.
H.
TiO2 (wt. %)
CaO/Al2O3
Zr (ppm)
143Nd/144Nd
87Sr/86Sr
Nb (ppm)
MgO (wt. %)
MgO (wt. %)
Samburu Basalts
Getra Basalts
Early Miocene
Flood Phonolites
Simien-Axum
Early Rift Dev.
Zr/Nb
La/Yb
>5% MgO
PAL
EM2
HIMU
Afar Plume
DMM
208Pb/204Pb
206Pb/204Pb

Figure 5

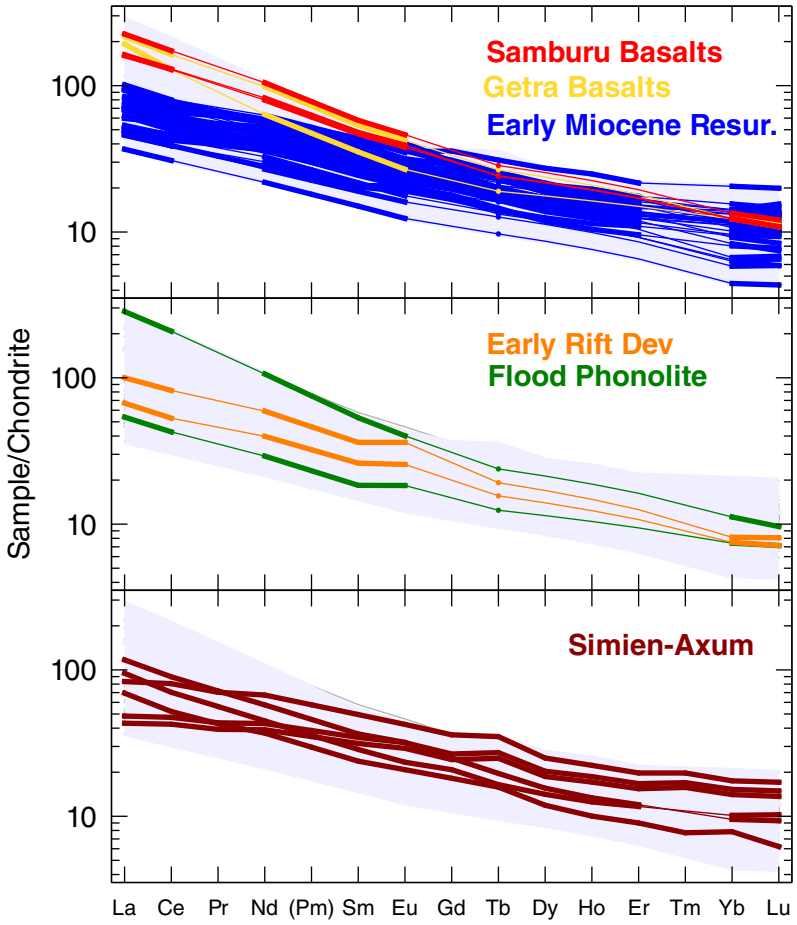
Samburu Basalts
Getra Basalts
Early Miocene Resur.
Early Rift Dev
Flood Phonolite
Simien-Axum
Sample/Chondrite
100
10
La
Ce
Pr
Nd
(Pm)
Sm
Eu
Gd
Tb
Dy
Ho
Er
Tm
Yb
Lu

Figure 6

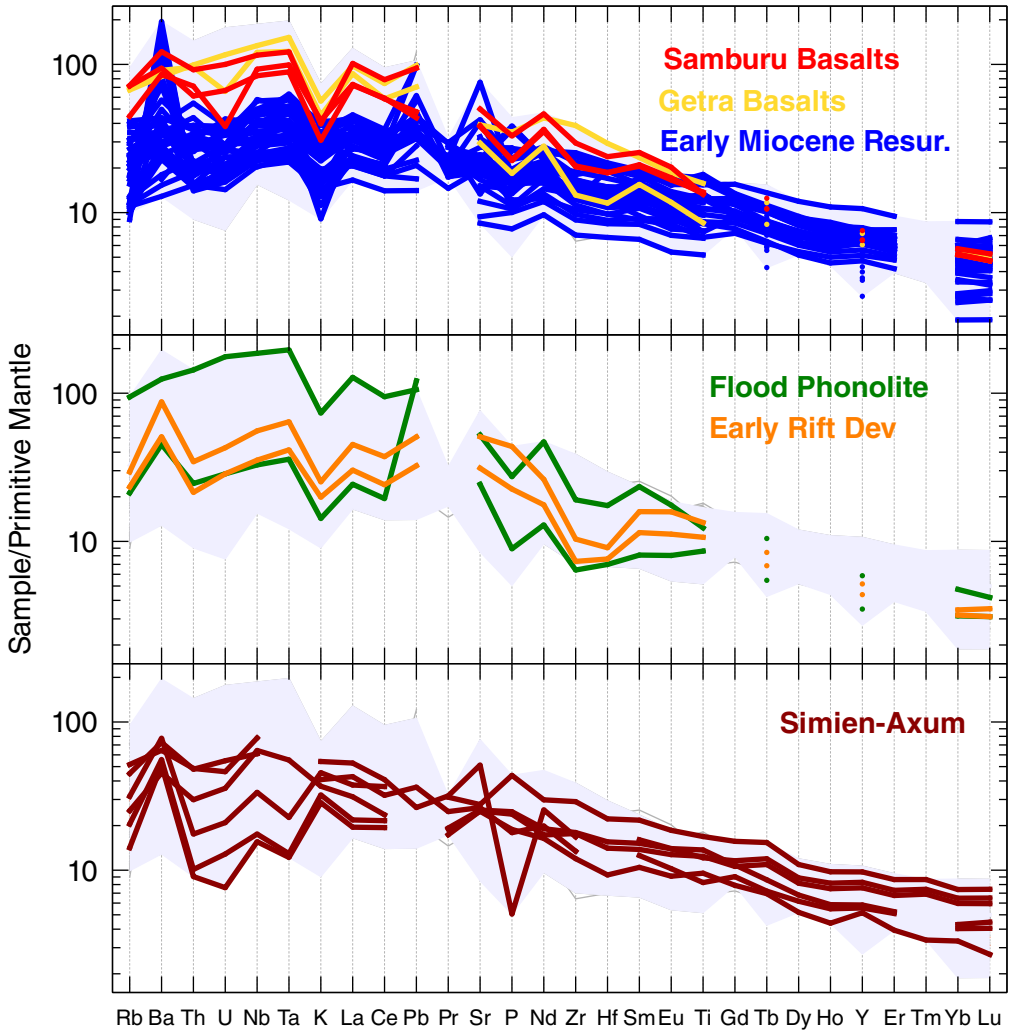
Samburu Basalts
Getra Basalts
Early Miocene Resur.
Flood Phonolite
Early Rift Dev
Simien-Axum
Sample/Primitive Mantle
100
10
Rb Ba Th U Nb Ta K La Ce Pb Pr Sr P Nd Zr Hf Sm Eu Ti Gd Tb Dy Ho Y Er Tm Yb Lu

Figure 7

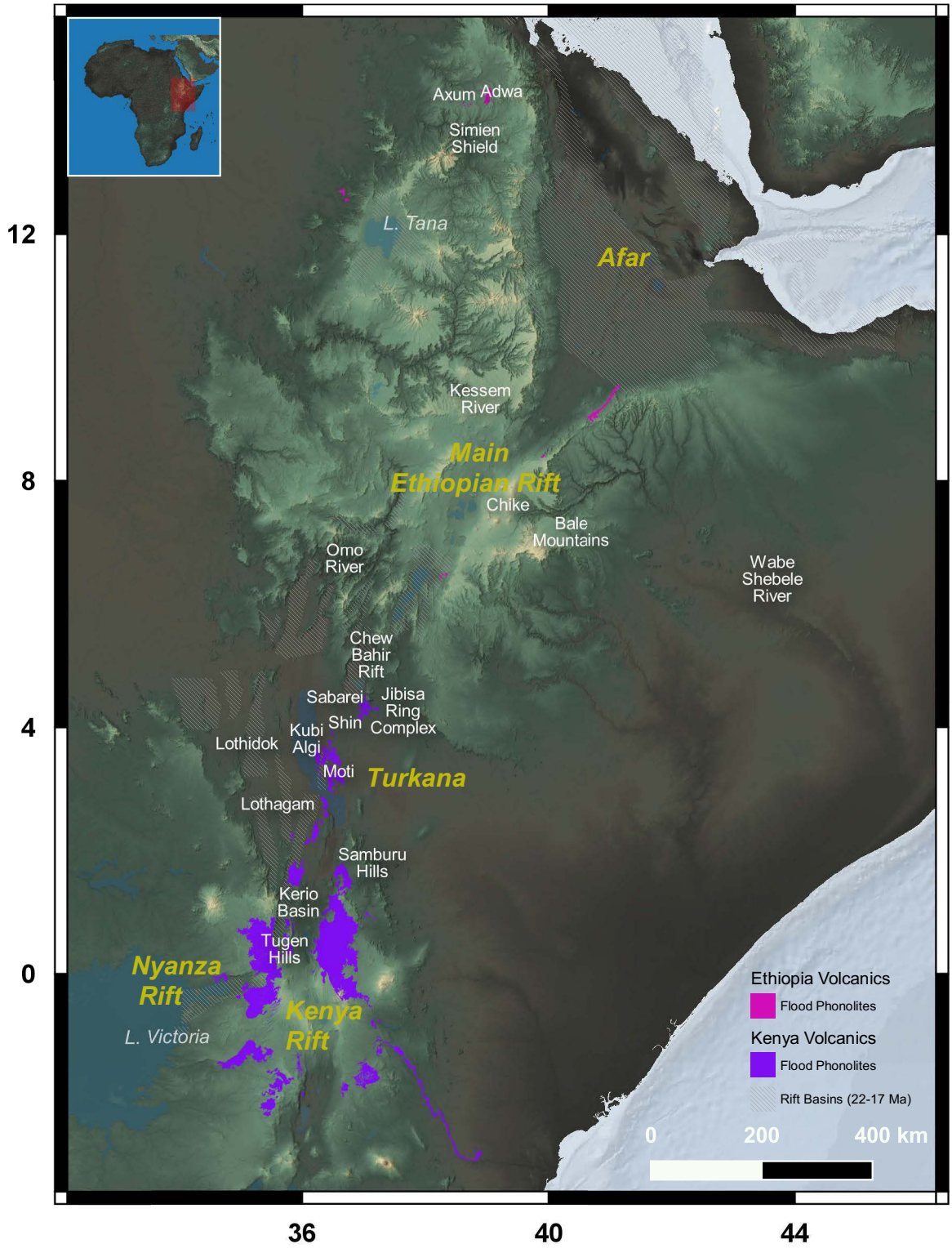
Axum
Adwa
Simien Shield
L. Tana
Afar
Kessem River
Main Ethiopian Rift
Chike
Bale Mountains
Omo River
Wabe Shebele River
Chew Bahir Rift
Sabarei
Jibisa
Ring Complex
Shin
Kubi Algi
Lothidok
Moti
Turkana
Lothagam
Samburu Hills
Kerio Basin
Tugen Hills
Nyanza Rift
L. Victoria
Kenya Rift
Ethiopia Volcanics
Flood Phonolites
Kenya Volcanics
Flood Phonolites
Rift Basins (22-17 Ma)
0
200
400 km
12
8
4
0
36
40
44

Figure 8

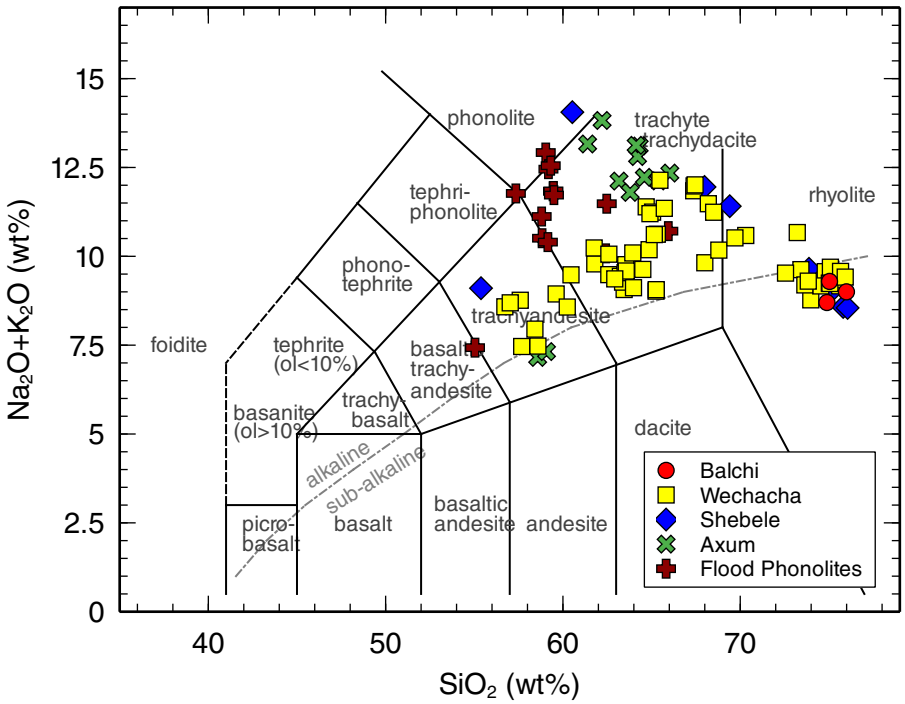
phonolite
trachyte
trachydacite
rhyolite
tephri-
phonolite
phono-
tephrite
trachyandesite
foidite
tephrite
(ol<10%)
basalt
trachy-
andesite
basanite
(ol>10%)
trachy-
basalt
dacite
alkaline
sub-alkaline
picro-
basalt
basalt
basaltic
andesite
andesite
Balchi
Wechacha
Shebele
Axum
Flood Phonolites
Na2O+K2O (wt%)
SiO2 (wt%)
0
2.5
5
7.5
10
12.5
15
40
50
60
70

Figure 9

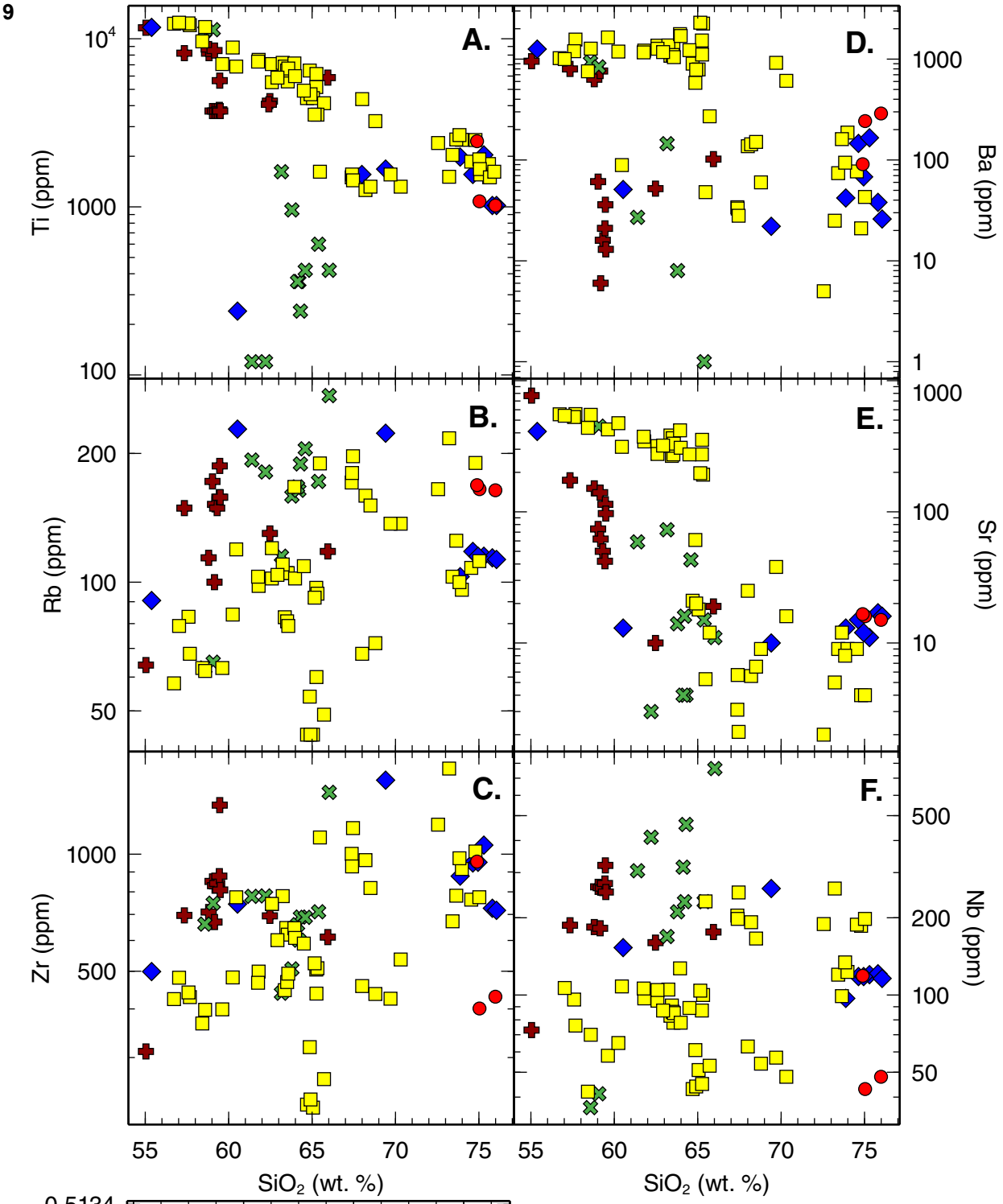
A.
B.
C.
D.
E.
F.
Ti (ppm)
Rb (ppm)
Zr (ppm)
Ba (ppm)
Sr (ppm)
Nb (ppm)
SiO2 (wt. %)
SiO2 (wt. %)

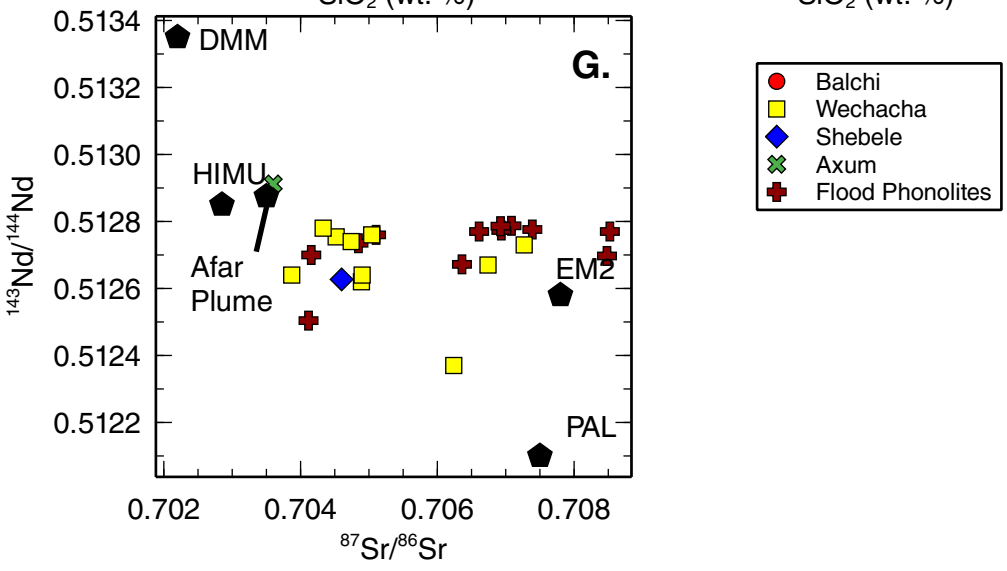
G.
DMM
HIMU
Afar
Plume
EM2
PAL
143Nd/144Nd
87Sr/86Sr
Balchi
Wechacha
Shebele
Axum
Flood Phonolites

Figure 10

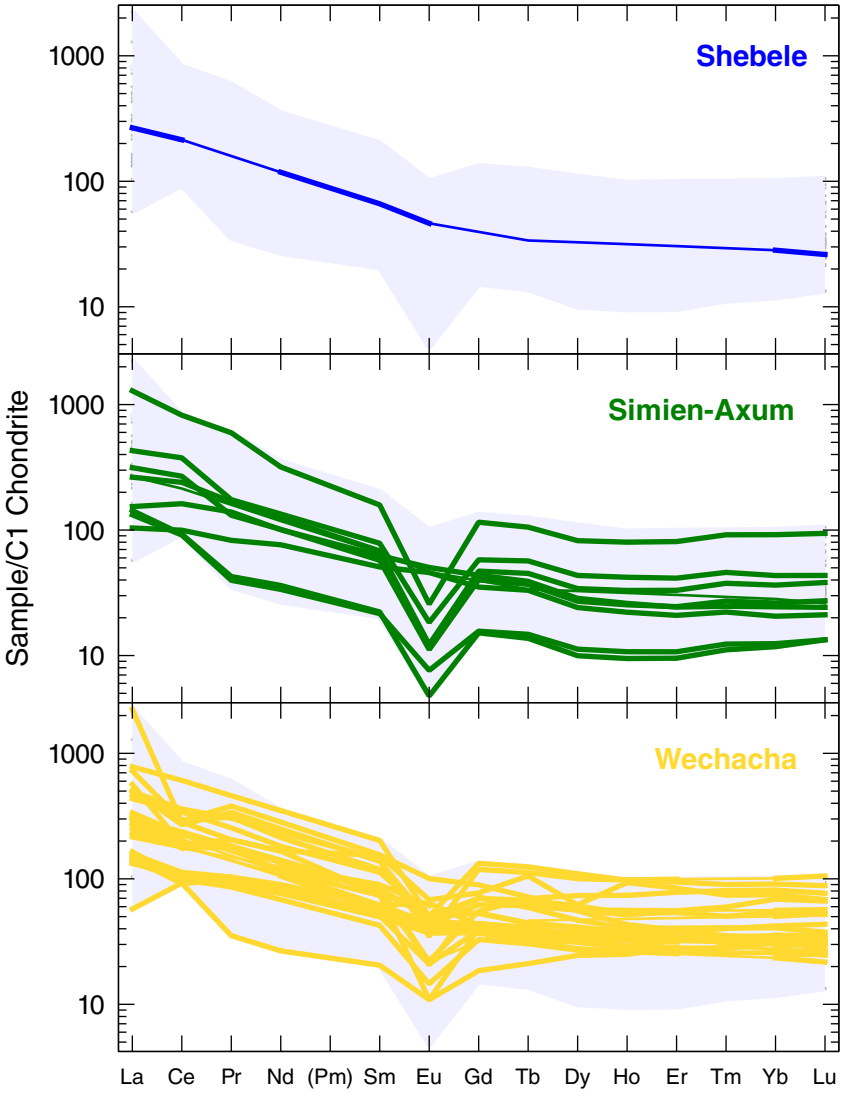
Shebele
Simien-Axum
Wechacha
Sample/C1 Chondrite
1000
100
10
La
Ce
Pr
Nd
(Pm)
Sm
Eu
Gd
Tb
Dy
Ho
Er
Tm
Yb
Lu

Figure 11

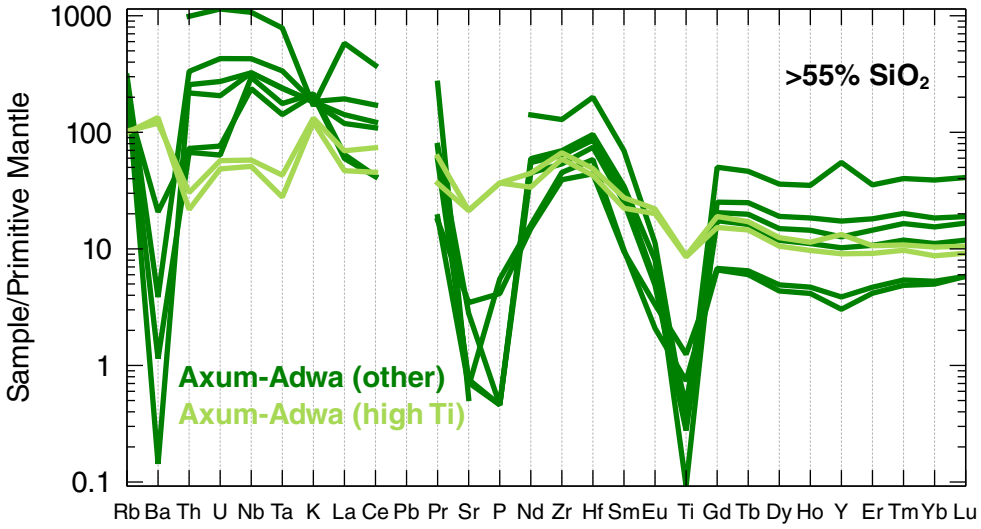
1000
100
10
1
0.1
Sample/Primitive Mantle
>55% SiO2
Axum-Adwa (other)
Axum-Adwa (high Ti)
Rb Ba Th U Nb Ta K La Ce Pb Pr Sr P Nd Zr Hf Sm Eu Ti Gd Tb Dy Ho Y Er Tm Yb Lu

Figure 12

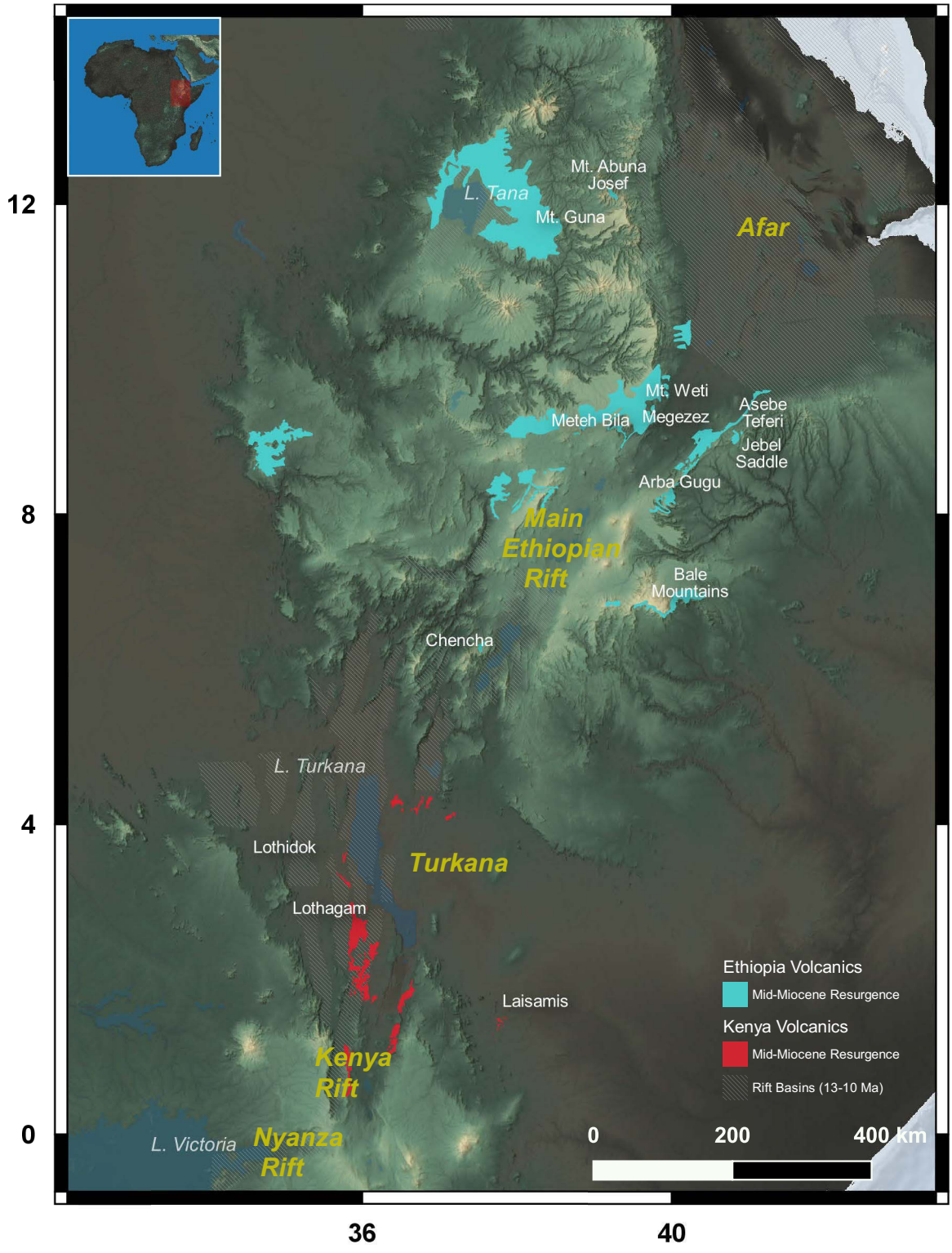
Mt. Abuna Josef
L. Tana
Mt. Guna
Afar
Mt. Weti
Asebe Teferi
Meteh Bila
Megezez
Jebel Saddle
Arba Gugu
Main Ethiopian Rift
Bale Mountains
Chencha
L. Turkana
Lothidok
Turkana
Lothagam
Laisamis
Kenya Rift
L. Victoria
Nyanza Rift
Ethiopia Volcanics
Mid-Miocene Resurgence
Kenya Volcanics
Mid-Miocene Resurgence
Rift Basins (13-10 Ma)
0
200
400 km
12
8
4
0
36
40

Figure 13

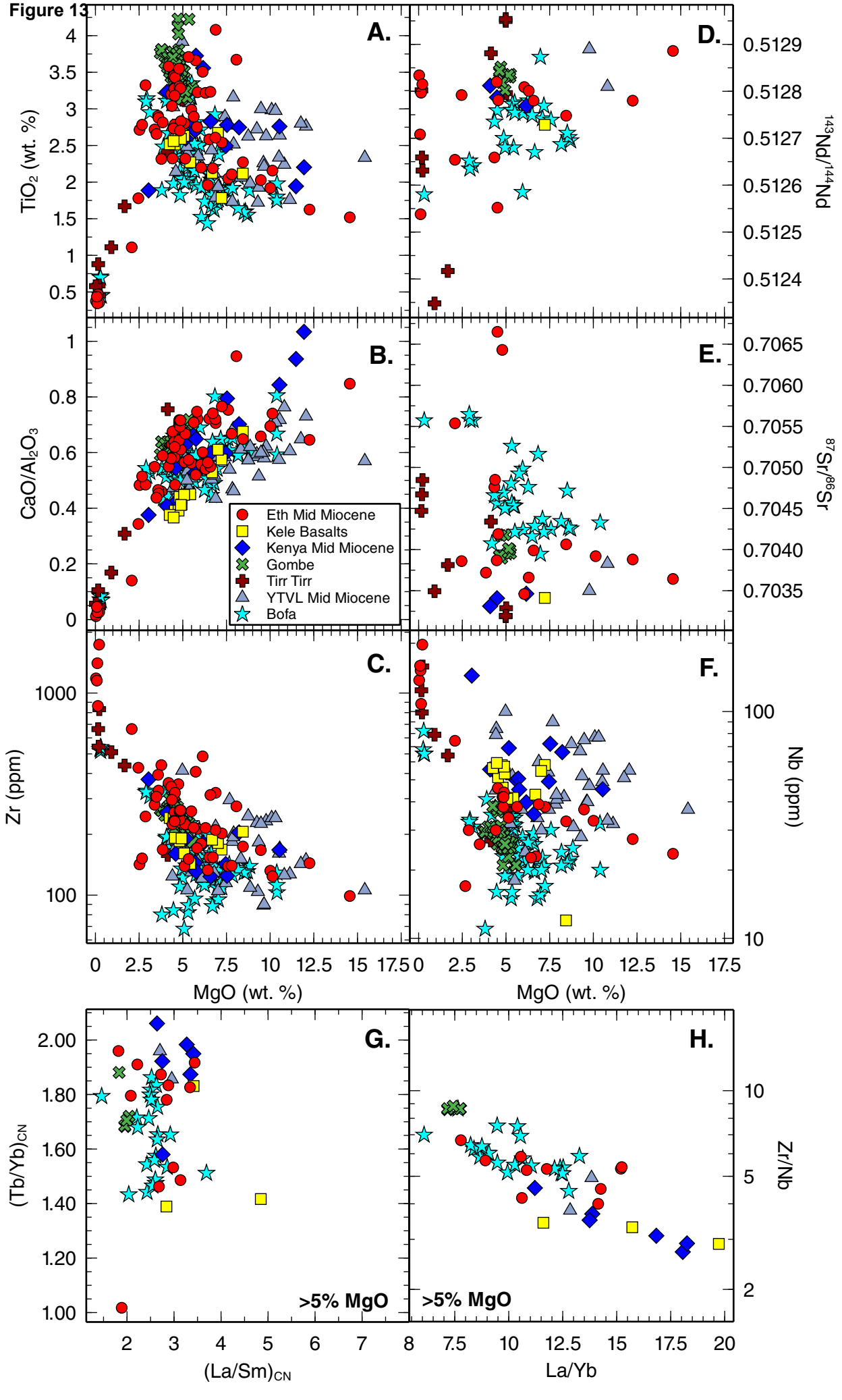
A.
B.
C.
D.
E.
F.
G.
H.
TiO2 (wt. %)
CaO/Al2O3
Zr (ppm)
143Nd/144Nd
87Sr/86Sr
Nb (ppm)
MgO (wt. %)
MgO (wt. %)
(Tb/Yb)CN
(La/Sm)CN
La/Yb
Zr/Nb
Eth Mid Miocene
Kele Basalts
Kenya Mid Miocene
Gombe
Tirr Tirr
YTVL Mid Miocene
Bofa
>5% MgO
>5% MgO

Figure 14

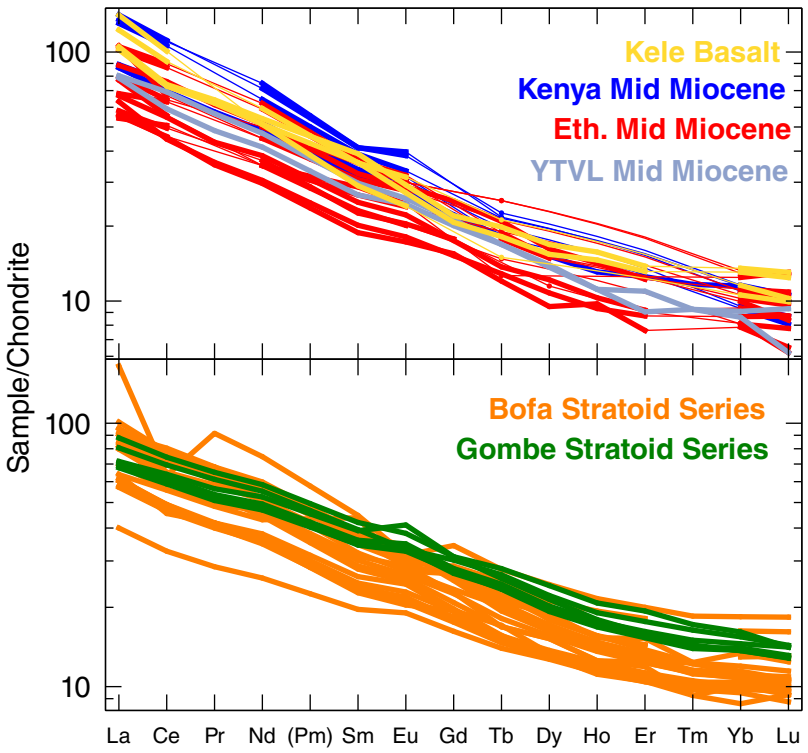
Kele Basalt
Kenya Mid Miocene
Eth. Mid Miocene
YTVL Mid Miocene
Bofa Stratoid Series
Gombe Stratoid Series
Sample/Chondrite
100
10
100
10
La Ce Pr Nd (Pm) Sm Eu Gd Tb Dy Ho Er Tm Yb Lu

Figure 15

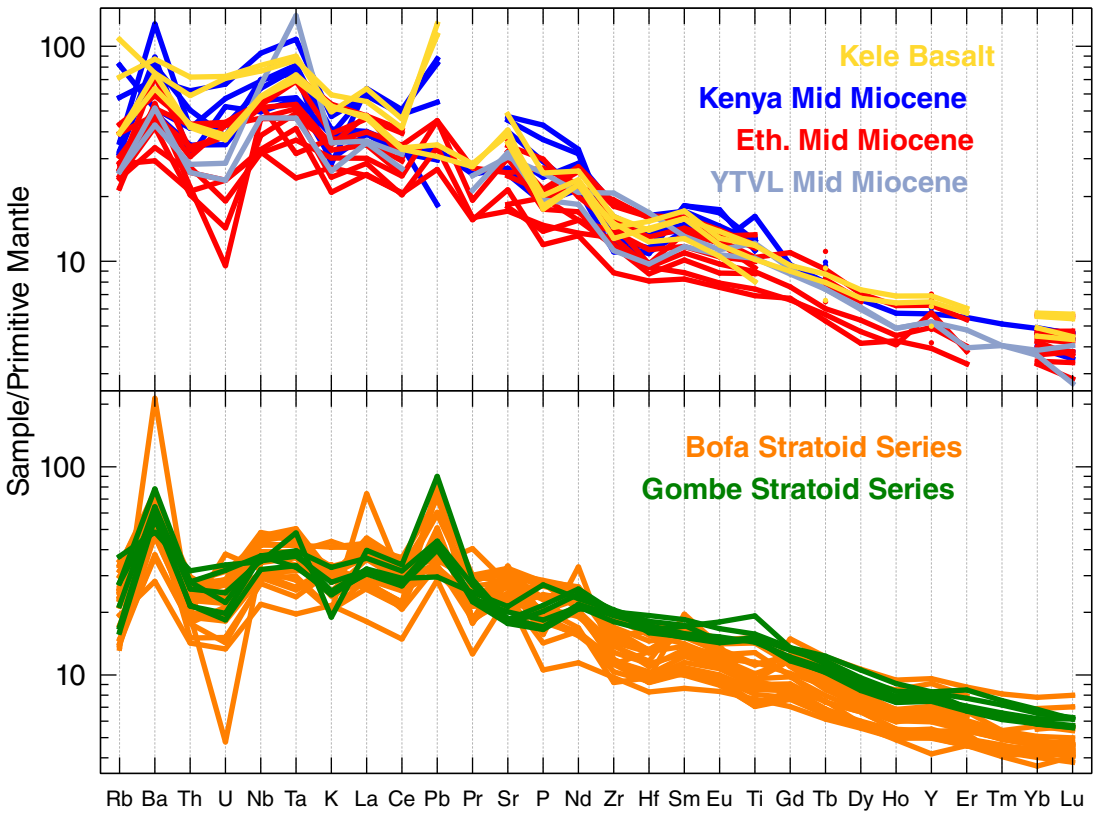
Kele Basalt
Kenya Mid Miocene
Eth. Mid Miocene
YTVL Mid Miocene
Bofa Stratoid Series
Gombe Stratoid Series
Sample/Primitive Mantle
100
10
100
10
Rb Ba Th U Nb Ta K La Ce Pb Pr Sr P Nd Zr Hf Sm Eu Ti Gd Tb Dy Ho Y Er Tm Yb Lu

Figure 16

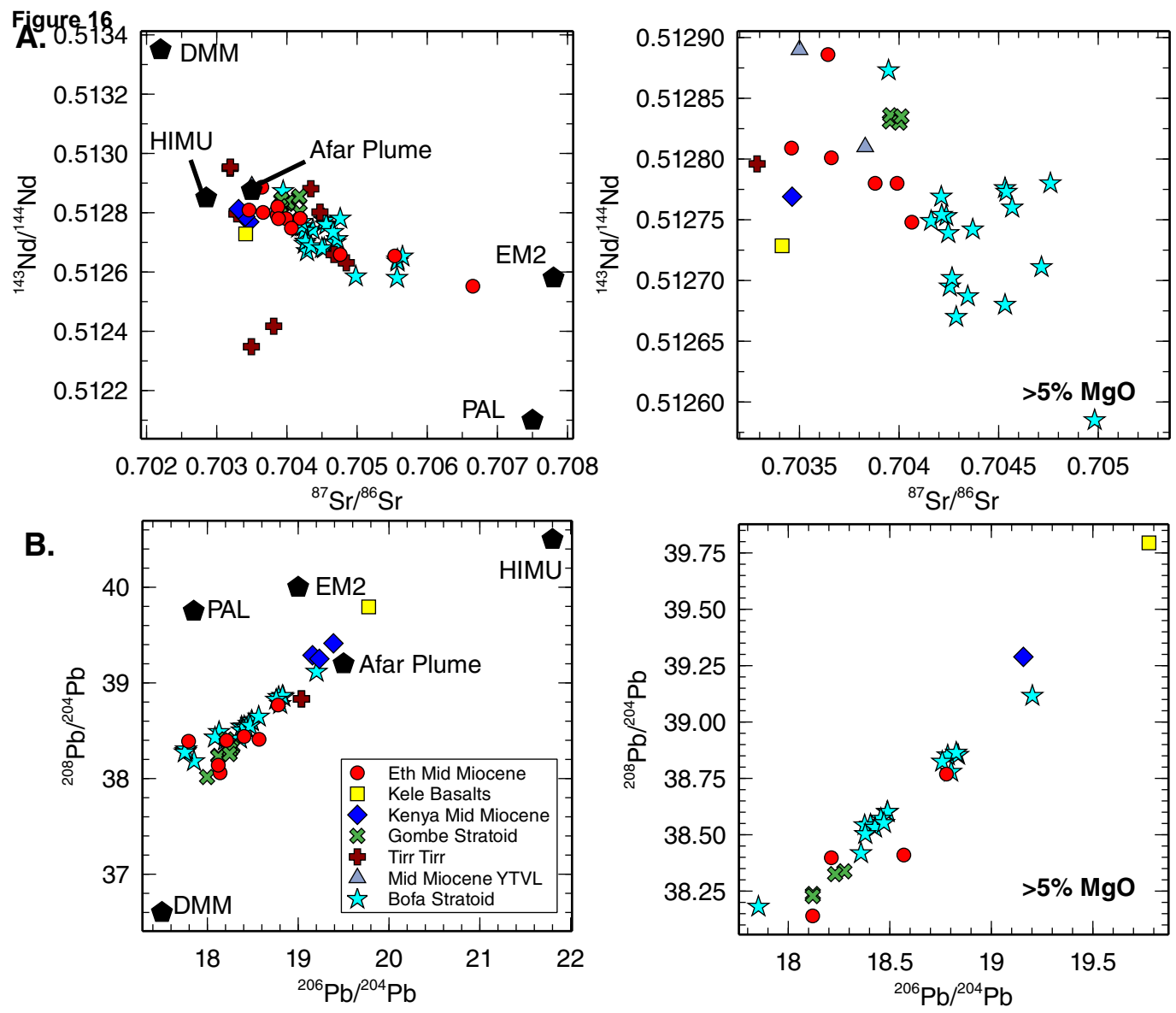
A.
DMM
HIMU
Afar Plume
EM2
PAL
0.5134
0.5132
0.5130
0.5128
0.5126
0.5124
0.5122
143Nd/144Nd
0.702 0.703 0.704 0.705 0.706 0.707 0.708
87Sr/86Sr
0.51290
0.51285
0.51280
0.51275
0.51270
0.51265
0.51260
143Nd/144Nd
>5% MgO
0.7035 0.704 0.7045 0.705
87Sr/86Sr
B.
HIMU
EM2
PAL
Afar Plume
DMM
40
39
38
37
208Pb/204Pb
18 19 20 21 22
206Pb/204Pb
Eth Mid Miocene
Kele Basalts
Kenya Mid Miocene
Gombe Stratoid
Tirr Tirr
Mid Miocene YTVL
Bofa Stratoid
39.75
39.50
39.25
39.00
38.75
38.50
38.25
208Pb/204Pb
>5% MgO
18 18.5 19 19.5
206Pb/204Pb

Figure 17

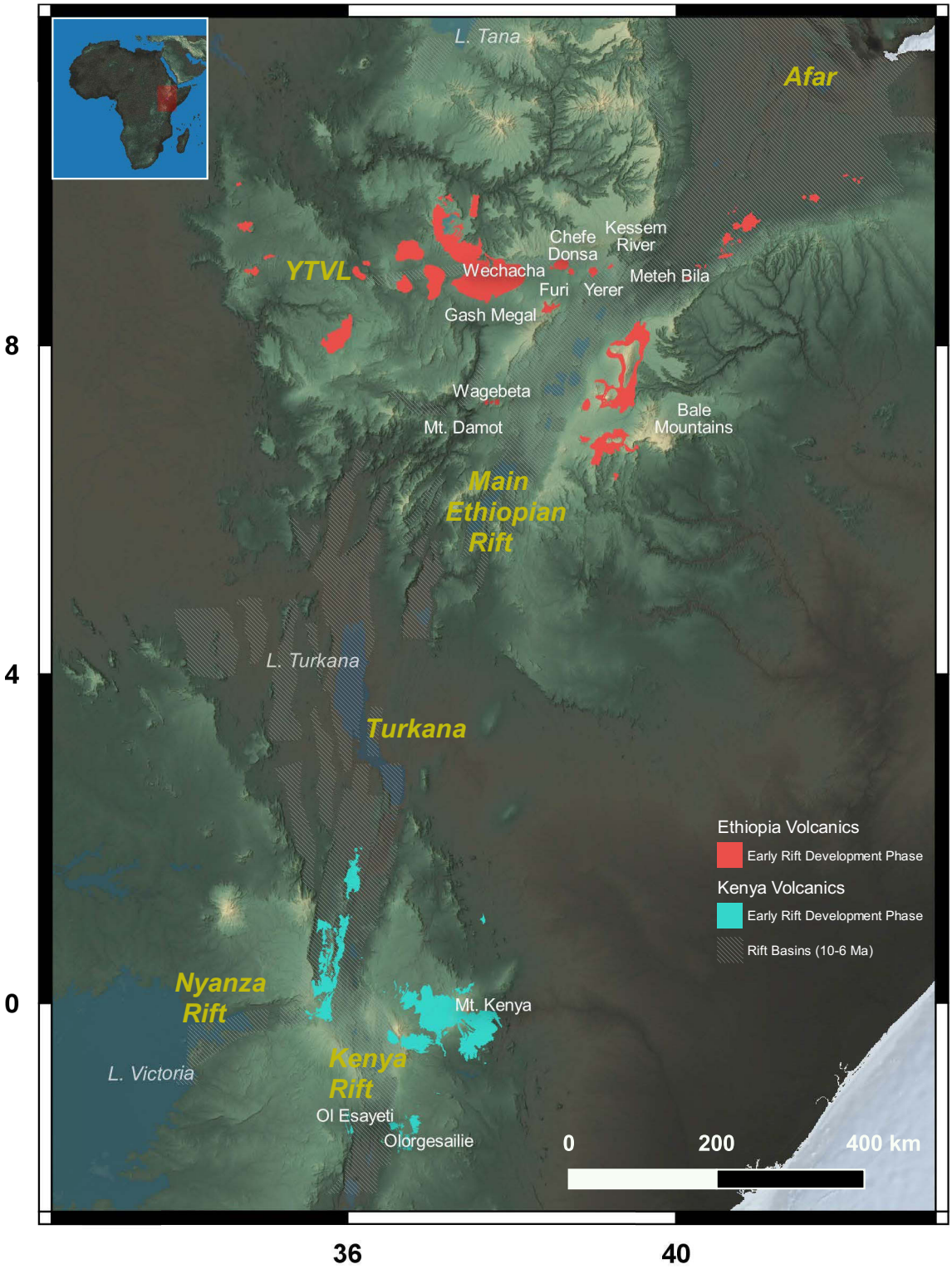
L. Tana
Afar
YTVL
Chefe Donsa
Kessem River
Wechacha
Furi
Yerer
Meteh Bila
Gash Megal
Wagebeta
Mt. Damot
Bale Mountains
Main Ethiopian Rift
L. Turkana
Turkana
Ethiopia Volcanics
Early Rift Development Phase
Kenya Volcanics
Early Rift Development Phase
Rift Basins (10-6 Ma)
Nyanza Rift
Mt. Kenya
L. Victoria
Kenya Rift
Ol Esayeti
Olorgesailie
0
200
400 km
8
4
0
36
40

Figure 18

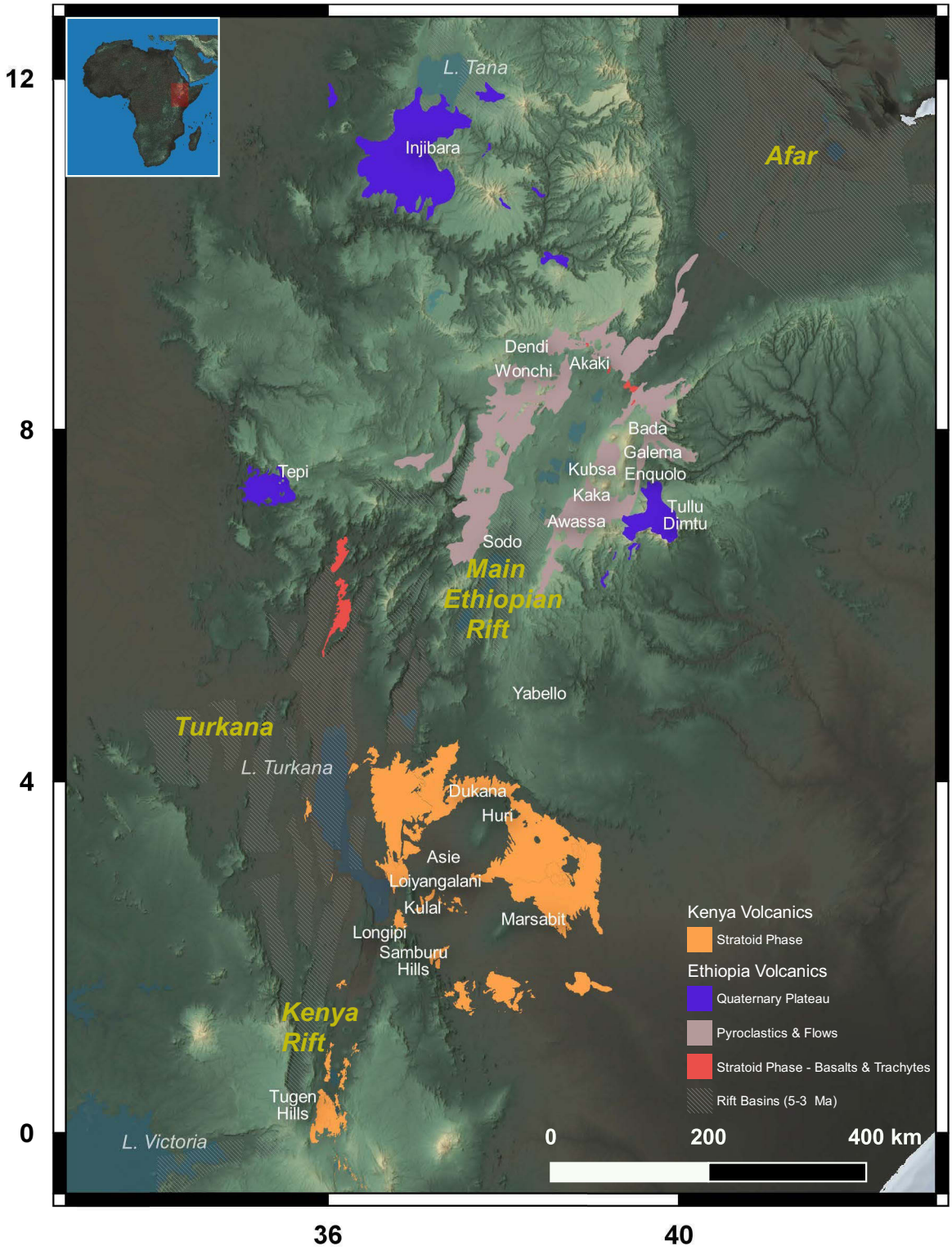
12
8
4
0
36
40
L. Tana
Injibara
Afar
Dendi
Wonchi
Akaki
Bada
Galema
Enquolo
Kubsa
Kaka
Awassa
Tullu
Dimtu
Tepi
Sodo
Main
Ethiopian
Rift
Yabello
Turkana
L. Turkana
Dukana
Huri
Asie
Loiyangalani
Kulal
Marsabit
Longipi
Samburu
Hills
Kenya
Rift
Tugen
Hills
L. Victoria
Kenya Volcanics
Stratoid Phase
Ethiopia Volcanics
Quaternary Plateau
Pyroclastics & Flows
Stratoid Phase - Basalts & Trachytes
Rift Basins (5-3 Ma)
0
200
400 km

Figure 19

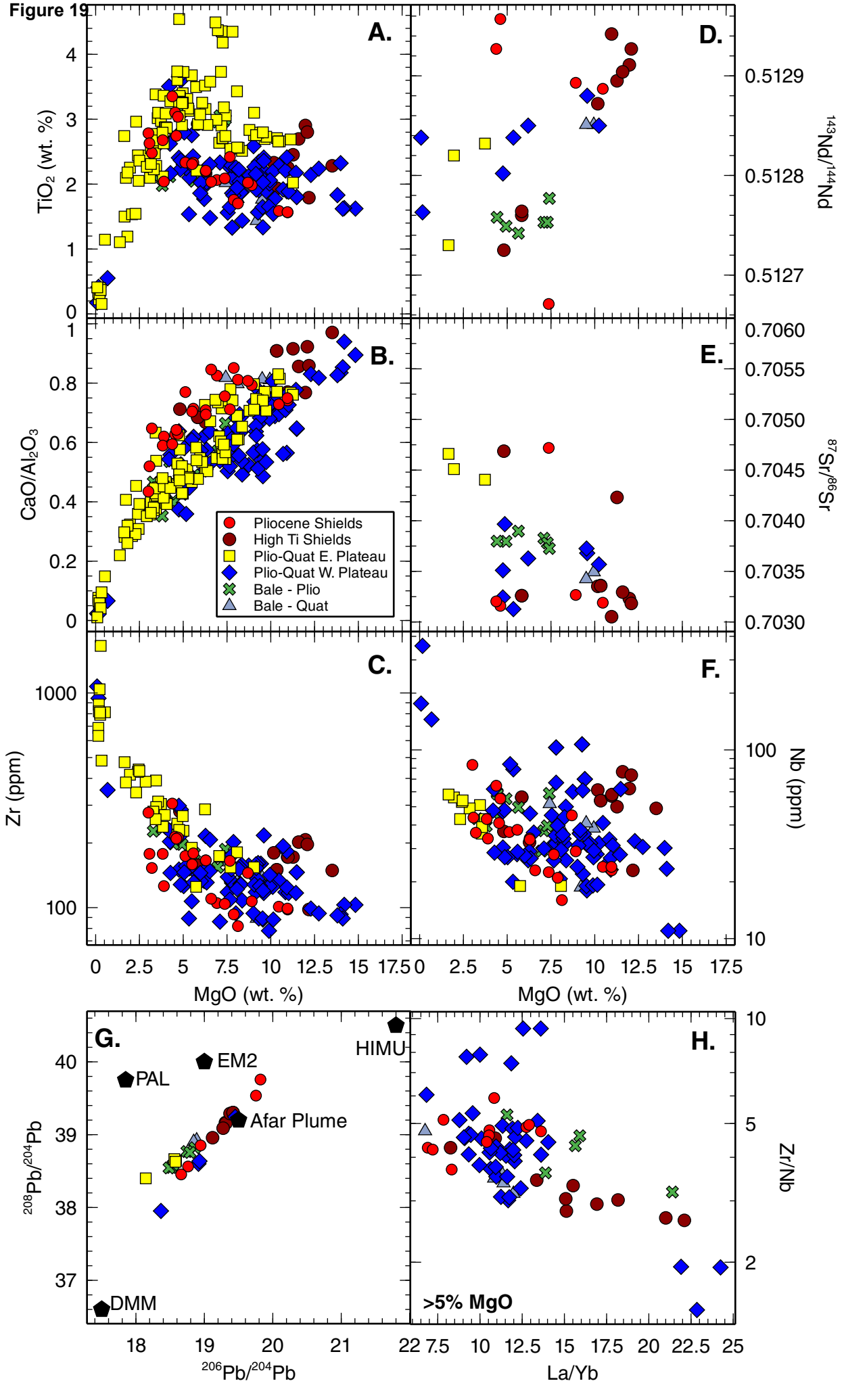
A.
B.
C.
D.
E.
F.
G.
H.
TiO2 (wt. %)
CaO/Al2O3
Zr (ppm)
143Nd/144Nd
87Sr/86Sr
Nb (ppm)
MgO (wt. %)
MgO (wt. %)
Pliocene Shields
High Ti Shields
Plio-Quat E. Plateau
Plio-Quat W. Plateau
Bale - Plio
Bale - Quat
HIMU
EM2
PAL
Afar Plume
DMM
208Pb/204Pb
206Pb/204Pb
>5% MgO
La/Yb
Zr/Nb

Figure 20

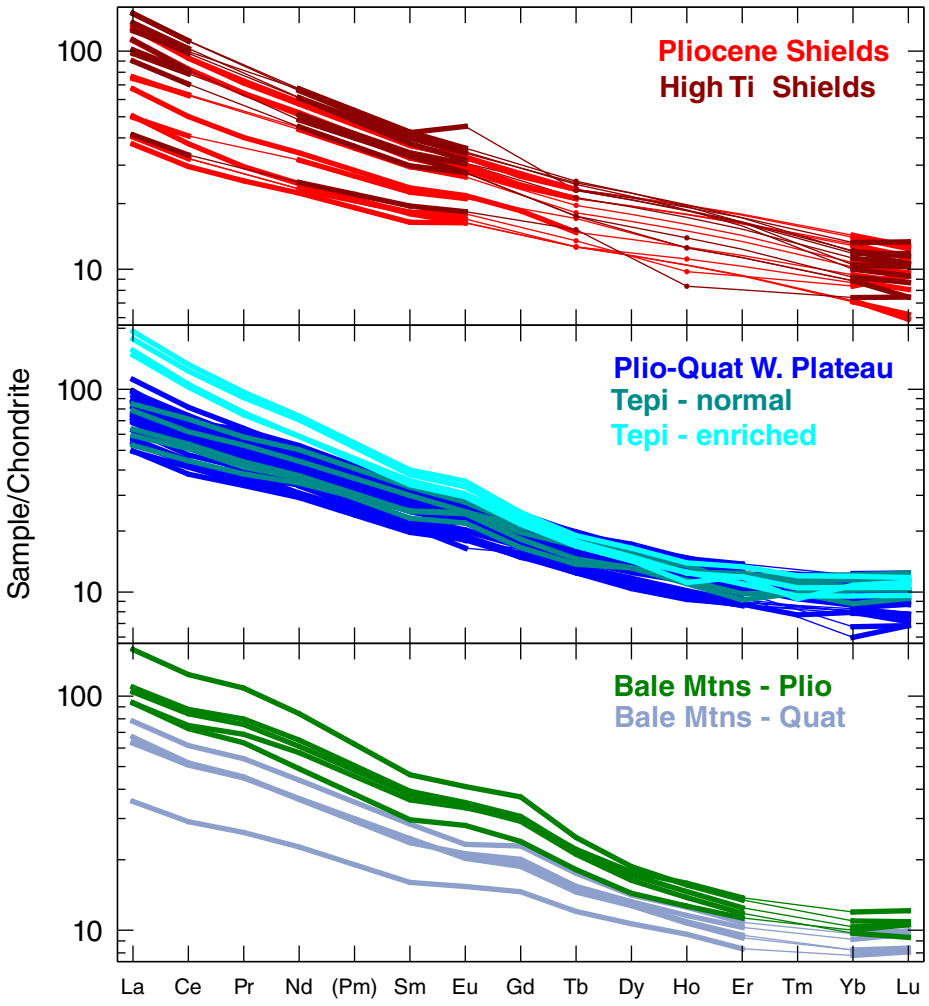
Pliocene Shields
High Ti Shields
Plio-Quat W. Plateau
Tepi - normal
Tepi - enriched
Bale Mtns - Plio
Bale Mtns - Quat
Sample/Chondrite
100
10
La
Ce
Pr
Nd
(Pm)
Sm
Eu
Gd
Tb
Dy
Ho
Er
Tm
Yb
Lu

Figure 21

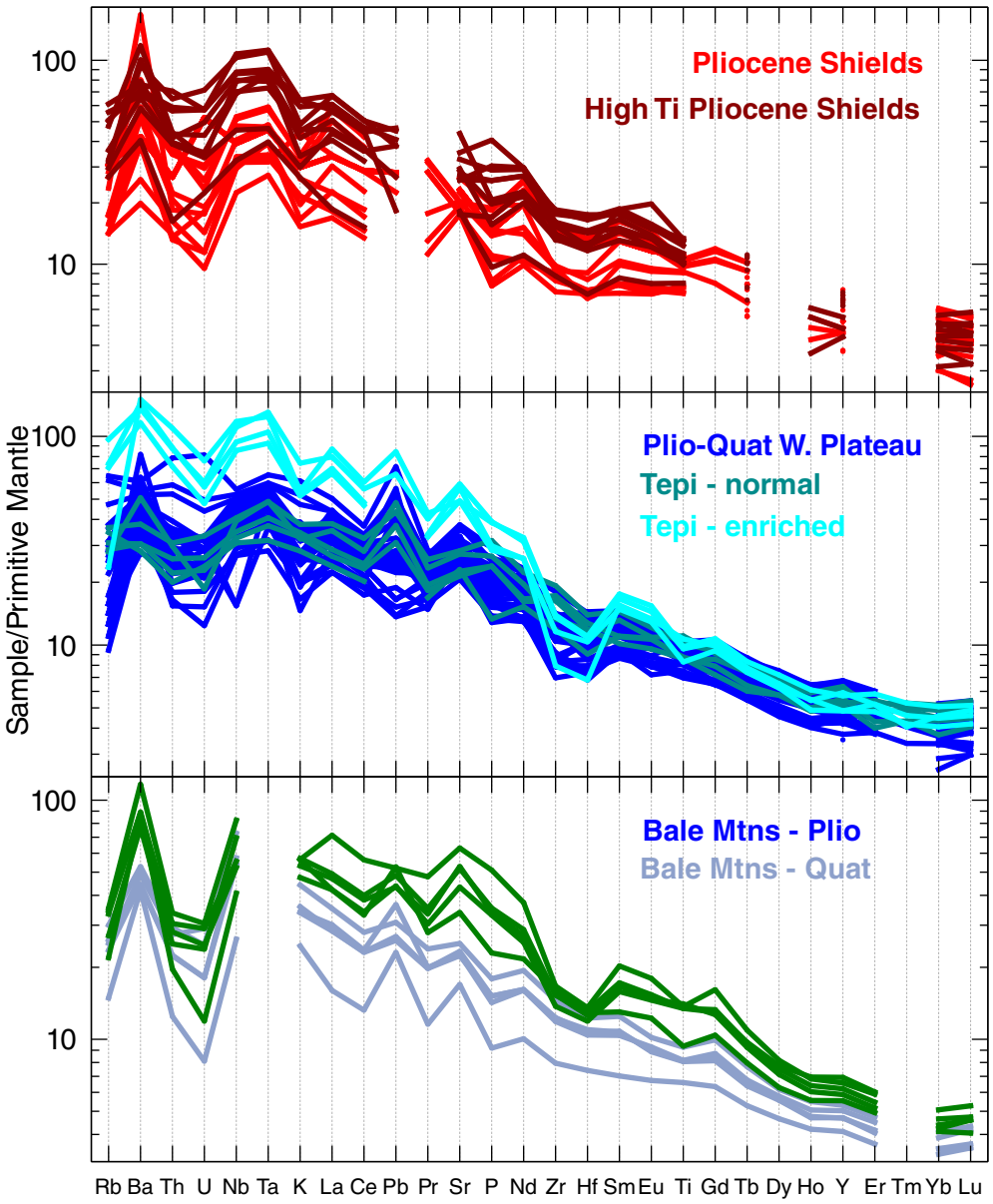
Pliocene Shields
High Ti Pliocene Shields
Plio-Quat W. Plateau
Tepi - normal
Tepi - enriched
Bale Mtns - Plio
Bale Mtns - Quat
Sample/Primitive Mantle
100
10
Rb Ba Th U Nb Ta K La Ce Pb Pr Sr P Nd Zr Hf Sm Eu Ti Gd Tb Dy Ho Y Er Tm Yb Lu

Figure 22

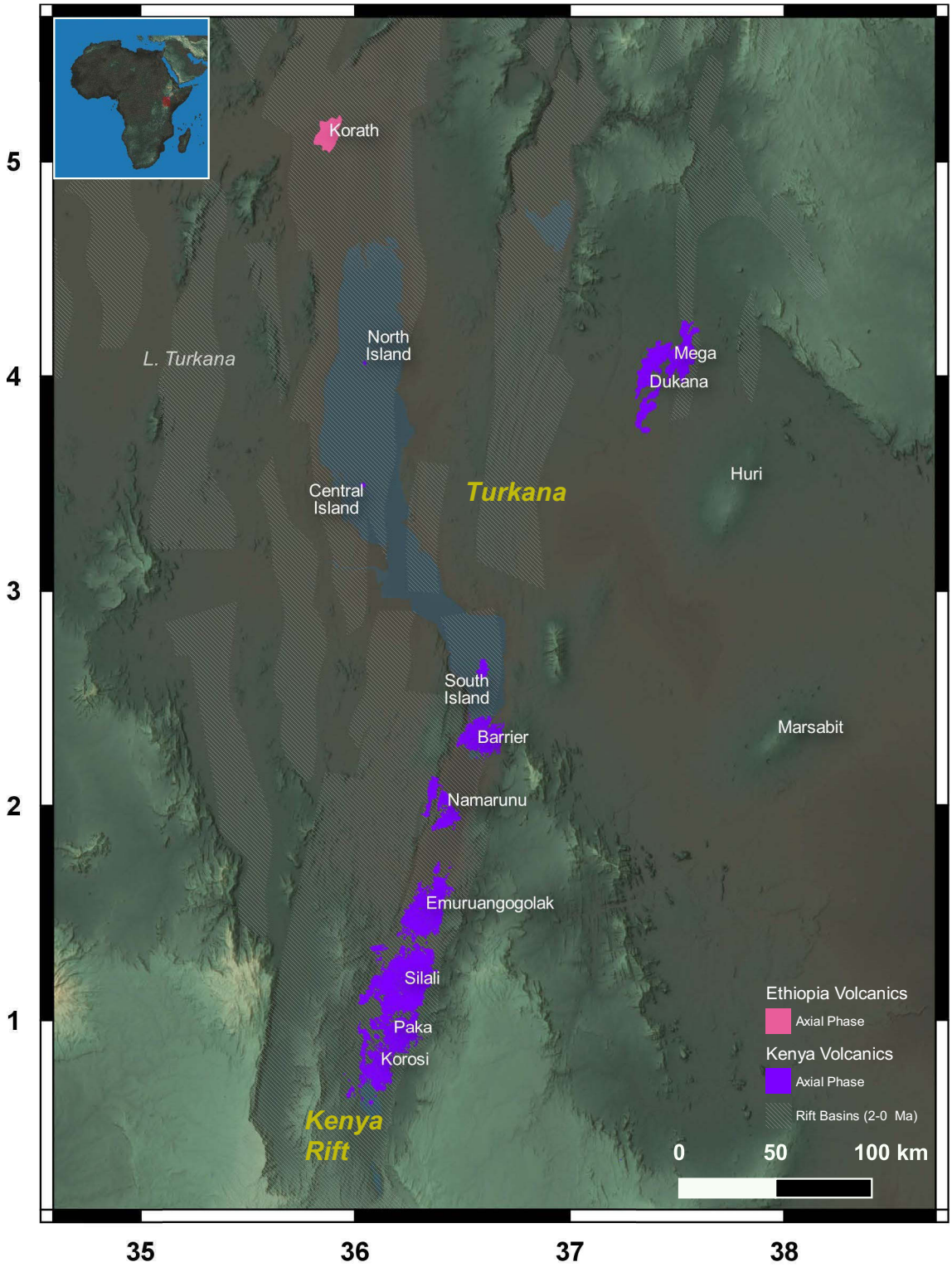
Korath
L. Turkana
North Island
Central Island
Turkana
Mega
Dukana
Huri
South Island
Barrier
Marsabit
Namarunu
Emuruangogolak
Silali
Paka
Korosi
Kenya Rift
Ethiopia Volcanics
Axial Phase
Kenya Volcanics
Axial Phase
Rift Basins (2-0 Ma)
0
50
100 km
5
4
3
2
1
35
36
37
38

Figure 23

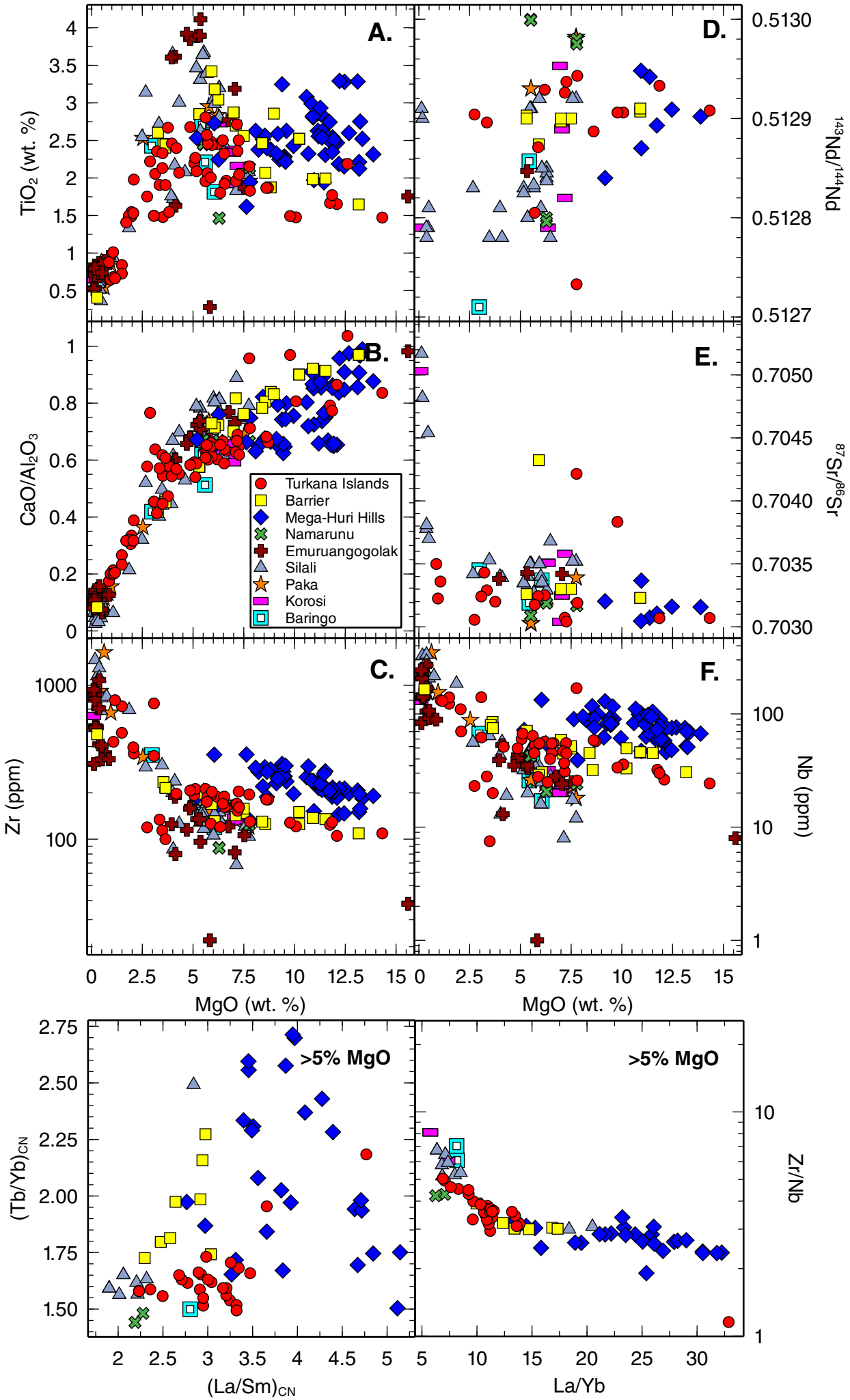
A.
B.
C.
D.
E.
F.
TiO2 (wt. %)
CaO/Al2O3
Zr (ppm)
143Nd/144Nd
87Sr/86Sr
Nb (ppm)
MgO (wt. %)
MgO (wt. %)
Turkana Islands
Barrier
Mega-Huri Hills
Namarunu
Emuruangogolak
Silali
Paka
Korosi
Baringo
>5% MgO
>5% MgO
(Tb/Yb)CN
(La/Sm)CN
La/Yb
Zr/Nb

Figure 24

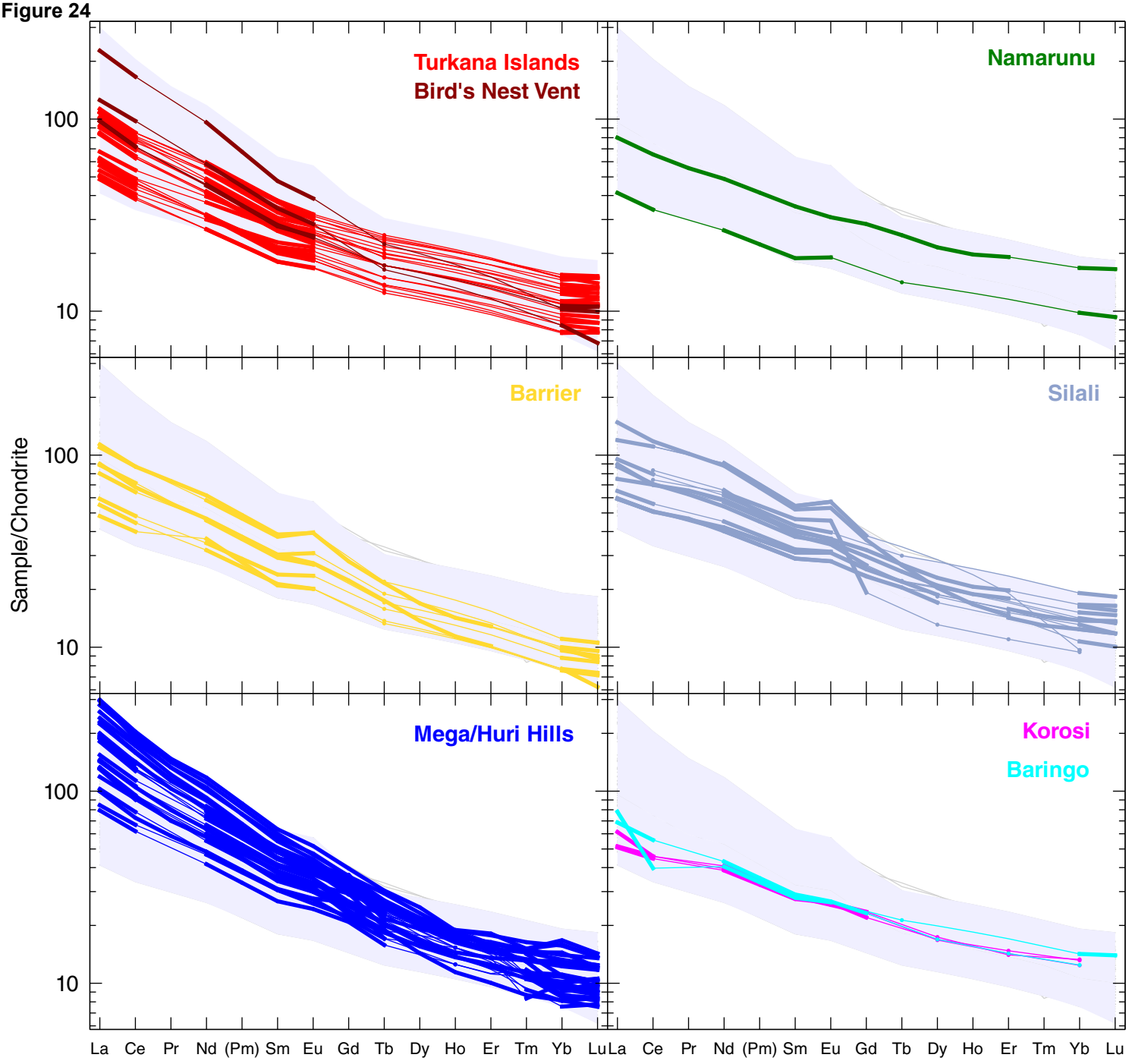
Turkana Islands
Bird's Nest Vent
Namarunu
Barrier
Silali
Mega/Huri Hills
Korosi
Baringo
Sample/Chondrite
100
10
La Ce Pr Nd (Pm) Sm Eu Gd Tb Dy Ho Er Tm Yb Lu

Figure 25

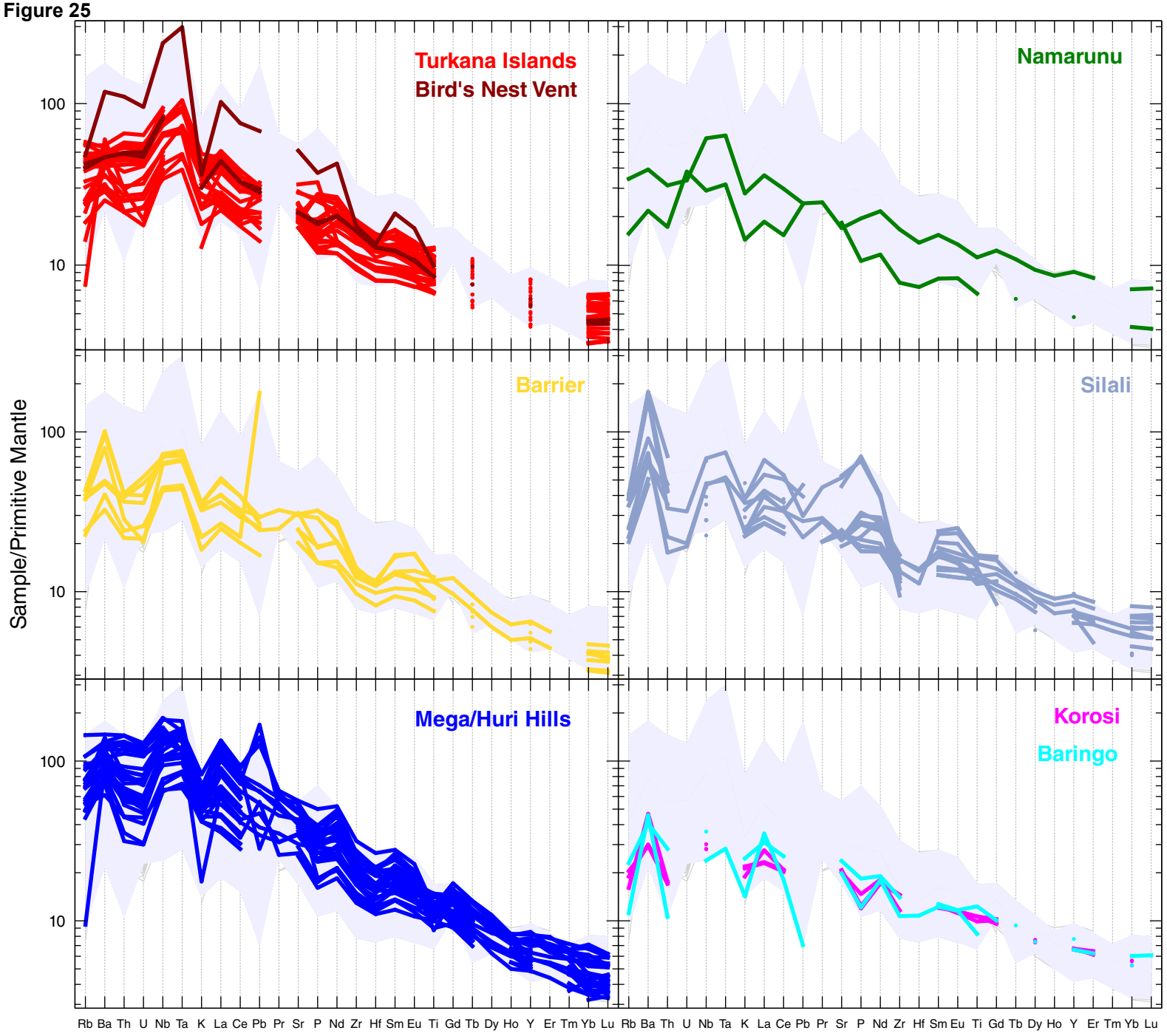
Turkana Islands
Bird's Nest Vent
Namarunu
Barrier
Silali
Mega/Huri Hills
Korosi
Baringo
Sample/Primitive Mantle
100
10
Rb Ba Th U Nb Ta K La Ce Pb Pr Sr P Nd Zr Hf Sm Eu Ti Gd Tb Dy Ho Y Er Tm Yb Lu

Figure 26

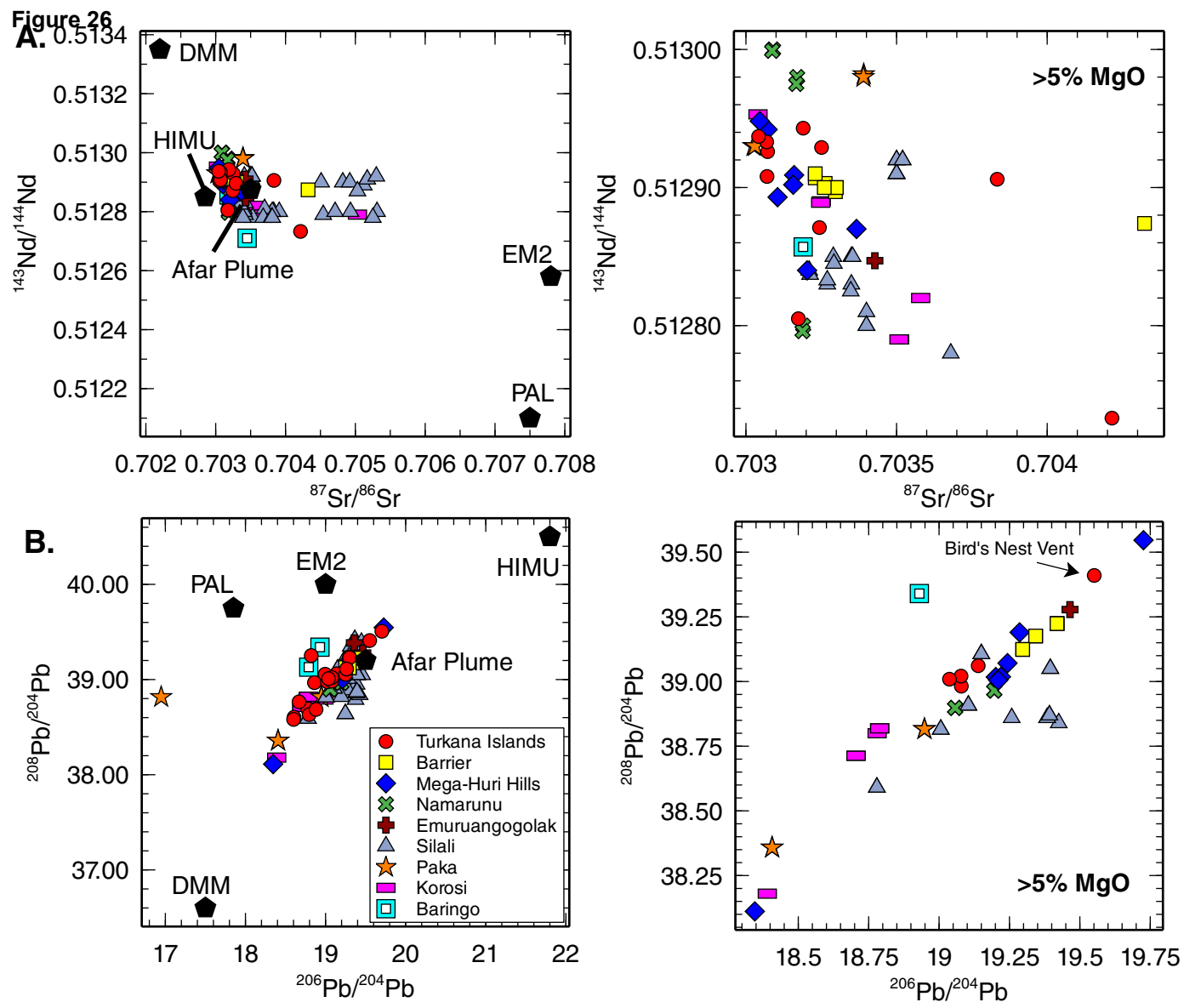
A.
DMM
HIMU
Afar Plume
EM2
PAL
0.5134
0.5132
0.5130
0.5128
0.5126
0.5124
0.5122
143Nd/144Nd
0.702 0.703 0.704 0.705 0.706 0.707 0.708
87Sr/86Sr
0.51300
0.51290
0.51280
>5% MgO
0.703
0.7035
0.704
B.
EM2
HIMU
PAL
Afar Plume
DMM
40.00
39.00
38.00
37.00
208Pb/204Pb
17 18 19 20 21 22
206Pb/204Pb
Turkana Islands
Barrier
Mega-Huri Hills
Namarunu
Emuruangogolak
Silali
Paka
Korosi
Baringo
Bird's Nest Vent
39.50
39.25
39.00
38.75
38.50
38.25
>5% MgO
18.5 18.75 19 19.25 19.5 19.75

Figure 27

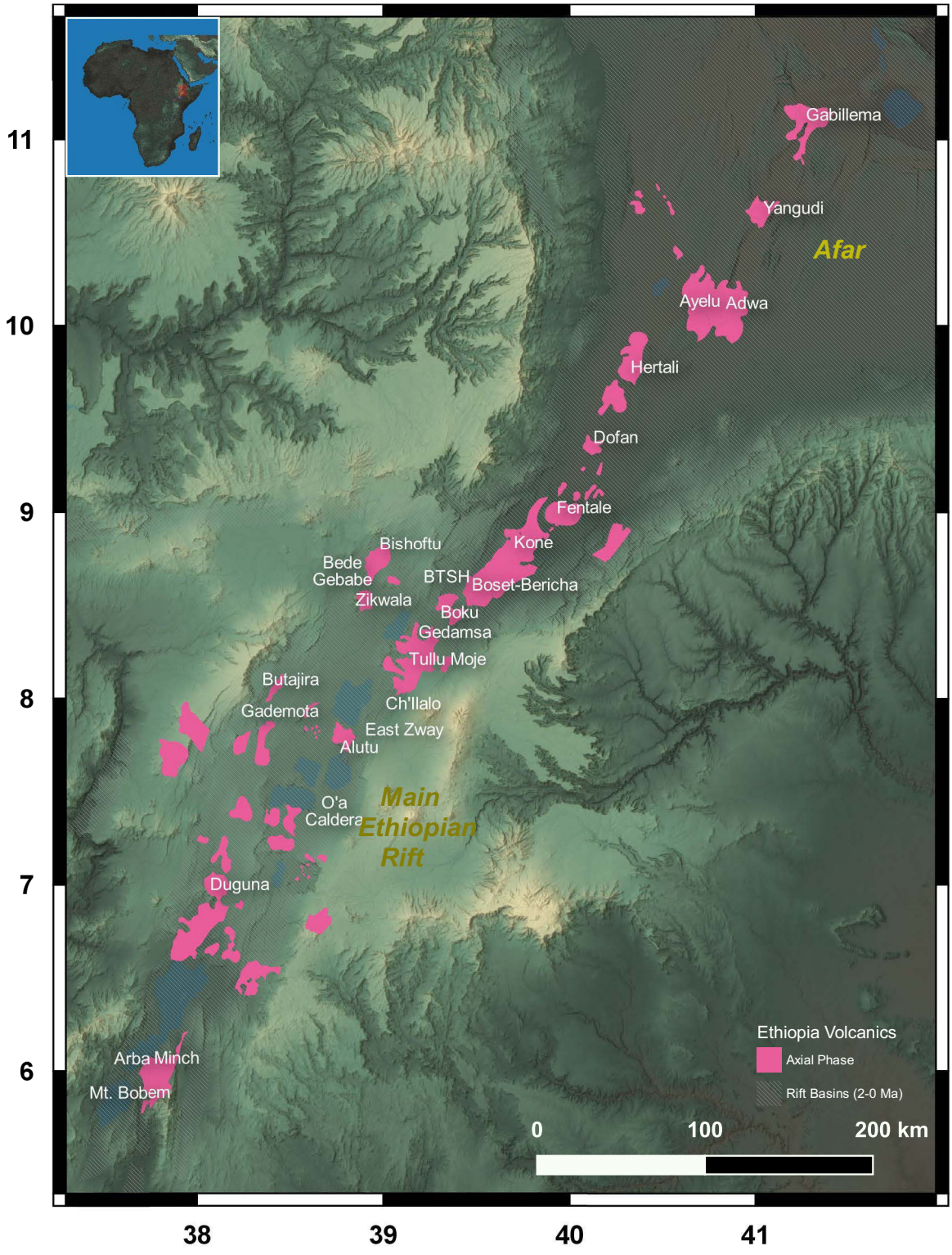
Gabillema
Yangudi
Afar
Ayelu
Adwa
Hertali
Dofan
Fentale
Bishoftu
Kone
Bede
Gebabe
BTSH
Boset-Bericha
Zikwala
Boku
Gedamsa
Tullu Moje
Butajira
Gademota
Ch'llalo
East Zway
Alutu
O'a
Caldera
Main
Ethiopian
Rift
Duguna
Arba Minch
Mt. Bobem
Ethiopia Volcanics
Axial Phase
Rift Basins (2-0 Ma)
0
100
200 km
11
10
9
8
7
6
38
39
40
41

Figure 28

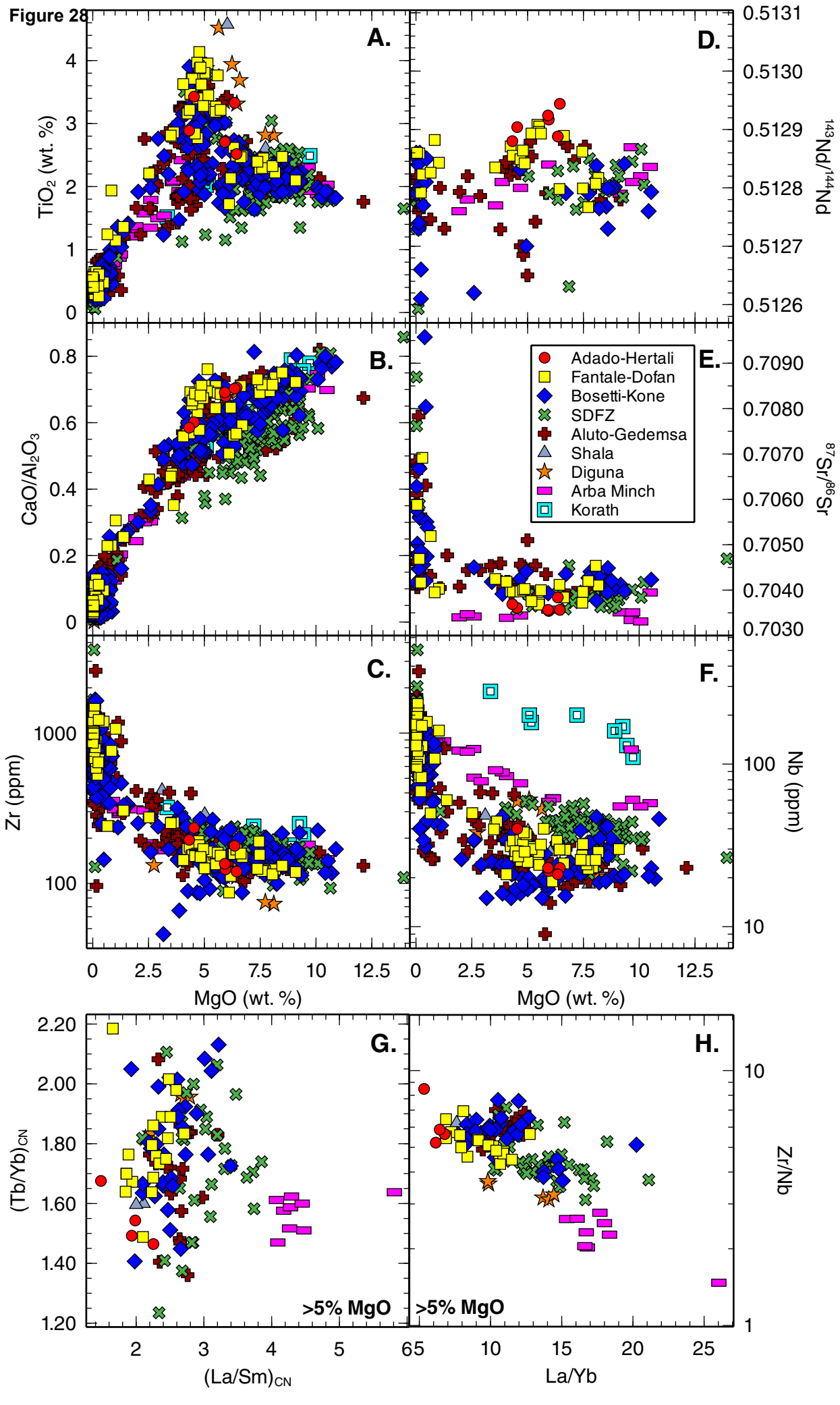
A.
B.
C.
D.
E.
F.
G.
H.
TiO2 (wt. %)
CaO/Al2O3
Zr (ppm)
143Nd/144Nd
87Sr/86Sr
Nb (ppm)
(Tb/Yb)CN
Zr/Nb
MgO (wt. %)
MgO (wt. %)
(La/Sm)CN
La/Yb
Adado-Hertali
Fantale-Dofan
Bosetti-Kone
SDFZ
Aluto-Gedemsa
Shala
Diguna
Arba Minch
Korath
>5% MgO
>5% MgO

Figure 29

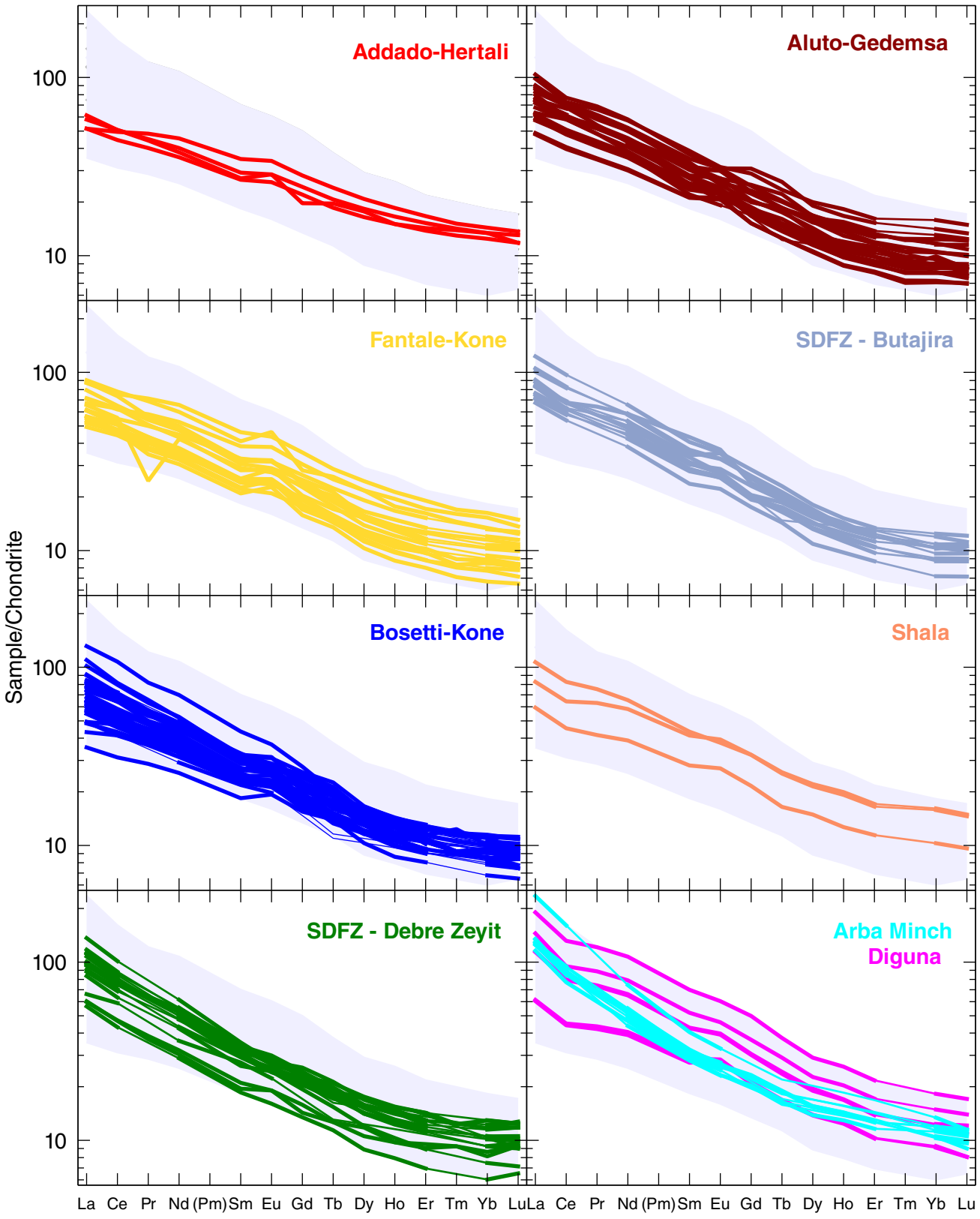
Addado-Hertali
Aluto-Gedemsa
Fantale-Kone
SDFZ - Butajira
Bosetti-Kone
Shala
SDFZ - Debre Zeyit
Arba Minch
Diguna
Sample/Chondrite
100
10
La Ce Pr Nd (Pm) Sm Eu Gd Tb Dy Ho Er Tm Yb Lu

Figure 30

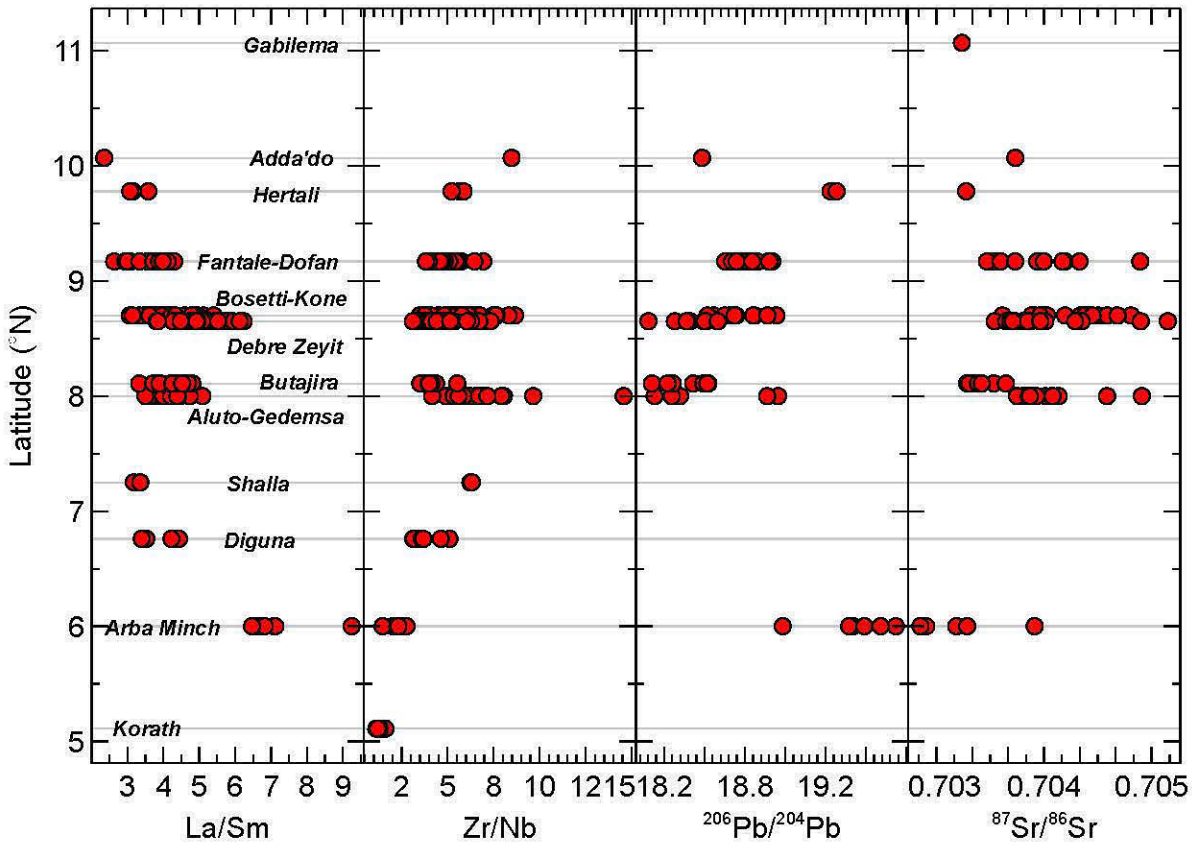
Gabilema
Adda'do
Hertali
Fantale-Dofan
Bosetti-Kone
Debre Zeyit
Butajira
Aluto-Gedemsa
Shalla
Diguna
Arba Minch
Korath
Latitude (°N)
11
10
9
8
7
6
5
3 4 5 6 7 8 9
La/Sm
2 5 8 10 12 15
Zr/Nb
18.2 18.8 19.2
206Pb/204Pb
0.703 0.704 0.705
87Sr/86Sr

Figure 31

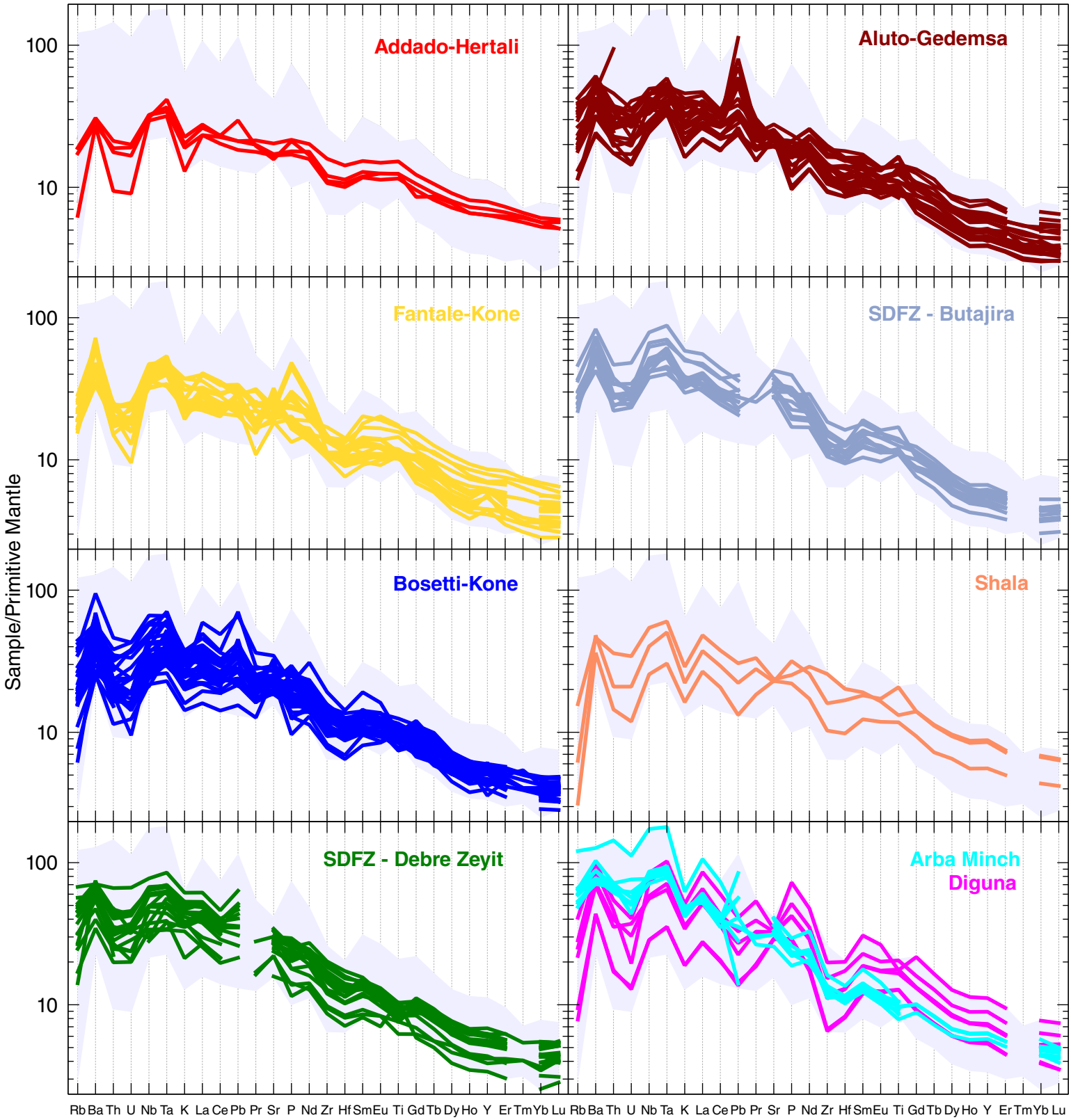
Addado-Hertali
Aluto-Gedemsa
Fantale-Kone
SDFZ - Butajira
Bosetti-Kone
Shala
SDFZ - Debre Zeyit
Arba Minch
Diguna
Sample/Primitive Mantle
100
10
Rb Ba Th U Nb Ta K La Ce Pb Pr Sr P Nd Zr Hf Sm Eu Ti Gd Tb Dy Ho Y Er Tm Yb Lu

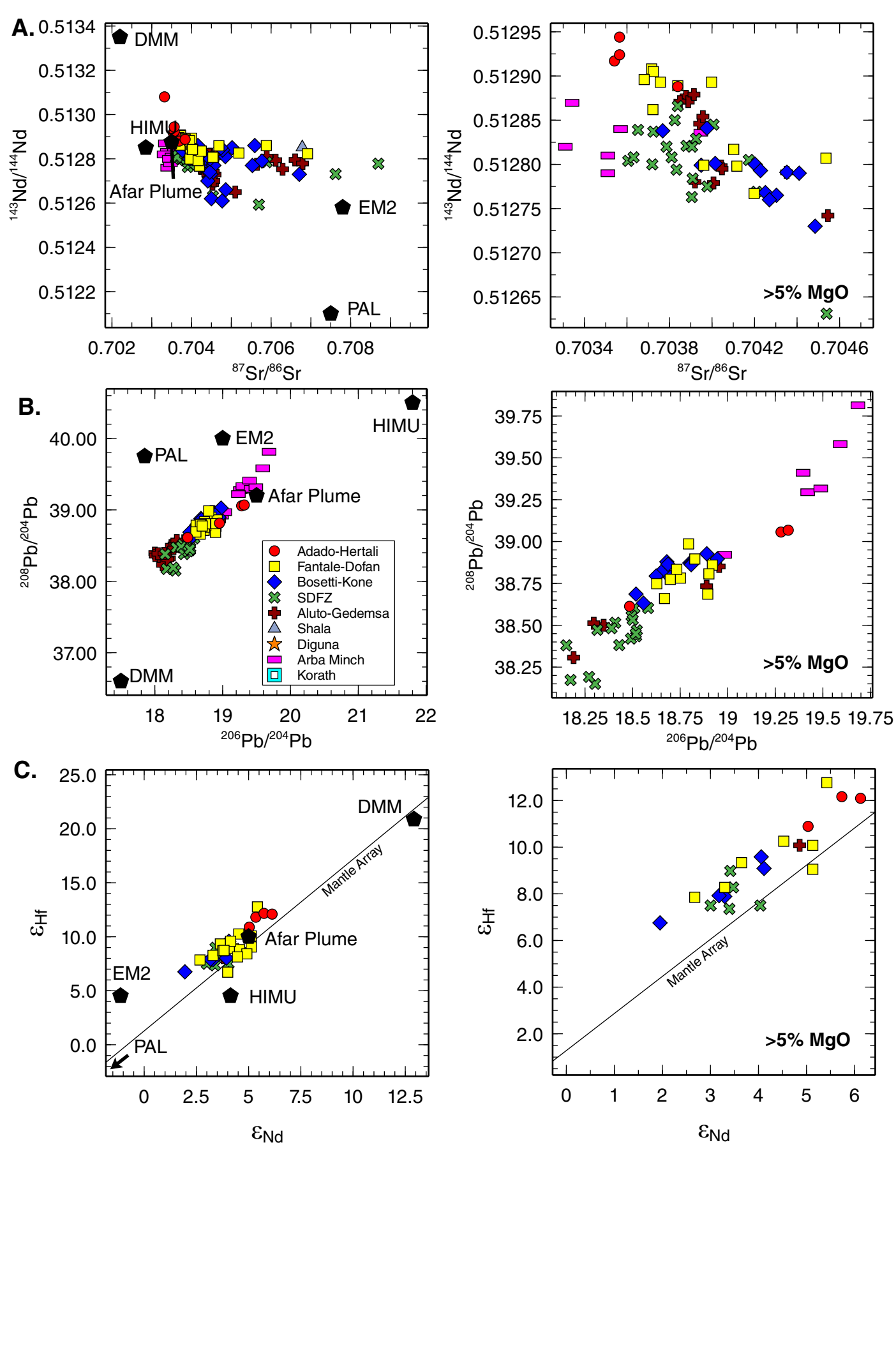
A.
DMM
HIMU
Afar Plume
EM2
PAL
0.5134
0.5132
0.5130
0.5128
0.5126
0.5124
0.5122
143Nd/144Nd
0.702
0.704
0.706
0.708
87Sr/86Sr
0.51295
0.51290
0.51285
0.51280
0.51275
0.51270
0.51265
>5% MgO
0.7034
0.7038
0.7042
0.7046
B.
HIMU
EM2
PAL
Afar Plume
DMM
40.00
39.00
38.00
37.00
208Pb/204Pb
18
19
20
21
22
206Pb/204Pb
Adado-Hertali
Fantale-Dofan
Bosetti-Kone
SDFZ
Aluto-Gedemsa
Shala
Diguna
Arba Minch
Korath
39.75
39.50
39.25
39.00
38.75
38.50
38.25
>5% MgO
18.25
18.5
18.75
19
19.25
19.5
19.75
C.
DMM
Mantle Array
Afar Plume
EM2
HIMU
PAL
25.0
20.0
15.0
10.0
5.0
0.0
εHf
0
2.5
5
7.5
10
12.5
εNd
12.0
10.0
8.0
6.0
4.0
2.0
Mantle Array
>5% MgO
0
1
2
3
4
5
6

Table 1

Magma Type	Characteristics	Origin
I – Incompatible element depleted family of magmas	Extreme depletions in most elements forming a relatively flat incompatible trace element normalized pattern. Subtype Ia exhibits positive anomalies in LILE (e.g. Ba).	Associated with Eocene and Oligocene Flood basalts and remains of uncertain origin.
II – OIB Family of magmas	Exhibits a typical OIB-like pattern in a primitive mantle normalized diagram. Type IIa extend to MgO-rich compositions and are less silica undersaturated. Type IIb have lower SiO_2 and elevated CaO and incompatible trace elements	Origin of Type IIa is controversial and may be associated with material within the Afar plume, lithospheric material metasomatized by the plume, or delaminated. Type IIb are likely derived from melting of lithospheric mantle metasomses.
III – The Moderate Family of Magmas	Typified by a distinctive Ba peak, a U-Th trough, and a Nb-Ta peak. The slope of the REE are controlled by the depth and degree of melting.	The most common magma type within the East African Rift and is interpreted to be a melt of a plume-influenced upper mantle.
IV – Intermediate Composition	Typified by a pattern that is a simple mix of Type II and Type III magma	Contamination of a Type III magma as it passes through the lithosphere and either assimilates a metasome or mixes with a Type II melt.
V – Potassic Metasomes	Typified by a relatively flat pattern in the most incompatible trace elements within the primitive mantle normalized figure, with small negative anomalies in U and K, and a mild depletion in Zr-Hf.	Melts derived from a phlogopite-bearing lithospheric mantle metasome. Well-developed within the Virunga Province in the Western Branch.
VI – Depleted Source	Typified by extreme depletion in the most incompatible trace elements that resemble MORB, but with unusual positive anomalies in LILE	Uncertain – may be a plume component but more work needed.

Table 1: Classification of magma types erupting in the East African Rift. This classification adds to that presented in Rooney (2017) and is presented in more detail in Part V of the synthesis series. These magma types are predominantly identified on the basis of commonalities in patterns in primitive mantle normalized incompatible trace element diagrams. Other magma groups may emerge as further work is undertaken in the region and this list should therefore be viewed as preliminary and subject to addition in the future.

the silicic interludes that are evident within the rifts, are generally absent. Moreover, from 4 Ma to present, there is a progressive decrease in magmatic activity from an initial fissural basalt, to a series of large shield volcanoes, to modern belts of cinder cones. The results of this synthesis suggest widespread pulsed basaltic events precede silicic flare-ups throughout the EARS, and the lack of such flare-ups in Turkana may relate to the Mesozoic rifting in that region which modified the continental lithosphere.

Keywords: Rift, magmatism, East Africa, Kenya, Ethiopia, East African Rift System

1. INTRODUCTION

East Africa is the archetypal example of continental rifting, featuring in most every introductory geology textbook. Our modern understanding of continental rifting springs from the pioneering work in East Africa during the 19th century, which produced a definition of a rift as “A linear valley with parallel almost vertical sides, which has fallen due to a series of vertical faults” (Gregory, 1896). This definition, which has influenced subsequent studies, has resulted in a focus on field-scale observations evident within in a single basin or valley. The interconnection of observations on rift-scale is less common but not solely a modern phenomenon. Early work by Eduard Suess (Sueß, 1891) used existing basin-scale observations to reveal that these rift valleys in East Africa were interconnected into a single system (Mohr, 2009). In this second part of the synthesis of the Cenozoic Magmatism of East Africa, I follow the methods of Prof. Dr. Suess and utilize the existing observations to provide insights on the East African Rift system as a whole. This contribution seeks to collate knowledge from the rich literary canon that defines the scientific studies on East African magmatism, and act as a guide to further reading and research. It is clear that much remains unknown about the magmatism of East Africa, requiring significant new analytical programs and field studies. Indeed as a different Dr. Suess once

noted “The more that you read, the more things you will know. The more that you learn, the more places you'll go.”

The East African Rift System (EARS) extends continuously from Mozambique to Afar. In the very north, the mature rifting in Afar transitions to sea floor spreading within the Gulf of Aden. To the south and west, the impingement of the rift upon the Tanzania craton results in the North Tanzania Divergence and Western Branch of the EARS. In this part of the synthesis I focus upon the Eastern Branch of the EARS extending from the southern boundary of the Afar Depression to central Kenya. This region is dominated by the Main Ethiopian Rift and Kenya Rift, but betwixt these narrow archetypal rift valleys, the existence of the broad Turkana basin has complicated attempts at applying simple rifting models to East Africa, in the absence of lithosphere-scale constraints. The narrative of this contribution explores the temporal evolution of magmatism within these three specific areas and reconciles the similarities and differences in the erupted lava composition on the basis of both the lava source and the influence of the lithosphere being rifted.

The process of continental rifting fundamentally perturbs the stability of the continental lithosphere, potentially resulting in mass exchange with the underlying asthenosphere and overlying atmosphere (Brune et al., 2017). Thus, rather than simply existing as an inert barrier or conduit for magmas to pass through, the continental lithosphere instead represents a rich reservoir capable of generating melts and influencing the composition of lavas that pass through it. The potential complexity imposed upon the magmatic system within the EARS by rifting a Proterozoic mobile belt *and* an Archean craton (e.g., Foley et al., 2012) necessitates a modular approach to discussions on the origin of lavas within the EARS (Fig. 1). Examining the geochemical variation of the EARS as a whole, it is self-evident that a significant division exists between lavas erupted in the shadow of the Tanzania craton and those within the mobile belt (Fig. 2). Accordingly, this contribution initially separates regions where lavas experience the

influence of the Tanzania craton (western branch of the EARS, North Tanzania Divergence, and southern Kenya rift) from the Pan-African Mobile belt (northern Kenya rift, Turkana, Main Ethiopian Rift, Afar, Yemen). This contribution explores magmatism within the less mature portions of the Eastern Branch of the EARS from central Kenya to central Ethiopia.

Historically, there has been an appreciation that decompression of the upper mantle due to lithospheric thinning can cause rift magmatism (e.g., McKenzie and Bickle, 1988). However, there is now a growing awareness that during lithospheric extension magmatism and deformation are linked. Thus, insights into the progressive development of a rift can be achieved through a systematic temporal study of rift magmatism. Despite the EARS being acknowledged as the ideal in terms of a modern rift, there remains substantial ambiguity as to the temporal evolution of magmatism during rift development. The expression of modern volcanism within both the Kenya Rift and Main Ethiopian Rifts exhibits considerable overlap, consisting of axial grabens, large central silicic volcanoes, and interlinking small volume basaltic cinder cones. These observations suggest commonalities in the currently active processes through both rifts. While such similarities may seem unremarkable given our current perspective of an interconnected East African Rift System, this interconnection is a relatively recent phenomenon having occurred during the Quaternary (Ebinger et al., 2000; Corti et al., 2019). These observations raise obvious questions: (A) Is the common manifestation of magmatism within the Kenya Rift and Main Ethiopian Rift the result of the modern interlink between the two rifts? Or (B) Have the individual magmatic histories within these two rifts developed in parallel with the modern linkage simply connecting rifts at a similar stage of evolution? And (C) How does the Turkana Depression, located between these two rifts, provide insight on the development of the EARS in this region?

To address these questions, this contribution presents a detailed comparative chrono-magmatic study of eruptives within all three regions – The Main Ethiopian Rift, Northern Kenya

Rift, and Turkana Depression. Achieving an effective comparison requires the collation of a large number of mapped and analyzed units into distinctly related temporal bins. The proliferation of unit names, in particular within the Kenya Rift, has been a significant barrier to progress in this regard. To that end, much attention is devoted to naming and arranging the various units on the basis of the geochronologic constraints, geochemical characteristics, and stratigraphic position. While this approach may seem formulaic and lacking in narrative within large sections of this contribution, the collation of the names of these units into one place, in addition to indicating where such units can be found and their age, is a significant advance in developing a more synergistic understanding of magmatic processes within the EARS.

2. Episodes of Lithospheric Modification

When considered at a plate-scale level, lavas within the Eastern Branch of the EARS, extending from central Kenya to central Ethiopia, should exhibit similar characteristics. For example, within this region, the EARS cuts across similarly aged Pan-African mobile belt lithosphere (Fig. 1). Furthermore, there is a growing recognition that much of the mantle beneath East Africa is thermally (Rooney et al., 2012c), and chemically (Hilton et al., 2011) influenced by a common deep mantle upwelling emanating from below the asthenosphere. But despite these commonalities, fundamental differences are observed between lavas erupted in northern Kenya, Turkana, and Ethiopia that require further explanation.

Over the last 20 Ma, magmatic activity in the Turkana Depression and Main Ethiopian Rift differed from that in the Kenya Rift. Rocks from the Kenya Rift are typically more alkaline (e.g., flood phonolites) in comparison to rocks in Turkana and Ethiopia. The origin of this heterogeneity may be linked with the longer period of magmatic activity in Turkana and Ethiopia,

which manifests as flood basalt events extending into the Eocene. These earlier flood basalt events in Turkana and Ethiopia may have destabilized the lithosphere (e.g., Furman et al., 2016), melted ancient metasomes (Rooney et al., 2014b), or created new metasomes (Beccaluva et al., 2009). The Tanzania craton, which is known to influence rift magmatism in the southern EARS also likely contributes to the heterogeneity between the two regions (Foley et al., 2012). Such processing of the lithosphere prior to rift development and craton influence may help explain the differing magmatic response to lithospheric extension between the Kenya Rift and the EARS further north.

While Turkana and the Main Ethiopian Rift exhibit similarities in comparison to the Kenya Rift, differences are also evident. Both of these regions experienced large-volume flood basalt events prior to rift development, yet lavas in Turkana exhibit notable isotopic differences in comparison to the Main Ethiopian Rift (Fig. 2). The origin of this difference may be linked to an episode of prior rifting and modification of the lithosphere (and in particular the lithospheric mantle) during the Mesozoic Karoo event (Fig. 1). The Anza Graben, which passes through Turkana, has fundamentally changed the lithospheric structure in Turkana, reducing crustal thickness to ca. 25 km (KRISP), in comparison to the 35 – 40 km crust within the Main Ethiopian Rift (Maguire et al., 2006). These observations highlight the controlling influence of the lithosphere, and its history, in regulating the composition of rift lavas. In many instances it can be difficult to resolve which contributions to rift lavas derive from lithospheric and sub-lithospheric sources, however examining the temporal evolution of magmatism within a region (and between regions) can help reveal magma generation and evolution processes.

This synthesis series focuses upon East African Cenozoic magmatism. Following the Eocene and Oligocene Flood Basalt episodes, magmatism and rifting became interlinked. From the Miocene onwards, the influence of the continental lithosphere became a central process in magma generation and evolution. Insights into the relationship between magmatism and rift

development are most clearly evident when magmatic episodes are interpreted within the framework of faulting and basin development. Existing synthesis studies that have focused on basin development provide an important template for probing the evolution and modification of the lithosphere during this period. Purcell (2018) and Macgregor (2015) present a series of detailed maps that chart the development of rift basins over time. These papers have roughly constrained the sequence of basin evolution as follows: A) Increasing tectono-magmatic activity ca. 22 – 17 Ma, correlating with the initial development of the EARS. Purcell suggests that Turkana is a 'seed point' from which the rift develops both to the north and south during this period of time. B) Migration of activity within the various rifts in Turkana, and polarity reversals of faults termed 'major changes in tectonic and volcanic activity' by Purcell occurred during the period from 13 – 10 Ma. This period correlates with the second major rift phase of Macgregor (2015), during which he describes Turkana as a nexus of rifting during the Mid-Miocene. This period of basin development also shows significant rift activity within the Afar Depression. C) The development of the Main Ethiopian Rift at ca. 10 – 6 Ma (Purcell, 2018). It should be noted that MacGregor (2015) instead agrees with the ca. 5 Ma date presented by Bonini (2005) and there thus remains debate as to the specifics of rift development in Ethiopia. D) The modern phase of activity was preceded by deepening of rifts in Turkana at ca. 5 – 3 Ma (Purcell, 2018), and propagation of rifting away from Turkana both to the north and south (Macgregor, 2015). These structural observations are consistent with the concept of the controlling influence of pre-existing lithospheric structure on the rifting process; the previously thinned Anza Graben, from which the Turkana Depression developed, provides a natural focus for extension. This synthesis series thus acknowledges the fundamental differences in tectono-magmatic activity near the thick Archean craton and the thinner Proterozoic mobile belts and addresses magmatism in these regions separately.

3. The Samburu and Getra-Kele Basaltic Events (20 to 16 Ma)

The first volume of this series of synthesis papers explored the large-scale flood basalts and widely distributed flows that occurred episodically from ca. 45 Ma to 22 Ma, and dominated the East African Cenozoic landscape (Rooney, 2017). The narrative within that initial exploration of East African Cenozoic volcanism terminated with an event characterized by widely distributed lavas dated ca. 26.9 to 22 Ma – The Early Miocene Resurgence Phase. This, the second volume in the synthesis, continues where the first volume left off – the terminal stages of the Early Miocene Resurgence Phase at ca. 20 Ma.

In this contribution I revise and update the divisions used in volume I . The Early Miocene Resurgence Phase (originally 26.9 Ma to 22 Ma) is typified by a pulse of alkaline basaltic activity that follows a long hiatus after eruption of the regional flood basalts and associated terminal pyroclastics (e.g., Abbate et al., 2014). The initiation of this event is therefore clear, however the termination of the event is far less certain, and appears to vary depending on location. In particular, the event appears to continue in Southern Ethiopia and Turkana, where the Early Miocene Resurgence Phase begins at ca. 24 Ma, but persists to ca. 17 Ma. This Early Miocene Resurgence Phase is thus more temporally extensive than I had first contemplated. This observation becomes important when considering the initial magmatic events south of Lake Turkana.

The ca. 20 Ma Samburu lavas represent the first magmatic events within the nascent Kenya Rift. This phase of volcanic activity was widespread, and is dominated by fissure-fed mafic lavas that form low shields with a maximum thickness of ~1070m (Hackman, 1988). The composition of these mafic lavas are typically alkaline to highly alkaline (Hackman, 1988; Kabeto et al., 2001). The Samburu Event is herein described within the context of the Early Miocene Resurgence Phase, however, the Samburu Event initiates later. This suggests a

progressive migration of magmatic activity southward away from Turkana – a theme that will persist in discussions of rift magmatism within this volume.

3.1 Kenya Rift

Within many summaries of magmatism within the Kenya (formerly Gregory) Rift, magmatic units are typically described from the two shoulders and then the median graben. Given this contribution is a regional overview, this level of detail is not preserved herein. The interested reader is directed to the citations within this contribution for such differentiation. Along the Northern Kenya Rift (Fig. 3), The Early Miocene Resurgence Phase is equivalent to the lower Nachola formation that extends from 19.2 Ma to 17.4 Ma, along the eastern rift margin (Sawada et al., 1998). This age range derives from the average of two K/Ar dates of 19.6 Ma and 18.8 Ma each with an error of 0.6 Ma; the reader is referred to Itaya and Sawada (1987) and Tatsumi & Kimura (1991) for original data. This phase may also comprise the Kapcherat Formation along the western rift margin (Smith, 1994), but little is known about this formation and I do not include it on the map for this period.

Within the North Central Kenya Rift, an early rifting phase created two half-graben basins (Kerio and Baringo) into which post-faulting volcanism flowed (Hautot et al., 2000). The initial stages of volcanism within the Baringo basin are represented by the Samburu Basalts (~1000m thickness). The age range of the Samburu Basalts is poorly constrained with an upper limit of 20.7 Ma ± 0.6 and a lower limit of 14.2 Ma ± 0.4 (see Hackman, 1988). Many papers use 11 Ma as a lower limit for the Samburu Basalts, however, the earliest date of 11.8 Ma was regarded as ‘doubtful’ by Hackman (1988). Walsh (1969) mapped Samburu Basalts also within the Kerio basin, however subsequent work did not confirm this observation (Chapman et al., 1978). I use the term Samburu Series to denote this phase of activity given the potential

diversity in magmatic products. There is some ambiguity with respect to the assignment of lavas to the Samburu Series or the subsequent Flood Phonolite Series given the overlap in dates and the large errors associated with K-Ar dates from the 1970s. Thus, some future re-organization is possible with enhanced dating precision (Note that all dates presented in this contribution are K-Ar unless specifically labelled $^{40}Ar/^{39}Ar$). The eruption of the Samburu Series in Kenya was coincident with a phase of faulting whereby tilting, fault-block downthrows and warping suggest some degree of tectonic instability within the lithosphere even at this early stage (Hackman et al., 1990).

3.2 Turkana and Southern Ethiopia

This time period is coincident with a widespread basaltic event (Fig. 3) broadly equivalent to the Samburu Basalts of the Kenya rift. At Lothidok, the upper Kalakol Basalts, which had commenced after the deposition of the Eragaleit Beds (coarse grained sandstone), have an eruption range from 24.2 Ma (± 0.3) to 17.9 Ma (± 0.3) (Boschetto et al., 1992). Subsequent magmatic activity is in the form of tuffs dated at 17.5 Ma (± 0.2), 16.8 Ma (± 0.2), and 16.6 Ma (± 0.2). A composite section within the Asille Group (Irile fossil site and Nabwal Hills fossil site) indicates that the Bakate Formation (alkali basalts, sediments, and rhyolites) has a lower Irile Member, whose lower age is constrained by the underlying Langaria Formation (rhyolites)(26.9 Ma ± 0.2) (McDougall and Watkins, 2006). The upper temporal limit for this member is ca. 17 Ma (± 2 mean reported by McDougall and Watkins, 2006). The Irile member is overlain by the Buluk and Il Jimma Members that contain thin basaltic flows (17.15 Ma ± 0.2) and tuffs (16.6 - 16.1 Ma) (McDougall and Watkins, 1985, 1988). Less stratigraphically constrained occurrences of basalts at Nkalabong (20.6 Ma ± 2) (Brown and Nash, 1976), Nakoret 17.5 Ma± 0.9 to 21.3

Ma (± 1.1), and Muruanasigar (19.2 Ma ± 1.0) (Morley et al., 1992) further support a widespread basaltic event in Turkana during this phase of magmatic activity.

In southern Ethiopia this basaltic phase is represented by the 400m thick Teltele and Surma Basalts (Fig. 3), which have been described as a 'flood basalts' (Davidson, 1983; Ebinger et al., 2000), though I prefer to use the term stratiform in order to distinguish from the Eocene-Oligocene traps phase. These basalts have an array of dates that extend from 23.0 Ma (± 1.2 $^{40}Ar/^{39}Ar$) to 18.7 Ma (± 0.8) (Davidson and Rex, 1980; Ebinger et al., 1993, 2000). Overlying these basalts are tuffs associated with the Jibisa Ring Complex – part of the later Flood Phonolite episode. In addition to the Teltele and Surma basalts, the Getra-Kele basalts form a volumetrically important basaltic eruption in Southern Ethiopia that has a bimodal clustering of ages (17.0 to 19.1 Ma, and 11.12 to 12.9 Ma) (Woldegabriel et al., 1991; Ebinger et al., 1993, 2000; George et al., 1998). These age clusters are separated by the Mimo Trachyte (Ebinger et al., 1993), and I therefore suggest that the Getra-Kele Formation is a composite of the ca. 20 Ma basaltic event discussed here, and the subsequent Mid-Miocene Resurgence Phase (see later). It should be noted that the spatial distribution of Getra-Kele basalts is not currently well-constrained.

An additional basaltic sequence, which is not currently shown on the geological maps of the region, has been identified by paleontologists working on Kajong fossil site on the eastern shore of Lake Turkana. This formation was described by Williamson & Savage (1986), though first mentioned by Savage & Williamson (1978) as the Loiyangalani Formation, and is comprised of 'at least 200m of fine grained olivine basalts and subsidiary pyroclastics'. The lower bounds of the Loiyangalani Formation is best constrained by $^{40}Ar/^{39}Ar$ dates of Brown et al. (2016) as an average of two samples from the base of the sequence at 19.11 Ma (± 0.17 $^{40}Ar/^{39}Ar$). It should be noted that the upper contact of the Loiyangalani Formation is not described in the current literature; thus, its relationship with the Jarigole Volcanics is unknown.

Given the lack of existing constraints, I have opted to place the Jarigole Volcanics into the 16 to 8 Ma time bin given their dominantly phonolitic composition (Wilkinson, 1988).

3.3 Geochemical Composition of the Samburu Series

The Samburu Series magmas (comprised of the Nachola, Chembalao, Samburu, and Kapcherat basalts) are not immediately distinctive from other magmas erupted in Northern Kenya (Fig. 4). Other units of the Samburu Series that remain unanalyzed include: The Tangulbei Formation of the Aruru Shield, the Morilo Formation of the Morilo Shield, The Ngusero Formation, and the Bogoria Formation (see Hackman, 1988). Geochemical data from rocks erupted during the Samburu Phase and the Early Miocene Resurgence Phase are examined together (with the exception of Gerba Guracha – see Rooney et al., 2014b, 2017; Rooney, 2017 as rocks from this volcano exhibit quite distinct compositions that are not seen in this portion of the rift). There is a wide array of compositions evident within rocks from this phase. Zr and Nb show a general trend of increasing concentration with decreasing MgO, but the scatter of these values is more consistent with a different composition in terms of the primary magmas. Magmas from Getra (of the Getra Kele formation) generally overlap the Samburu Basalts and have similarly elevated values of Nb in comparison to the Early Miocene Resurgence Phase (Fig. 4). This observation is consistent with evidence of a greater incompatible trace element enrichment in these two suites in comparison to others during this phase in terms of low Zr/Nb and high La/Yb (Fig. 4).

These differences are apparent in terms of the chondrite-normalized plot (Fig. 5), which exhibits a strong enrichment in LREE for Getra and Samburu in comparison to the Early Miocene Resurgence Phase data (Teltele, Lodwar, Jarigole, Ogden, and Choke/Guguftu). While this incompatible trace element enrichment is also evident in terms of a primitive-mantle

normalized figure (Fig. 6), the patterns do vary significantly. For the Early Miocene Resurgence Phase, there are an array of Type II and Type III lava styles (Fig. 6). However, lavas from Getra and Samburu exhibit pronounced negative K anomalies, variably developed negative Zr-Hf anomalies, and a hybrid Type II pattern with strong enrichment in the more incompatible trace elements (Fig. 6). The reader is directed initially to the first volume of this review series (Rooney 2017) for a discussion on the various lava types that have been defined. A fuller description of all lava types is presented in the final volume of the synthesis. A summary of the magma types (I – VI) is presented in Table 1.

No obvious correlation exists between decreasing MgO and isotopic ratios, though the variability of the lavas may mask potential contamination (Fig. 4). The very limited isotopic data that is available shows the Getra and Samburu lavas plotting at the most radiogenic end of the array defined by the Early Miocene Resurgence Phase samples in terms of $^{206}Pb/^{204}Pb$-$^{208}Pb/^{204}Pb$. While the Type II patterns and radiogenic Pb isotopes evident in Samburu and Getra Kele might suggest some type of contribution from a lithospheric metasome to their formation, radiogenic Pb isotopes at Jarigole (the Early Miocene Resurgence Phase samples that also exhibit radiogenic Pb) are interpreted as derived from the convecting mantle (Furman et al., 2006). Further work on lavas from this phase is required to resolve the potential contribution from various mantle reservoirs to the genesis of these basalts. What is clear is that the Getra Basalts, which are located at the northern boundary between the Turkana Depression/southern Ethiopia, and the Samburu Basalts, which are located in a similar position to the south, show similar geochemical characteristics. We tentatively suggest that the compositional and isotopic data for these suites requires the involvement of a lithospheric metasome in their genesis, consistent with early rift perturbation of the regional lithospheric mantle destabilizing easily fusible metasomes in these localities.

3.4 Summary

The Samburu Event is fundamentally a basaltic one, where large volumes of lava erupted onto the pre-rift surface. The extant data suggests that this is a phase of shield building, with some evidence of lava flows dipping radially away from a central point (e.g., Hackman, 1988). This basaltic event appears coincident with the development of faulting that may indicate the initial stages of lithospheric instability that would eventually develop at a rift (Hackman et al., 1990; Hautot et al., 2000). This interpretation is consistent with the synthesis studies of MacGregor (2015) and Purcell (2018) who both highlight this phase of activity as an important period of extension. The compositional data suggests a significant sub-lithospheric source to these lavas (Type III), though some contribution from lithospheric reservoirs is evident. As introduced above, the Samburu Event cannot be meaningfully separated from the preceding “Early Miocene Resurgence Phase”, which is a widespread event throughout East Africa (Rooney, 2017). Indeed, the shield building event represented by the ca. 20 Ma Samburu Series is remarkably similar to the ca. 23 Ma shield building event (Early Miocene Resurgence Phase) that dominates the NW Ethiopian Plateau (Choke and Guguftu shields: Kieffer et al., 2004). The extant data would suggest that in Southern Ethiopia, Turkana, and the Northern Kenya Rift, the Early Miocene Resurgence Phase identified in Part I of this synthesis series may have continued into the Samburu Event. These observations further support a model whereby the Early Miocene Resurgence Phase and Samburu Event are coincident with a spatially widespread period of extension within the African lithosphere. Further high-precision geochronology is required to assess any potential hiatus in magmatism between the two events. The terminal stages of the Samburu Event are less difficult to establish, as what follows is a phase of significant silicic volcanism.

4. The Flood Phonolites and Silicic Eruptive Phase (16 – 12 Ma)

Following a phase dominated by largely mafic magmatism at restricted localities in the region, the subsequent Flood Phonolite phase marked a significant departure in terms of both the aerial extent of magmatic activity and the volume of highly alkaline lavas (Fig. 7). This phase is dominated by the eruption of the Plateau Phonolites (Lippard, 1973), which are viewed as a flood lava event (e.g., Smith, 1994). During this phase, these phonolites extend throughout all portions of the soon-to-be Kenya Rift, however the most intense phase occurred from ca. 13 to 11 Ma (Smith, 1994). The termination of this phase coincides with a hiatus in volcanism, and an eventual shift towards trachyte magma types. As implied by the name, the flood phonolites spilled out onto the pre-existing landscape, banking onto shield volcanoes of the previous Samburu Series (e.g., Golden, 1978).

4.1 Northern Kenya Rift

Within the Northern Kenya rift, magmatic activity subsequent to 16 Ma is transitional between magmatic events within the central Kenya Rift and those in Turkana. Within the Samburu Hills this phase spans the upper Nachola Formation and Aka Aiteputh Formation. This phase is distinct given that basalt is volumetrically more significant in this region (Sawada et al., 1998). The upper Nachola Formation (~16.6 -15 Ma) is comprised of ~100m of trachyphonolite (Kabeto et al., 2001).

Throughout Kenya, this phase is typically represented by the eponymous flood phonolites, however the base of the sequence in the Kerio basin is represented by the Elgeyo Formation (15.1 Ma ±3.2 to 15.6 Ma ± 3.2 Ma) (Baker et al., 1971) – a series of massive mafic lavas and agglomerates (Chapman et al., 1978). Walsh (1969) initially noted that the Elgeyo formation (basalts) unconformably overlay the Samburu Basalts (Basaltic Shield Phase), which were tilted and eroded. The relationship between the two units remains unclear as subsequent work by

Chapman et al. (1978) showed an absence of Samburu Basalts in the Kerio basin. Despite the Elgeyo basalts being the lowermost mafic unit in the region, in this synthesis the Elgeyo Basalts have been assigned to the Food Phonolite phase rather than the preceding Samburu Series phase. The rationale for this decision is that the Elgeyo formation is in conformable contact with the overlying Chof Phonolite formation (Chapman et al., 1978). This rationale is consistent with equivalent rocks from the Tugen Hills, where the Saimo Basanites are clearly underlain by a thick phonolite sequence (Martyn, 1969). Hautot et al., (2000) correlated the Elgeyo Formation and the 339m thick Chof Phonolite, dated at 15 Ma (± 0.5)(Chapman et al., 1978), with the 1200m thick Sidekh Phonolite Formation (16 Ma ± 0.6 to 14.4 Ma ±0.5) (Chapman et al., 1978). Hautot et al., (2000) postulated a second phase of phonolitic volcanism and correlated the 480m thick Uasin Gishu Phonolite erupted between 13.6 Ma (± 0.6) and 12 Ma (± 0.3) (Baker et al., 1971), with the 1050m thick Tiim Phonolite (14.3 Ma ± 0.5 to 12.5 ± 0.3 Ma) (Chapman et al., 1978; Sawada et al., 2002), and the 750 m thick Rumuruti Phonolites (11.6 Ma ± 0.3 to 10.3 Ma ± 0.3) (Chapman et al., 1978). On the basis of a strict temporal division, some of these later phonolite units might be assigned to the Mid-Miocene Resurgence Phase (commencing ca. 12 Ma), but this phase is poorly expressed in the north-central Kenya Rift and thus it would seem that this Flood Phonolite phase continued in this region later than others further to the north.

The nomenclature for this phase is quite diverse, in particular near the rift shoulders where additional units have been identified that are not traditionally viewed as Flood Phonolites, but are temporally contiguous with this phase. The most recent geological maps for the region have introduced (in stratigraphic order) names such as Murgomul Volcanics, Lopet Phonolites (15.0 – 15.2 Ma) (Hackman, 1988), Katomuk Tuffs, Komol Volcanics (13.6 to 14.2 Ma) (Hackman, 1988), and that these units are themselves different from the more detailed maps produced a decade prior (Truckle, 1977). It is advisable that any interested reader consult these publications for a fuller list of units attributed to the Flood Phonolite phase.

4.2 Turkana and Southern Ethiopia

Within the Turkana depression, a hiatus in basaltic lava flows manifests as an accumulation of sediments (including volcanoclastics) until about ca. 16 Ma (Brown and McDougall, 2011). This phase of sedimentation is then interrupted by a small-scale renewed phase of basaltic volcanism that is observed at some well-studied localities. There then follows a phase of rhyolite volcanism (explosive and extrusive) to the north, and Plateau Phonolites along what is thought to be the rift axis at this time (McDougall and Watkins, 1988; Hackman et al., 1990). A widespread renewed phase of basaltic magmatism at ca. 13-12 Ma terminates this time period (Mid-Miocene Resurgence Phase – see below)

It is notable that the existence of Plateau Phonolites within the Turkana basin and Southern Ethiopia is rather limited. The most northerly exposure of Plateau Phonolites in Turkana are the Jarigole Volcanics (Fig. 7). To the southwest, the Emuruabwin Tephrites are thought correlative on the western side of Lake Turkana (Ochieng et al., 1988). The Plateau Phonolites thus form a somewhat narrow belt of activity as the magmatism to the east and west of these units is basaltic. The Jarigole Volcanics, which comprise a significant magmatic sequence of dominantly phonolites and tephrites (1350 km^2) on the eastern shore of Lake Turkana, have created some confusion as to the magmatic sequence in Turkana. Existing K-Ar dating has suggested that the volcanics erupted between 23.2 and 16.9 Ma (Wilkinson, 1988). However, the volcanics (as currently mapped) are a composite of the Jarigole Phonolites and the Loiyangalani Formation. We have no clear basis for dividing the mapped unit excepting small-scale maps produced for individual localities (e.g., Brown et al., 2016). However, I have placed the Loiyangalani Formation in the prior Samburu Series phase. Furman et al., (2006) designated a suite of trachytic to picritic samples from this area as ‘Jarigole’, and assigned the age of the Jarigole Volcanics to these rocks (17-23 Ma). In this region, basaltic compositions from this time period should be assigned to the ca. 20 Ma Loiyangalani Formation (see above).

Given the association with the Plateau Phonolites in Kenya, it is probable the Jarigole Volcanics are closer to 16.9 Ma date, but more investigation is needed.

In addition to the Plateau Phonolites, small phonolite centers are described by Hackman et al. (1990). The Moti, Kubi Algi, and Shin volcanic centers (13.3 Ma ± 0.1 to 12.8 Ma ± 0.1) are aligned, and may represent the orientation of rifting during this time (McDougall and Watkins, 1988; Hackman et al., 1990). On the western side of Lake Turkana (Lothidok), the first magmatic event during this phase is a phonolite dated at 13.8 Ma (± 0.4), which is followed by a tuff at 13.2 Ma (± 0.2) (Boschetto et al., 1992). The sequence at Lothagam is broadly parallel with phonolites from 14.2 Ma (± 0.2) to 12.2 Ma (± 0.1). In Southern Ethiopia, the Weyto and Mimo trachytes/phonolites (16.7 Ma ± 0.6 to 12.4 Ma ± 0.4 $^{40}Ar/^{39}Ar$) are localized volcanic centers and associated flows that occur along faults (Ebinger et al., 1993, 2000), further supporting the association between extension and the occurrence of these magma types.

In the northeast, near the Ethiopian border, magmatism in the Asille Group and the Sabarei Volcanics have a parallel pattern that consists of a lower basalt at ca. 16.2 Ma (± 1 Ma) (Key and Watkins, 1988) that is followed by a phase of explosive volcanism preserved as tuffs within the Gum Dura Formation of the Asille Group (15.8 Ma ±0.1 $^{40}Ar/^{39}Ar$) (McDougall and Watkins, 2006) and rhyolites (and other evolved products including phonolites) in the Sabarei area. In Southern Ethiopia, rhyolites and tuffs are also found during this phase (14.0 Ma ± 1.0 to 14.9 Ma ± 0.6 $^{40}Ar/^{39}Ar$) (Ebinger et al., 1993). It is thought that these volcanic sequences are all derived from the Jibisa Ring Complex, a volcanic edifice occurring at the intersection of lineaments associated with the Chew Bahir Rift and the Pliocene rifting in Turkana (Hackman et al., 1990; Ebinger et al., 2000). There then followed a pause in explosive magmatism where fluvial sediments accumulated in the Asille area (Il Yia member) with some basalts interbedded (Nakwele member) (Key and Watkins, 1988).

4.3 MER and Northern Ethiopia

Further north in Ethiopia, the Shebele Trachytes erupted from 17 to 12 Ma (WoldeGabriel et al., 1990), and are broadly similar to the Weyto and Mimo trachytes/phonolites from Turkana and Southern Ethiopia. The Shebele Trachytes are typically only found at the base of deep river incisions, and have been noted from: (1) The Webe Shebele River, where a 16.5 Ma (± 0.2) - 16.1 Ma (± 0.7) trachyte is underlain by pyroclastic layers and a mugearite (16.9 Ma ± 0.8) (Williams et al., 1979; WoldeGabriel et al., 1990); (2) the Omo River canyons (i.e. the units noted above); (3) the Kessem (also spelled Cassam, Kesem, and Kasam in other works) River Gorge, where a 15.6 Ma (±0.3) trachyte and 13.1 Ma (± 0.3) rhyolite occur (Justin-Visentin and Zanettin, 1974); and (4) The Damole/Cawa ignimbrite and flood trachyte from the Bale Mountains at ca. 19 to 15 Ma (Mohr and Zanettin, 1988). Observations from Woldegabriel et al., (1990) suggested a local origin for the flows and pyroclastics, and a probable source at Mt. Chike. This heavily dissected phonolite volcano is dated from samples taken towards its middle and upper slopes at 12.1-11.6 Ma (± 0.6 Ma). We have also added the Arba Guracha silicic volcanics to this unit whose age was initially constrained to ca. 10 – 14 Ma with one radiometric date at 10.3 (± 0.2) (Chernet et al., 1998). Note that the maps shown for these units are of the Arba Guracha silicics unit from the Geological Map of Ethiopia. Lavas of this phase are not evident on either plateau away from the then nascent rift. In western Ethiopia, ca. 10 Ma basaltic lavas erupted onto a heavily laterized flood basalt sequence (e.g., Abebe et al., 1998). It is thus apparent that during this phase, evolved lavas dominated but were restricted to discrete volcanic centers associated with developing rift faults.

Curiously, in the northern Ethiopian plateau a different magmatic event is observed. Reactivation of magmatic activity occurred on the Simien Shield volcano (dominantly constructed during the Oligocene), where a few flows of alkali basalt are evident at the summit and are dated to 18.65 Ma (± 0.19 $^{40}Ar/^{39}Ar$) (Kieffer et al., 2004). Beneath these alkali basalts

are an undated ~10m rhyolitic tuff and trachytes. A parallel sequence is evident at Axum, where a basalt and trachyte complex has been dated to between 18.97 Ma (± 0.2 $^{40}Ar/^{39}Ar$) and 15.6 Ma (± 0.6) (Hagos et al., 2010; Natali et al., 2013). Critically, however, this volcanic event was also linked with fractures, block tiling, and extension (Natali et al., 2013). Activity along a 'Adwa-Axum line' has previously been noted by Abbate and Sagri (1980) to extend to the Red Sea where the axis is offset, suggesting a pre-existing structural lineament.

4.4 Geochemical Characteristics of lavas erupted during the Flood Phonolite and Silicic Eruptive Phase

I have divided the data from this phase and the later 'Early Rift Development phase' on the basis of composition, as both exhibit bimodal activity with a Daly Gap. Data from each side of the Daly Gap is plotted together for these two phases. While it may seem that a sizeable amount of data exists from mafic volcanics during the Flood Phonolite phase (Fig. 4), little of this data is sufficiently complete enough to construct chondrite or primitive mantle normalized diagrams (Fig. 5, 6). An exception to this are the Simien-Axum volcanics, which are treated separately given the geographic separation between the NW Ethiopian Plateau, and where the majority of the flood phonolites erupted (south of Turkana). In a general sense there is significant overlap between the mafic lavas erupted during the two phases in question from all regions (Fig. 4). Both the Early Rift Development Phase lavas and Flood Phonolite Phase lavas show increasing $^{87}Sr/^{86}Sr$ with decreasing MgO, suggesting some potential crustal assimilation. However, the variance is limited and no such correlation is evident in terms of $^{143}Nd/^{144}Nd$ (Fig. 4). The data from all regions plots close to the composition of the Afar plume, though it is difficult to resolve the various endmembers given the paucity of Pb isotope data (Fig. 4). The REE slopes from the Early Rift Development and Flood Phonolite phases are similar, and both

are distinct from the somewhat flatter slopes evident in the Simien-Axum lavas (Fig. 5). More insight is gained into the origin of these lavas when considering the primitive mantle normalized figure, where clear heterogeneity in the origin of the mafic endmembers of the Flood Phonolite phase is evident (Fig. 6). Within these data it is clear that Early Rift Development phase and Flood Phonolite phase lavas exhibit pronounced negative Zr-Hf anomalies (Fig. 6), which is suggestive of the influence of apatite in the source of these lavas (a fuller discussion of this is presented in Part III of the synthesis). While most of these lavas exhibit a Type III lava signature, which is typically suggestive of an origin within the convecting upper mantle, some interaction with the lithospheric mantle is probable. Support of this concept comes from a single sample of the Flood Phonolite phase lavas that exhibits a strong Type II signature (Fig. 6) – suggestive of a more direct origin from metasomatized sub-continental lithospheric mantle. In contrast, lavas from the Axum-Simien field show no such influence and exhibit a typical Type III lava signature (Fig. 6). In summary, for mafic lavas from the Flood Phonolite and Early Rift Development phases it would seem that some metasomatic influence is evident on their trace element patterns. However, the lack of any obvious isotopic deviation towards more lithospheric values might reflect a more recent lithospheric enrichment of the lithospheric mantle (Baker et al., 1998; Beccaluva et al., 2009).

Oddly, there is very little trace element geochemical information on phonolitic compositions erupted during the Flood Phonolite phase. The lack of data requires a reliance on other contemporaneous magma suites that are better characterized. The majority of the Shebele Trachytes follow a differentiation path towards rhyolite, broadly parallel to other (later) silicic units in the region (Fig. 8; 9). The exception to this is the Weyto Phonolite (the Shebele Trachyte sample that plots within the phonolite field; Fig. 8), which unsurprisingly follows a differentiation pathway towards a terminal phonolite. This phonolite differentiation pathway is not immediately clear when considering the Weyto Phonolite in isolation, and is instead illuminated

by the data from the Axum-Adwa volcanic complex (Natali et al., 2013). Natali et al. (2013) successfully modelled the evolution of SiO_2-saturated trachytes and SiO_2-undersaturated syenites in this region from fractional crystallization of basalts. However, some unusual characteristics are evident whereby some samples have a significant enrichment in Na_2O and depletion in SiO_2 that has been explained in terms of fenitization of the syenites (Natali et al., 2013). While late stage magmatic processes have no doubt impacted the composition of these rocks, this process is unable to explain the parallel Ti depletion from 65% SiO_2 towards a minimum at 59% SiO_2 (Fig. 9), while other elements are rising (e.g., Nb). This process results in quite unusual differences in the trace element content of rocks containing similar values of SiO_2 (Fig. 10; 11). I contend that these observations are consistent with a magmatic evolution process whereby trachytic magmas evolve towards lower SiO_2. White et al. (2012) modelled the evolution of Suswa volcano (Kenya Rift) through open system fractional crystallization processes to reach trachyte in a similar manner to the models for Axum-Adwa. However a second step was added to the fractionation process where a fractionating assemblage dominated by anorthoclase was used to model the differentiation pathway from trachytes to phonolites at Suswa. The removal of a fractionating assemblage that was rich in SiO_2 due to dominance of anorthoclase, resulted in parallel depletion of SiO_2 and K_2O, an increase in the incompatible trace element content, and depletion of Ti in the residual liquids due to magnetite fractionation. Thus, a model whereby phonolites are generated in the Axum-Adwa volcanic complex via anorthoclase fractionation is possible, though further study is necessary. In a general sense it would appear that the primary heterogeneity in the evolution of evolved liquids in this region occurs within the trachyte field with some systems progressing towards rhyolite while others yield phonolite (Fig. 8). The Flood Phonolite phase lavas do not exhibit vectors that permit clear assessment of this model for their origin, but typically plot towards the Axum data (Fig. 8; 9). Despite a lack of trace element data, Sr-Nd isotopic data do exist for the Flood Phonolites Phase lavas (Fig. 8). These data are consistent with a mix from more primitive

values close to the Afar Plume (and the composition of the mafic endmembers of the Flood Phonolites: 3) towards lithospheric-type reservoirs.

4.5 Summary

The Flood Phonolites and Silicic Eruptive phase represents an important period during which silicic volcanism dominated the magmatic products in the region. As discussed above, a number of basaltic intervals are recorded within the Plateau Phonolites which could, with more detailed geochronology, be assigned to the Samburu Series or instead may represent the conjugate mafic material involved in generating the phonolite lavas. While this event had a modest expression within the Turkana Depression, the volumetrically significant activity within both the not-yet-developed Kenya Rift, and Main Ethiopian Rift provides insight into the origin of this magmatism. Importantly, the occurrence of these magmas along what would become the rift margin, and in conjunction with faulting (Ebinger et al., 2000), suggests a linkage between extensional processes, the development of the rift in Ethiopia and Kenya, and this silicic magmatic event.

5. Mid-Miocene Resurgence Phase (12 to 9 Ma)

This phase heralds the return of wide-scale basaltic volcanism throughout the region, extending from the border with Afar southwards as far as the Northern Kenya Rift (Fig. 12). This event is not well expressed in the north-central portions of the Kenya Rift, where sedimentary material was deposited during this phase (Dunkley et al., 1993). Magmatism during this event typically manifests as stratiform basaltic flows. Within Turkana and Northern Kenya, this event had been previously recognized by Bellieni et al. (1986) as the “first cycle” fissural volcanism, however, the extent to which this event was mapped was somewhat limited. Modern stratigraphic and

geochronologic constraints further clarify these observations and it is now apparent that this is a much more widespread pulse of basaltic volcanism, beginning ca. 12-13 Ma in Turkana, and aligned along a NNW – SSE orientation. The full extent of the Mid-Miocene Resurgence Phase is not yet fully constrained, however, the extant data indicate that this event is roughly parallel to the boundary of the Tanzania craton and both margins of the Afar Depression. When probing the northern boundary of this event, it has become apparent that magmatism during this phase is far more extensive than has been previously recognized. Here, for the first time, I expand this Mid-Miocene basaltic event to include similar activity that occurred within the Ethiopian sector of the EARS.

5.1 North Kenya Rift, Turkana, and Southern Ethiopia

Given the enlargement in the spatial distribution of the Mid-Miocene Resurgence Phase that I am proposing, it is important that the units which I am assigning to this newly expanded temporal bin are appropriately identified. To that end, it is necessary to examine existing units and their relationship with this large-scale basaltic event. The Mid-Miocene Resurgence Phase is comprised of a number of stratigraphically well-constrained formations (Fig. 12): (A) The Upper Nakwele Formation Basalts, the majority of which erupted after 13.0 Ma (± 0.1) Ma (McDougall and Watkins, 1988), and correlatives throughout the region such as the Tatesa Hill Basalts (12.1 Ma ± 1) (Key and Watkins, 1988); (B) The Loperi Basalts at 10.9 to 12.4 Ma, which cap an important fossil sequence to the West of Lake Turkana (Lothidok), and regional equivalents such as the highest basalt within the Nabwal Arangan beds at Lothagam (9.12 Ma ± 0.15) (McDougall and Feibel, 1999), (C) The Lakhapelinyang Basalt, which has been roughly dated at between 13.9 Ma (± 0.2) and 15 Ma (± 0.2) (Boschetto et al., 1992). (D) South of Marsabit shield volcano and north of Mt. Kenya are basalts from the Laisamis area, which are dated from 12.2 Ma (± 3) to 9.9 Ma (± 1) (Brotzu et al., 1984). These basalts were the first to be

termed '1st cycle Plateau Basalts' by Bellieni et al. (1986). Major element data show that these basalts are extremely primitive (~9 wt. % MgO) and are geochemically distinct from the more evolved '2nd cycle plateau basalts' that are correlative with the Gombe Group (see later). (E) The younger cluster of ages within the Getra Kele basalts (11.12 to 12.9 Ma) (Woldegabriel et al., 1991; Ebinger et al., 1993, 2000; George et al., 1998) appears to be correlated with the 1st Plateau Basalt series and is thus included here. (F) Basaltic flows and dikes at Chencha in Southern Ethiopia also correlate with activity during this phase (12.32 Ma ± 0.17 to 12.39 Ma ± 0.10 $^{40}Ar/^{39}Ar$) (Rooney, 2010). (G) The Aiteputh formation occurs in the Northern Kenya Rift during the flood phonolite phase, however subsequent magmatic activity within the Aiteputh formation (15-9.9 Ma) is dominantly basaltic, in stark contrast to other regions in the Kenya rift. Note that the Aiteputh Formation and later Kongia Formation (7.3 -5.3 Ma) are marked as a single unit on maps of the area (Kamolingaran Basalt: Dunkley et al., 1993). This basaltic episode could be correlative to the Lomujal Basalts along the western margin (which also overlie a phonolite) and dates from 16.1 Ma (± 0.5) to 13.7 Ma (± 0.3) (Truckle, 1977), however more precise dating is required to confirm this.

Within the north-central Kenya rift (where this phase is not well-expressed magmatically), this phase correlates with the Ngorora formation – an 800m thick fluvial-lacustrine formation (Dunkley et al., 1993; Hautot et al., 2000). Along the rift margin in this region the ca, 10.6 Ma Alengerr Tuffs are also evident (Hackman, 1988).

This major event marked the termination of magmatic activity in Turkana and Southern Ethiopia for at least 5 Ma until the eruption of the 2nd plateau basalt phase, which we term the Stratoid phase (see subsequent section of the same name). In the Northern Kenya Rift there is a distinct hiatus in volcanism from 9.9 to ~7.5 Ma that is coincident with downwarping, faulting and tilting in the developing rift (Sawada et al., 1998). Slightly further south (in the Baringo region) there then followed a hiatus in volcanism, which is correlated with a second phase of

deformation and sedimentation (Mugisha et al., 1997; Hautot et al., 2000). In these more southerly regions magmatism eventually continued as the ‘Early Rift Development phase’.

5.2 Main Ethiopian Rift and adjacent plateaus

There has been a broad recognition that the time period from ca. 12-10 Ma in Ethiopia was coincident with a large volume of erupted basaltic lavas, however existing nomenclature and difficulties in establishing the lateral extent of these units has resulted in a lack of clarity as to how extensive magmatism was during this phase. For example, the Tarmaber (Termaber) Formation, which is a prominent unit on the geological map of Ethiopia, is considered to extend from ca. 26 to 13 Ma (Berhe et al., 1987). Originally defined as a collection of shields, the long period that the formation occupies has resulted in some ambiguity as to the relationship between rock types. This issue was recognized by previous authors, resulting in a subdivision into a Tarmaber Guassa (early Miocene) and Tarmaber Megezez (mid to late Miocene) (Mohr and Zanettin, 1988). This division of the Tarmaber parallels that of the Getra Kele Formation from Southern Ethiopia, which also exhibits an Early and Mid-Miocene pulse. While the Tarmaber Guassa and Megezez division is apparent in the more recent geological maps of Ethiopia, the currently mapped divisions require revision. In this contribution I have attempted to examine the Tarmaber in order to resolve the Early and Mid-Miocene events. In reality, the scale of mapping is not yet of sufficient detail to fully separate the units. For example, around Lake Tana, a flow is dated by Prave et al. (2016) at 23.75 Ma (± 0.02 $^{40}Ar/^{39}Ar$), yet this unit is currently mapped as contiguous with Mt. Guna (10.76 Ma ± 0.05 $^{40}Ar/^{39}Ar$) (Kieffer et al., 2004). In this instance, I have assigned the map shape as Mid-Miocene Resurgence Phase though it also contains flows from the Early Miocene Resurgence Phase. Clearly more detailed mapping and a focused geochronological campaign is required to firmly separate lavas from these two

distinct events, thus the maps presented herein should only be viewed as tentative indicators as to where Early and Mid-Miocene eruptive events may be found.

In this work we abandon the 'Tarmaber' name given the extensive history it has within the literature (and potential confusion that would result from another redefinition of this term). Instead, we note that the Tarmaber Guassa of Mohr & Zanettin (1988) is roughly correlative with the Early Miocene Resurgent phase of Rooney (2017), and that the mid to late Miocene Tarmaber Megezez formation is herein assigned to the Mid-Miocene Resurgence Phase. It should be noted that the map of the Early Miocene Resurgence Phase presented in Rooney (2017) shows **all** Tarmaber outcrops and does not discriminate between Tarmaber Guassa and Tarmaber Megezez. As a result, some units presented in in the map by Rooney (2017) are a mixture of both of these events and the reader will notice overlap between units from that map and that presented here for the Mid-Miocene Resurgence Phase.

Defining units associated with the Mid-Miocene Resurgence Phase in north-central Ethiopia is facilitated by the widespread hiatus in magmatism (excepting localized silicic activity) that defined the period between the Early Miocene Resurgence Phase (ca. 22 Ma) and Mid-Miocene Resurgence Phase (ca. 10.5 Ma). It should be noted that this region-wide Mid-Miocene Resurgence Phase is a basaltic event limited to ca. 1-2 Ma in duration, following which, the expression (or existence) of magmatism became largely localized. We define the initial part of the Mid-Miocene Resurgent phase as being comprised of two parts:

(A) *Basaltic shield volcanoes that are typically located along rift-related faults.* This activity is defined in other publications as the Tarmaber or Tarmaber-Megezez formation. The Tarmaber, Megezez, Weti, Mt. Arba Gugu, and Abuna Josef volcanoes typify this magmatic activity, and occur along the rift border fault and reactivated Yerer Tullu Wellel Volcanic Tectonic Lineament (YTVL) (Zanettin, 1992; Wolde and Widenfalk, 1994; Abebe et al., 1998). Radiometric dates constrain this activity to ca. 10.4 Ma (± 0.2) to 10.5 Ma (± 0.2), though no attempt has been

made to fully constrain the commencement or termination ages of these volcanoes (George, 1997; Chernet et al., 1998). Jebel Saddle, a basaltic shield volcano in the vicinity of Asebe Teferi, may also fall into this category but the precise chronology has yet to be established (Kazmin et al., 1981).

(B) *A widespread fissural basaltic volcanic event.* A widespread ca. 200-400m thick (sometimes described up to 600 m: Berhe et al., 1987) basaltic fissural event overlies the laterized Oligocene flood basalts, Early Miocene Resurgence Phase shields, and the ca. 16 Ma evolved magmatism described above. Previous work in the region has highlighted the wide-scale nature of this event within Ethiopia (Mohr and Zanettin, 1988; Abebe et al., 2005; Bonini et al., 2005), though the broader context in terms of events in Turkana has not been clear until now. The precise date at which this magmatic event commences is uncertain in this region due to the lack of $^{40}Ar/^{39}Ar$ dating, and that current dates are clustered in a region where the base of the sequence is not exposed (WoldeGabriel et al., 1990). Extant K-Ar data suggest that the event commenced by at least ca. 10.5 Ma. The best constraints are currently derived from the section at the Kessem River Gorge where precise $^{40}Ar/^{39}Ar$ dating suggests the event commences at 10.56 Ma (Wolfenden et al., 2004). This event is represented by a number of different magma units – some of which have been correlated by previous authors:

(i) The Guraghe-Anchar basalts (defined by Abebe et al., 2005) are a widespread magmatic event erupting up to 300m of basalts. Extant radiometric dates extend from 10.6 Ma (+/ 0.5) to 8.39 Ma (± 0.64) and are consistent across studies (WoldeGabriel et al., 1990; Abebe et al., 2005). These basalts have also been referred to as the Guraghe Basalt on the margin of the northwestern Ethiopian Plateau (WoldeGabriel et al., 1990) and the Anchar basalts along the conjugate margin of the southeastern Ethiopian plateau (Kazmin et al., 1980). These basalts thicken towards the rift.

(ii) The Upper Trap Series. Kazmin et al. (1980) suggested that the Anchar Basalts were synonyms of the Upper Trap series proposed by (Juch, 1978). However, The Upper Trap Series, are viewed as a distinct correlative unit by Mohr & Zanettin (1988). The Upper Trap series are basalts with minor intercalated silicic horizons that occur along the southeastern margin of Afar. The unit is typically 400m thick, but is thickest towards the rift basin. The unit is constrained to between 10.7 and 9.2 Ma (Juch, 1978), consistent with modern stratigraphic constraints that date the unit to 10.31 Ma ± 0.51 (Suwa et al., 2015). It should be noted that overlying this unit along the SE Afar margin are rhyolites dated from 9.02 Ma (± 0.16) to 9.36 Ma ± 0.20 and the paleontologically-dated sedimentary-volcanoclastic Chorora Formation (see part IV of the synthesis series), further constraining the upper age limit of the sequence (Suwa et al., 2015).

(iii) The lower portion of the Kessem Formation. This unit is best observed within the Kessem River Gorge and at Meteh Bila (along the rift margin) and has been loosely defined by Wolfenden et al. (2004) as a volcanic package consisting of basalts and volcanoclastics which is tilted and thickens towards the rift. The Kessem Formation was temporally constrained to between 10.6 and 6.6 Ma, however the upper part of the sequence is volcanoclastic and defined primarily at the Meteh Bila locality. In contrast, the basaltic section, which is best exposed at the Kessem River Gorge, was constrained to between 10.56 Ma (± 0.02 $^{40}Ar/^{39}Ar$) and 10.144 Ma (± 0.012 $^{40}Ar/^{39}Ar$) (Wolfenden et al., 2004), consistent with the basaltic event elsewhere. These flows are inter-fingered with flows from the contemporaneous 10.4 Ma ± 0.2 Megezez shield volcano (Wolde and Widenfalk, 1994; Chernet et al., 1998; Wolfenden et al., 2004). We thus divide the Kessem Formation into a lower dominantly basaltic unit and upper dominantly volcanoclastic unit, which will be addressed later. The lower basaltic member of the Kessem formation is equivalent to the Fursa Basalts of Justin-Visenten et al. (1974).

(iv) The Lower aphyric basalts and Upper Basalts from western Ethiopia. These lavas, defined by Berhe et al. (1987) form a ~500 m thick pile dominantly in western Ethiopia in the vicinity of the YTVL. The flows are basaltic but may be intercalated with trachytes from adjacent volcanoes. This basaltic activity is described as fissural, after which central volcanoes developed along the YTVL (Abebe et al., 1998; Tommasini et al., 2005). The duration of this event is not precisely constrained – existing geochronology suggests a duration from 11.2 Ma (± 2.2) to 9.1 Ma (± 1.4) (Berhe et al., 1987), though the fissural phase in this region has been described as continuing to 7 Ma (Abebe et al., 1998; Tommasini et al., 2005). The existing geological map of Ethiopia does not map this unit around the city of Nekemte, though smaller-scale maps of the region do recognize the presence of these fissural units in this area.

(v) The Reira Basalts. This unit is described as a 600m thick unit of basalts with variable textures ranging from aphyric to plagioclase and pyroxene-phyric and containing scoriaceous horizons with paleosols located on the southwestern Ethiopian plateau (Berhe et al., 1987). The unit is temporally poorly constrained between ca. 15 and 5.3 Ma. Further data is needed on this unit to confirm the assignment of it to this phase.

(vi) The Astit formation from along the Ankober border fault north of Addis Ababa, fringing the NW Afar rifted margin. This formation, defined by Wolfenden et al. (2005), contains basalt lavas and pyroclastics that are ca. 500m thick. Similar to the lower Kesem Formation, Wolfenden notes that the flows of this formation are interweaved with those of the Mezezo trachytic shield complex (a small complex north of Megezez shield – see Wolfenden et al., 2004 for location). Wolfenden et al. (2005) note the 10.87 ± 0.06 Ma (Ukstins et al., 2002) for basalt from this section is from a flow from the top of this complex, thus constraining the age of the Astit formation.

Notwithstanding the widespread pulse of basaltic volcanism during this phase throughout Ethiopia, in the northern portions of the NW Ethiopian plateau synchronous activity at Mt. Guna

(10.76 Ma ± 0.05 $^{40}Ar/^{39}Ar$) (Kieffer et al., 2004) took the form of a phonolite shield volcano. It is notable that this event is not the first instance where this portion of the NW Ethiopian plateau exhibited magmatic events that did not comport with the regional magmatic activity (i.e. Mid-Miocene activity around Axum and the Simien shield discussed above). A possible explanation for this magmatic event is the position of the Guna shield volcano within the hypothesized Debre Tabor Graben (Chorowicz et al., 1998). It is thus possible that local tectonics in this region have a controlling influence on the magmatic events – a concept explored further for Quaternary magmatic activity noted in this area. On the map of Ethiopia, Mt. Guna is assigned to the Tarmaber Guassa, and Mt. Guguftu and Gerba Guracha to Tarmaber Megezez; given the radiometric dates available since the publication of that map (Kieffer et al., 2004; Rooney et al., 2017), I assign Mt. Guna to the Mid-Miocene Resurgence Phase, and Mt. Guguftu & Gerba Guracha to the Early Miocene Resurgence Phase (discussed in volume 1).

5.3 Geochemical Characteristics of the Mid-Miocene Resurgence Phase Lavas

From the Mid Miocene (ca. 12 Ma to Pliocene), a number of significant magmatic events occurred within the northern East African Rift system. The geochemical behavior of these lavas is, however, distinctive. The Mid-Miocene Resurgence Phase events extend from northern Kenya to the junction of the MER with the Afar Depression and have been divided broadly on the basis of geographic location. Mid-Late Miocene rocks from the YTVL have the lowest values of CaO/Al_2O_3 at equivalent MgO, which when coupled with typically flat evolution of TiO_2 (Fig. 13) is suggestive of deep titaniferous clinopyroxene fractionation. Fractionation of clinopyroxene in the deep crust is a characteristic process common in many lavas erupting outside of the rift. These YTVL lavas also show incompatible trace element enrichment, plotting at high Nb values (Fig. 13). Taken together these data may suggest smaller degrees of melting with a less

developed magmatic system along the YTVL. While the Mid-Miocene events along the rift margin in Ethiopia show significant scatter, they commonly extend to high TiO_2 and plot at elevated CaO/Al_2O_3 (Fig. 13), inferring a less significant role for deep clinopyroxene fractionation. When combined with the typically lower values of Nb, the Mid-Miocene lavas erupted along the rift margin might represent a larger magmatic event, consistent with the large volumes inferred from mapped lava distribution. Temporally equivalent rocks from Southern Ethiopia (Kele basalts) and northern Kenya largely overlap and exhibit trace element enrichment over the Ethiopian rift margin lavas. The differences between the Ethiopian rift margin, southern Ethiopia and northern Kenya is particularly apparent in terms of element fractionation whereby Kenya and southern Ethiopia rocks plot at the most enriched ends the data array (Fig. 13).

In comparing REE trends among the four Mid-Miocene Resurgence Phase lava series it is evident that the slopes differ significantly: Kenya Mid-Miocene lavas exhibit a relatively steep slope with a depletion in the HREE (Fig. 14); in contrast, lavas from the Ethiopian rift margin and along the YTVL appear to have a broadly flatter HREE profile and are less enriched in the more incompatible REE. Primitive mantle normalized patterns largely reflect the observations above, whereby Mid-Miocene Kenya and Kele basalts define the most enriched endmembers during this time phase. While all of the magma groups exhibit a broad Type III pattern (Fig. 15), significant scatter is pervasive. The most notable deviation from a more normal Type III pattern is the negative Zr-Hf anomaly evident in most Kenya Mid-Miocene samples (also seen in one sample from the YTVL). Such patterns are reflective of metasomatic additions to these lavas of uncertain affinity.

It is difficult to assess the role of crustal assimilation in these systems. While there is a general tendency for samples >5% MgO to exhibit less radiogenic $^{143}Nd/^{144}Nd$ and radiogenic $^{87}Sr/^{86}Sr$ (Fig. 13), no clear trends exist within the data. There are significant differences between the Mid-Miocene samples erupted in northern Ethiopia and those in southern Ethiopia

and Kenya. Notably, the southern Ethiopia and Kenya samples appear to have the influence of a HIMU-like component, manifesting as radiogenic $^{206}Pb/^{204}Pb$ and unradiogenic $^{87}Sr/^{87}Sr$ (Fig. 16). In contrast, samples from northern Ethiopia exhibit the opposite characteristics (Fig. 16), and their origin is consistent with a mix of the Afar plume, depleted mantle, and Pan-African lithosphere source (Rooney et al., 2012). The origin of the HIMU-like component remains unconstrained; while a negative Zr-Hf anomaly is evident in lavas from this group, lavas from Yabello (where the isotopic data is derived) do not manifest this anomaly clearly (Fig. 15). Thus, the heterogeneity between the two regions could relate to contributions from a potential metasomatic source, or components in a heterogeneous plume (Shinjo et al., 2011).

5.4 Summary and Synthesis of the Mid-Miocene Resurgence Phase from Turkana to Ethiopia

The connection of this Mid-Miocene Resurgence Phase between northern Ethiopia and Turkana/ southern Ethiopia is currently unclear. Ebinger et al. (1993, 2000) have roughly mapped the Getra-Kele Basalts extending to about 7°N (not shown on the maps herein as there is insufficient continuity to allow for a departure from the Geological Map of Ethiopia). This unit has been described above as having a lower Getra unit (early Miocene) and an upper Kele unit (mid-late Miocene) (Ebinger et al., 1993). The Kele member of the Getra-Kele commences ca. 12.9 Ma (Ebinger et al., 1993), consistent with the 12.32 Ma (±0.17 $^{40}Ar/^{39}Ar$) age for the Chencha Basalts at 6.3°N (which may be part of the Getra-Kele unit). Further north at Sodo (6.9°N) Woldegabriel and Aronson (1987) describe a Mid-Miocene unit as a ~300 m thick series of alternating basalts and tuffs dated to 10.5 Ma (± 0.5) to 10.2 Ma (± 0.49). There is thus a ca. 2 Ma gap in the date of the initiation of the Mid-Miocene basaltic pulse in the region between the Chencha Basalts and the Mid- to Late Miocene sequence (likely the Guraghe-Anchar Basalts) at Sodo. This observation is generally consistent with the ca. 10.5 Ma date of initiation for the basaltic event north of 7°N, and suggests a temporal lag between Turkana and Southern

Ethiopia in the commencement of large-scale fissural basaltic volcanism in the Mid-Miocene. However, more detailed geochronological work will be necessary to test this hypothesis.

The origin of the potential temporal lag is unclear, but may relate to rifting events dominated by extension that initiated in Turkana and Afar. The central Main Ethiopian Rift is considered to be the product of strain migration from the loci of extension in Afar and Turkana, though the precise timing of its formation remains controversial and may range from 5 – 10 Ma (Wolfenden et al., 2004; Bonini et al., 2005; Macgregor, 2015; Purcell, 2018). Northward, and southward migrating strain formed the rift border faults of the Main Ethiopian Rift ca. 10-11 Ma (Wolfenden et al., 2004, 2005). A tentative hypothesis to explain the magmatic observations may be that the Mid-Miocene magmatic event in the southern portion of the region related to extension migrating from Turkana northwards into southern Ethiopia. This is consistent with the broad region of rifting associated with the Omo River region and the ca. 12 Ma magmatic event observed throughout eastern Turkana (adjacent to the Omo rifts in southern Ethiopia). In contrast, the northern portion of the MER is controlled by extension migrating southward from Afar. The southward migration of strain is thought to have reactivated a rift-perpendicular Precambrian fault zone – the YTVL – and resulted in lithospheric thinning along its alignment (Abebe et al., 1998; Keranen et al., 2009). This hypothesis is supported by the significant volume of basaltic fissural lavas dating from this time erupting along the trace of the YTVL, mirroring the contemporaneous fissural activity along the rift margin. In aggregate, the existing data suggests that the Mid-Miocene Resurgence Phase is not entirely synchronous from north to south, but that this heterogeneity in the time of commencement reveals insights into the origin of this event.

The existing evidence suggests that extension is likely the driver of the Mid-Miocene Resurgence. Region-wide synthesis studies of the EAR basins highlight the Mid Miocene as a critical phase of extension in Turkana and Afar (e.g., Macgregor, 2015). Succinctly, the Mid-

Miocene Resurgence Phase seems linked with the commencement of a phase of extension throughout the region whose nexus is located in Afar and Turkana. Consequently, magmatic activity in the region that develops subsequent to the Mid-Miocene Resurgence Phase should be influenced by the presence of a developing rift. The stratigraphic record is consistent with this model - the thickness of geologic units younger than the Mid-Miocene Resurgence Phase varies a function of proximity to the rift margin.

6. Early Rift Development Phase (9 to 4 Ma)

The largely basaltic magmatic activity that manifested during the Mid-Miocene Resurgence Phase heralded the initial development of rifts in both Kenya and Ethiopia. This initial magmatic pulse was followed by a phase of faulting and sedimentation that was accompanied by explosive silicic volcanism and basaltic flows. This phase continued until another significant regional basaltic event that commenced ca. 4 Ma. It should be noted that this phase of activity is particularly well-expressed in the now developing Kenya and Main Ethiopian Rifts (Fig. 17).

6.1 Northern Kenya Rift, Turkana, and Southern Ethiopia

No significant magmatism was recorded in the Turkana basin or southern Ethiopia during this interval (Fig. 17). However, within the Northern Kenya Rift, this phase is represented by a number of important formations including the ~200 m thick, dominantly basaltic, Kongia Formation. Age dating of this unit suggests a range of 7.3 to 5.3 Ma, and is followed by a hiatus to 4.1 Ma, after which the Tirr Tirr Formation erupted (see subsequent discussion on the Stratoid Series). The Kongia formation may correlate with the Tirioko basalts, which are a widespread 6.6 – 4.5 Ma formation in this region (Webb and Weaver, 1975; Dunkley et al., 1993).

Following a dominantly sedimentary interval during the Mid-Miocene within the north-central Kenya Rift (Dunkley et al., 1993; Hautot et al., 2000), a more extensive sequence of magmatic activity has been reported. This activity (composite stratigraphy) commences with the 200-600 m thick Ewalel phonolite lavas and tuffs (8.8 Ma ± 0.3 to 7.1 Ma ± 0.4) (Chapman and Brook, 1978). The Ewalel phonolites are followed by a phase of erosion and tilting (Mugisha et al., 1997), onto which the ca. 150 m thick Eron Basalt is erupted (Chapman et al., 1978). The Mpesida Beds (6.36 Ma ± 0.03 $^{40}Ar/^{39}Ar$), which contain an ash flow and pyroclastic facies, are immediately overlain by the 355m thick Kabarnet flood trachytes (6.37 Ma ± 0.03 $^{40}Ar/^{39}Ar$) (Kingston et al., 2002), which are thought to have covered an area of ca. 1800 km^2 (Chapman et al., 1978). Overlying the Kabarnet Trachytes are the 550m thick Kaparaina Basalts (5.72 Ma ± 0.05 $^{40}Ar/^{39}Ar$) with a maximum duration of 0.4 Ma (Deino et al., 2002). The Kaparaina Basalts (and Narokwe, Barpelo, and Napeitom basalts) are also thought equivalent to the Tirioko Basalts (Truckle, 1977). Following this basaltic interval, air fall deposits and welded tuffs of the Chemeron formation began accumulating at ~5.3 Ma (Deino et al., 2002), though earlier tuffaceous sediments may have begun accumulating ca. 5.66 Ma (± 0.14) (Sawada et al., 2002).

Activity continued further to the south within the Kenya Rift and Northern Tanzania Divergence but this will be discussed in Part III of the synthesis series and is only shown here for completeness.

6.2 Northern Ethiopia

Following the synchronous basaltic volcanism that defined the Mid-Miocene Resurgence Phase, magmatic activity displays temporal and spatial variability. At a broad-scale, basaltic volcanism continued along the rift margins and YTVL after the termination of the Mid-Miocene Resurgence

Phase. Within the rift, magmatic activity is recorded dominantly as pyroclastic deposits. As this phase progressed, early basaltic volcanism, which had initially persisted along the rift shoulders and YTVL, transitioned to trachytic and more evolved volcanic activity focused on central volcanoes. Towards the end of this time period, a significant regional unconformity is evident within the rift – evidence of a tectonic reorganization that extends from Afar to the MER. The Early Rift Development phase terminates with the commencement of a new phase of widespread basaltic volcanism termed “the Stratoid phase”.

Central Ethiopian Rift and Addis Ababa Region: The upper part of the Kessem formation at the type locality where Wolfenden et al. (2004) defined it, has lithologies that are dominantly silicic pyroclastics (in contrast to the dominantly basaltic lower portion of the formation that falls within the Mid-Miocene Resurgence Phase). Pyroclastic deposits continued within the Keesem Formation until ca. 6.6 Ma, where thereafter a regional unconformity occurs (Wolfenden et al., 2004). This locality is proximal to the rift (Meteh Bila) and may thus express magmatic events in the rift during this interval. This period is not well-exposed at surface levels within the modern rift and thus is not expressed on the maps accompanying this contribution.

Western Ethiopian Plateau: During this time interval there is commonality on the western Ethiopian plateau in terms of a transition from dominantly fissural basaltic flows to more trachytic (and rhyolitic) central volcanoes. Basaltic activity continued (without apparent interruption) along the YTVL until ca. 5-7 Ma (Abebe et al., 1998, 2005; Tommasini et al., 2005). This phase of basaltic volcanism is best illustrated by the ca. 7.5 to 5 Ma Addis Ababa Basalts (occurring at the intersection of the YTVL and the MER), and continued fissural activity along the length of the YTVL (Abebe et al., 1998, 2005). As the Mid-Miocene fissural basaltic activity ended, magmatic events on the Western Ethiopian Plateau became more trachytic (and peralkaline) in composition, and migrated to distinct volcanic edifices that young towards the rift (Abebe et al., 1998; Tommasini et al., 2005; Rooney et al., 2012b). Prior studies have grouped

the volcanics in this region during this phase as the Wechacha Trachytes (Abebe et al., 2005), but only included the edifices of Yerer, Wechacha, and Furi (4.6 – 3.3 Ma). To these we also add the 3.119 Ma (± 0.010 Ma $^{40}Ar/^{39}Ar$) Chefe Donsa Maar (Rooney et al., 2012b), and Gash Megal peralkaline rhyolites (sometimes referred to as Mt. Guraghe), which are temporally poorly constrained, but thought to be younger than 5.2 Ma (Abebe et al., 2005). The Wagebeta calderas along this margin to the south are also active at this time and date from 4.20 Ma (± 0.2) to 3.63 Ma (± 0.2 Ma) (WoldeGabriel et al., 1990, 1999). Trachytes at Mt. Damot in the Sodo region represent the youngest magmatic event at 2.94 Ma ± 0.1 (WoldeGabriel et al., 1990). These events are roughly correlative with the Wechacha Trachytes to the north, and have been grouped together. It should be noted that, as defined above, the Wechacha Trachytes extend beyond the temporal limits of the Early Rift Development Phase. This overlap occurs because I consider the trachytes as the terminal (residual) phase of magmatic activity that began with the Mid-Miocene Resurgence Phase. This assertion is consistent with the co-location of the Wechacha Trachyte magmatic centers and regions where Mid-Miocene fissural basaltic activity had occurred (dominantly along the YTVL).

Bale Mountains and SE Ethiopian Plateau: The lack of clear geochronological control on the Mid-Miocene phase Reira Basalts makes it difficult to establish equivalences with the other regions. Importantly, the Reira Basalts are unconformably overlain by the Aroresa Trachytes and Dodola Ignimbrites. The sole geochronological constraint is 5.3 Ma (± 1) age for the Reira Basalts (Berhe et al., 1987). It should also be noted that in the most recent geologic map of this region, the Aroresa Trachytes of Berhe et al. (1987) are split such that there is a trachyte unit both above and below the Reira Basalts. This raises a question as to whether the Bale Mountains are perhaps exhibiting the same behavior as the better constrained Addis Ababa region where the fissural basalts and shield trachytes/basalts inter-finger.

South East Afar Margin: The Upper Trap Series (Mid-Miocene Resurgence Phase equivalent) is overlain, with an angular unconformity, by Pliocene volcanics that are dominantly silicic and occur towards the Afar Depression. These units will be examined in further detail in the discussion of volcanism in Afar (see subsequent synthesis volume).

6.3 Geochemical characteristics of the Early Rift Development Phase

Mafic lavas erupted during this phase exhibit a remarkable similarity to the earlier Flood Phonolite phase. Consequently, the characteristics of these lavas are described in more detail in that section. There are few samples where sufficient data is available to construct a primitive mantle normalized diagram but the two samples available suggest that the mafic lavas during this phase are derived from a similar source to one of the Flood Phonolite samples – both exhibit a broad Type III lava pattern but with pronounced negative Zr-Hf anomalies that may suggest a role for apatite in their source (Fig. 6). Succinctly, the extant data suggests a derivation from the convecting upper mantle in conjunction with some contribution from a recently created lithospheric mantle metasome, given the lack of any obvious ancient lithospheric mantle in the isotopic values (Fig. 4).

The Wechacha Trachytes occur predominantly in a series of large volcanic edifices along the intersection of the YTVL and the Main Ethiopian Rift. They comprise a remarkably coherent path of magma evolution extending from trachyandesite to rhyolite (ETHSIL1). A few lavas within the trachyte field from Wechacha and Menagesha volcanoes deviate in both total-alkali silica (Fig. 8) and TiO_2 (Fig. 9) towards the phonolite fractionation pathways described for Axum samples earlier. It is evident that magmas evolved along both a rhyolite and a phonolite path within the edifices represented by the Wechacha Trachytes. While fractional crystallization from basalt is the dominant mechanism proposed for magma evolution, open system processes are

necessary. MELTS modelling of the evolution of peralkaline magmas showed that the K_2O content of pristine basaltic lavas in the region are insufficient and requires magma mixing with more evolved melts in order to increase K_2O contents sufficiently (Rooney et al., 2012b). Such processes have been inferred for basalts in this region (Rooney et al., 2014a), and open system hybridization of magmas is evident in evolved systems elsewhere in the rift (e.g., White et al., 2012). Further open system behavior is evident in the more evolved Wechacha Trachyte lavas, which have $^{87}Sr/^{86}Sr$ values ranging up to 0.7075 (not shown), thus requiring crustal contributions to their evolution (Kabeto et al., 2009). In summary, while a small number of Wechacha Trachyte lavas show evidence of the beginning stages of anorthoclase fractionation enroute to phonolite, the terminal magmas in this region are universally rhyolites (Fig. 9). There is no extant geochemical data from the eastern Ethiopian plateau at this time.

6.4 Summary of the Early Rift Development Phase

This phase is well-represented in both the now evolving Kenya and Main Ethiopian Rifts, though the expression of this event differs significantly. While more diverse magma suites are evident when compared to the basalt-dominant Mid-Miocene Resurgence Phase, basaltic and trachytic volcanism is dominant within the Kenya Rift, while explosive silicic activity is more common within the Main Ethiopian Rift. There is also tentative evidence of more silicic activity closer to the surface expression of the rift valleys. The origin of magmatism during this phase may be linked with the lack of contemporaneous activity in Turkana. While not fully constrained at present, these observations tentatively point to lithospheric thinning focused in both the Kenya Rift and Main Ethiopian Rift (and not in Turkana) as a potential mechanism for melt generation.

7 The Stratoid Phase (ca. 4 to 0.5 Ma)

This phase of activity incorporates a wide array of magmatic events that commences with the areally-extensive Gombe Stratoid Series centered in Turkana, but also includes the later Bofa Stratoid Series from the Main Ethiopian Rift and the Rift Fill Series from the Kenya Rift (Fig. 18). Despite the morphological and temporal diversity in magmatism, I have amalgamated these events into a single phase as they represent an increased period of basaltic volcanism that impacts the entire study region. Importantly, this phase is also correlated with the recommencement of significant magmatic activity in Turkana, and suggests a fundamental shift in magmatism during this new phase in comparison to the Early Rift Development phase. The initiation of this event is likely linked with the deepening of the rift in Turkana (Purcell, 2018), and the migration of this strain away from Turkana (Macgregor, 2015).

7.1 Kenya Rift, Turkana, and Southern Ethiopia

7.1.1 The Gombe and Tirr Tirr Basaltic Platforms

Within the Kenya Rift, Turkana basin, and southern Ethiopia, magmatic activity recommenced after a ca. 5 Ma hiatus with the eruption of the Gombe Group, Tirr Tirr Formation and other regional equivalents, which when combined define the Stratoid Phase (Fig. 18). The most pronounced component of the Stratoid Phase are the Gombe Group lavas, which have been constrained isotopically as having erupted between 4.22 Ma and 3.97 Ma, based on two tuffs bracketing the Gombe Group lavas in Kenya (Gathogo et al., 2008). Basaltic magmas within the Gombe Group are remarkably homogenous and are reported as being relatively evolved with high TiO_2 (Haileab et al., 2004). This Group is also correlated with basalts of the Mursi, Harr, and Nkalabong Formations in Southern Ethiopia (Asfaw et al., 1991; Ebinger et al., 1993, 2000; Haileab et al., 2004), which are constrained to a similar age of eruption of between 4.18 to 4.29 Ma (Erbello and Kidane, 2018). The ‘Dida Galgalu’ lavas from the region surrounding the

Marsabit shield have also been assigned to the Gombe Group (Hackman, 1988; Key and Watkins, 1988; Haileab et al., 2004). These lavas were dated by Brotzu et al. (1984) at 4.5 Ma (± 0.3) to 7.7 Ma (± 0.4), however this temporal range is unlikely to be accurate (see discussion above). Haileab et al. (2004) tentatively assigned the 'Bulal Basalts', originally defined by Davidson et al. (1983), as also part of the Gombe Group. However, there is complexity with this assignation. Lavas from the Yabello area of southern Ethiopia that were mapped as Bulal Basalts are temporally (3.69 Ma ± 0.03 to 3.75 +/0.0.06 $^{40}Ar/^{39}Ar$) (Corti et al., 2019), and chemically (Fig. 13) part of the Gombe Stratoid Series. However, the Bulal Basalt dated by Ebinger et al. (2000) at 3.2 Ma (± 0.6) displays distinctively more silica-undersaturated composition than any known Gombe Group sample. This result likely reflects that the currently mapped Bulal Basalts are a composite of the Gombe Stratoid Series and an overlying (younger) shield volcano – a relationship commonly seen in Turkana. Difficulties in establishing a robust temporal correlation throughout the region are described by Haileab et al. (2004), who show that rocks of the Gombe Group are difficult to date directly and thus tend to exhibit a wide array of inconsistent K-Ar ages. In the accompanying maps I have not divided the Gombe Group lavas from the overlying shields.

The Tirr Tirr formation (Fig. 18), which forms a 300m thick basaltic plateau in the Samburu Hills section of the Northern Kenya rift (Dunkley et al., 1993), has been dated at between 3.94 Ma (± 0.74) (Tatsumi and Kimura, 1991) and 2.74 Ma (± 0.02 $^{40}Ar/^{39}Ar$) for the upper most flow (Dunkley et al., 1993). In the Northern Kenya Rift, the Tirr Tirr formation unconformably overlies the 5-7 Ma Kongia Formation (part of the Early Rift Development phase), consistent with the hypothesized faulting events from 5.3 to 4.1 Ma (Sawada et al., 1998), and indicates a smaller hiatus in volcanic activity in comparison to Turkana and southern Ethiopia. While most of the rocks within the Tirr Tirr formation are basaltic, there are subordinate trachytes and rhyolites (Dunkley et al., 1993). Haileab et al. (2004) noted the temporal similarity

of the Tirr Tirr formation to the Gombe Group, but also recognized that the lavas of the Formation were distinct from the Gombe Group lavas and thus no correlation was made. I have grouped the Tirr Tirr Formation within the Stratoid Phase, but currently I am unable to establish any relationship between the Tirr Tirr Formation and the Gombe Group. On the western side of the rift, the Nathelot Basalts and overlying Loriu Trachytes erupted at 4.5 Ma (± 0.4 Ma) (Dunkley et al., 1993 citing the thesis of Truckle 1977). These units are overlain by the ca. 2 Ma Lorikipi Basalts. Dunkley et al. (1993) interprets the Tirr Tirr Formation and Lorikipi Basalts as Pliocene flood basalts that filled in the rift depression around the predominantly Pliocene Namarunu trachyte volcano (see discussion on modern axial activity below).

7.1.2 Shield Building in Turkana

A shield building phase of activity immediately followed the plateau-forming eruptions (Fig. 18). This shield building phase created volcanic edifices in the following temporal order: Longipi (3.5 Ma ± 0.19 to 1.5 Ma ± 0.19 $^{40}Ar/^{39}Ar$) (Furman et al., 2006b), some Bulal Basalts 3.2 Ma (± 0.6) (Ebinger et al., 2000), Kulal (3.01 Ma ± 0.55 to 1.91 Ma ± 0.21) (Ochieng et al., 1988; Gathogo et al., 2008), Asie (2.7 Ma ± 0.35 to 2.07 Ma ± 0.13) (Key et al., 1987), Marsabit (1.70 Ma ± 0.35 to 0.76 Ma ± 0.17) (Key et al., 1987), and the Huri Hills (uncertain ages). On top of these shields are recent smaller monogenetic cones/maars and associated flows that continue into Ethiopia (Cinder cones on the Huri Hills shield continue to the NE as the Mega/Sidamo field in Ethiopia). Other monogenetic volcanic fields of similar age (e.g. Dukana, ~0.9 Ma) (Key and Watkins, 1988) may occur between the shield volcanoes. These shield volcanoes are constructed dominantly of either clinopyroxene-olivine, or olivine plagioclase phyric fissure-fed basaltic flows (e.g., Key et al., 1987). Evidence of subsequent magmatic activity is recorded in the detailed studies of tephra that form important time markers in the study of hominid evolution. The

interested reader is referred to papers that specifically examine the chronology of these events (WoldeGabriel et al., 2005; Brown and McDougall, 2011). However, I will note that within the Koobi Fora Formation north of Loiyangalani, three distinct basalt units have been recorded: (A) Kankam Basalt (ca. 3.2-3.3 Ma), Lenderit/Gus Basalt (2.02 Ma ± 0.02 to 2.18 Ma ± 0.03), and Balo Basalt 1.79 ± 0.002 Ma) (Gathogo et al., 2008). Within the Kenya Rift, the Lorikipi Basalts overlie the earlier trachyte platforms on the western margin and date to 2.33 Ma ± 0.2 $^{40}Ar/^{39}Ar$ to 4.0 Ma ± 0.1, and form an important part of the shield of Namarunu volcano (Dunkley et al., 1993). The Lorikipi Basalts may thus be associated with this shield building phase of magmatic activity that followed the trachytic platforms.

7.1.3 North-Central Kenya Rift

Within this portion of the rift, there again exists a disconnect between the significant magmatic events occurring further to the north during the early part of this phase and the largely sedimentary units occurring at this latitude. The Chemeron Formation is an important hominid-bearing unit and temporally occupies the late Rift Development phase and early Stratoid phase (Deino et al., 2002). The top of the Chemeron Formation is bracketed by the Ndau Mugearite at 1.57-2.13 Ma (Hill et al., 1986) and followed in the Tugen Hills by the Kapthurin Formation (which includes basalts at 0.61 Ma ± 0.04 and 0.552 Ma ± 0.015) and younger tuffs (Deino and McBrearty, 2002). The Chemakilani Basalt and Marigat Trachyte (ca. 1.8-2 Ma: Clément et al., 2003 citing earlier works) also occurs during this phase. Subsequent magmatic activity was more significant, with the Kwaibus Basalts (undated but reasoned to be ca. 0.89 to 0.95 Ma by Hackman (1988) on the basis of paleomagnetic constraints) filling the rift valley and then overlain by the Hannington Trachyphonolite series (Griffiths and Gibson, 1980). The Hannington Trachyphonolite (0.894 Ma ± 0.013 to 0.768 Ma ± 0.011) (Clément et al., 2003) and Loyamarok flow (0.855 Ma ± 0.013) (Clément et al., 2003) are associated with a low shield volcano in the

vicinity of Lake Bogoria and extend southward into the South-Central Kenya Rift (Baker et al., 1988). A further basaltic event (Koitumet/Goitumet) Basalts overlie the Hannington trachyphonolite. These basalts are thought to represent a broad ~7 km diameter basaltic dome (Hackman, 1988). We also assign the Baringo Trachytes (0.514 Ma ± 0.007) and Baringo Basalt (0.681 Ma ± 0.011) to this phase (Clément et al., 2003).

7.2 Northern Ethiopia

7.2.1 The Main Ethiopian Rift

Within the Main Ethiopian Rift, the clearest expression of the initial basaltic plateau phase of activity occurs in its southernmost extremities adjacent to Turkana. The Mursi Basalts, part of the ca. 4 Ma Gombe Stratoid Series centered on Turkana (discussed previously), extend as far north as Sodo. Within the central MER, existing stratigraphic constraints have resulted in significant ambiguity as to the existence of this event.

Existing stratigraphy for the MER during this phase has been quite variable with the units overlying the Mid-Miocene basalts termed either the Nazret Group/Pyroclastics (5.2 – 2.6 Ma) (Kazmin et al., 1980; Abebe et al., 2005), or Balchi Formation (ca. 9 – 1.5 Ma) (Mohr, 1983). Work by Wolfenden et al. (2004) redefined these units on the basis of a pronounced unconformity in the region that extended from 6.6 to 3.5 Ma. This unconformity is also an important marker in Afar, and broadly represents the boundary between magmatic units. Units prior to 6.6 Ma were amalgamated with the Kessem Formation (see previous discussion), while the units subsequent to this event were termed the Balchi Formation (ca. 3.5 to 2.5 Ma). Within the central Main Ethiopian Rift, the Balchi Formation (3.555 Ma ± 0.007 to 2.540 Ma ± 0.018 Ma $^{40}Ar/^{39}Ar$) is dominantly pyroclastic and is separated from the upper Kessem Formation by a distinct angular unconformity (Wolfenden et al., 2004). For units following the Pliocene Balchi

Formation of Wolfenden et al. (2005), we adopt the nomenclature of Abebe et al. (2005) whereby the Chefe Donsa Pyroclastics (2.54-1.7 Ma: Abebe et al., 2005) occur within the rift proper. This unit is distinguished from the underlying units due to the absence of welding. The lack of a large scale map showing the division between the units has necessitated using the catchall 'Nazret Series' unit from the Geological Map of Ethiopia to represent all these pyroclastic sequences. The interested reader is referred to the detailed map by Abebe et al. (2005) for the locations and extent of these units in the Addis Ababa region. The predominance of volcanoclastic rocks in the Central MER during this phase would seem to be at odds with the occurrence of a rift-wide basaltic stratoid event. However, broadly contemporaneous with these pyroclastic deposits is a widespread younger basaltic unit whose age remains poorly constrained – The Bofa Basalts.

Abebe et al. (2005) term all upper Pliocene basalts in the Central MER as 'Bofa Basalts' extending from 3.5 to 1.6 Ma. However, a clear temporal definition of the 'Bofa Basalts' has remained elusive (see Boccaletti et al., 1995). Moreover, pre-Stratoid Phase basalts during the Mid-Miocene to Pliocene have been variously termed: Wolenchiti Basalts, Bishoftu Basalts, Tullu Rie Basalts, and Eastern Margin Unit by other authors. Some of the complexity relates to a lack of isotopic dating, but also the presence of basaltic horizons within the pyroclastic sequences (e.g. the Nazret Series discussed above). While Kazmin et al. (1980) suggest an age range of 3.5 to 1.5 Ma for these units, later work found ages from 1.56 Ma ± 0.03 to 1.44 Ma ± 0.03 (Chernet et al., 1998). These ages are consistent with borehole work from Aluto (see Axial Phase below) that indicate the Bofa basalts are 800-1000m thick and have an age of 1.6 Ma ± 0.5 (Teklemariam et al., 1996). Abebe et al. (2007) posit that these basalts are equivalent to the 1.6 Ma (± 0.1) basalts occurring along the rift escarpment south of Awassa (WoldeGabriel et al., 1990) and thus form the base of an extensive basaltic episode in the region at ca. 1.6 Ma.

To resolve the existing nomenclature I adopt the new term ‘Bofa Stratoid Series’ to represent all basalts/trachytes in the central MER intercalated with the Balchi and Chefe Donsa pyroclastics, and extending until the development of axial volcanism. From the existing work, it is evident that the initial phase of basaltic volcanism expressed in Turkana is not well-developed in the central MER, and manifests primarily as pyroclastic activity with isolated basaltic flows. Such activity is to be anticipated given this portion of the rift was last to develop. However, at ca. 1.6 Ma, a clear and distinct stratoid basalt event is evident within the rift. These extensive lavas likely covered the rift floor and provided a source for later explosive caldera events (Hutchison et al., 2016a). Recent work by Ayalew et al. (2018) has provided new geochemical constraints on the Bofa Stratoid Series, which exhibit considerable range in composition, consistent with some degree of differentiation, and isotopic evidence of substantial crustal assimilation.

7.2.2 Western Ethiopian Plateau

The only volcanic event along the western rift margin from this phase is the creation of the Akaki basalt chain west of Addis Ababa along the YTVL. The precise chronology of the Akaki basaltic field is poorly constrained. Abebe et al. (2005) suggest a range from 2.9 to 2.0 Ma. It is probable that the picro-basalt dated by Chernet et al. (1998) south of Furi volcano at 2.03 Ma ± 0.04 is from the Akaki chain given the unusually strong mafic character of many of these basalts (Rooney et al., 2014a). The given age range is consistent with the stratigraphic relationship of the Akaki basalts overlying products of the Wechacha Trachytes (3.11 Ma) and the morphologically more eroded appearance of the Akaki cinder cones in comparison to those from the adjacent Quaternary Silti-Debre Zeyit fault zone. The existence of the Akaki basalts lavas near Addis Ababa, and the relative paucity of equivalent age material along the rift margin is likely a function of the intersection of the YTVL and Ethiopian Rift (Abebe et al., 1998; Rooney et al., 2014a).

Although likely younger and potentially contemporaneous with the modern Axial Phase, some other areas of magmatic activity are noted on the Western Ethiopian Plateau. I amalgamate all these regions here to permit a focus on the modern rift axis in the subsequent section. Adjacent to the evolving rift, magmatic activity around Mt. Wonchi (Wenchi) and Mt. Dendi is noted to be bimodal and is dated to less than 0.1 Ma (Abebe et al., 1998). Distant from the evolving Ethiopian Rift and margin, magmatic activity during this phase is also noted in the form of fissural flows, cinder cone fields, and associated basaltic flows. This activity is centered on the Tepi field in the south (Ayalew et al., 2005; Corti et al., 2018), and Lake Tana in the north (Meshesha and Shinjo, 2010). The existence of these fields has been linked to tectonic controls and lithospheric weaknesses on the Western Ethiopian plateau (Corti et al., 2018). The Tepi field, which is aligned ENE, is aligned with regional faults resulting from the Goba-Bonga volcanotectonic lineament (Corti et al., 2018). The precise age of the Tepi field is unknown, but it is considered recent (Ayalew et al., 2005; Corti et al., 2018). Recent magmatic activity in the Lake Tana region results from the intersection in this area of the Dengel Ber graben, Gondar graben, and Debre Tabor graben (Chorowicz et al., 1998), and is likely a Mesozoic reactivated structure (Hautot et al., 2006). Magmatism takes the form of xenolith-bearing cinder cones and fissural flows typically orientated NNE–SSW (Conticelli et al., 1999; Ferrando et al., 2008; Frezzotti et al., 2010; Beccaluva et al., 2011).

7.2.3 Eastern Ethiopian Plateau

In contrast to the Western Plateau, there is significant magmatic activity during this phase on the Eastern Ethiopian Plateau. Overlying the Reira Basalts and Aroresa Trachytes in the Bale Mountains are the Sanete Basalts, which occur in the vicinity of Sanete Mountain/Tullu Dimtu, and have been dated to 2.1 Ma (± 0.5) (Berhe et al., 1987). The younger Batu Trachyte has an age of 1.61 Ma (± 0.03 $^{40}Ar/^{39}Ar$), and compositions that are not entirely trachytic, as a result it

has been recently renamed to “Pliocene Bale” (Nelson et al., 2019). Closer to the rift, magmatism is represented by the 2.7 to 1.3 Ma ‘Chilalo Volcanics’ (Abebe et al., 2005). This magmatic group is comprised of the following dominantly basaltic to trachytic edifices dated by WoldeGabriel et al. (1990): Chilalo (2.54 Ma ± 0.1 to 1.74 Ma ± 0.1); Badda/Bada; Kada/Kaka (2.7 Ma ± 0.1); Kubsa; Enquolo/Hunkuolo (2.56 Ma ± 0.1). The Galema Range (previously Sagatu Ridge), which is comprised of a dike swarm that represents the feeder system of a now eroded cinder cone field, occurs between Badda and Kaka volcanoes and is dated at 1.97 Ma (± 0.02) (Kennan et al., 1990). The Galema Range is considered equivalent to cinder cone chains of the Wonji Fault Belt and Silti-Debre Zeyit Fault Zone within the rift proper (Chiasera et al., 2018). The occurrence of large silicic centers and cinder cones chains on the rift margin have important implications for strain migration during rifting (Chiasera et al., 2018). Late stage olivine-rich flows blanket the landscape and fill river valleys in this region. These flows, which have been dated to 0.66 Ma (± 0.11 $^{40}Ar/^{39}Ar$) (Nelson et al., 2019), form the upper reaches of the large shield volcano that dominates this portion of the Eastern Ethiopian Plateau.

7.3 Geochemical Characteristics of the Stratoid Series Phase

7.3.1 Geochemical Characteristics of the Gombe and Tirr Tirr Basaltic Plateaus

The Gombe Stratoid Series is a compositionally uniform massive platform of lavas extending from northern Kenya to southern Ethiopia. Initial work on these units recognized the tight cluster that the Gombe Stratoid Series lavas occupied (Haileab et al., 2004), and this is confirmed from the addition of new data (Fig. 13). Notable is the clustering of the data at ~5 wt. % MgO and 3.5 wt. % TiO_2, with somewhat depleted incompatible trace elements (Nb ~ 28 ppm) in comparison to Mid-Miocene events in the same region (~ 60ppm Nb) (Fig. 13). This depletion mirrors that of the younger Bofa Stratoid Series to the north, though that series exhibits far more geochemical

variability. The depletion in incompatible trace elements is best illustrated in a Zr/Nb-La/Yb plot whereby the Gombe Stratoid Series define the depleted endmember of the array (Fig. 13), consistent with the lack of LREE enrichment (Fig. 14). Gombe Stratoid Series lavas exhibit a consistent Type III magma pattern (Fig. 15). Similar to the major and trace element clustering of the Gombe Stratoid data, the isotopic values for this series are coherent, exhibiting unradiogenic $^{206}Pb/^{204}Pb$ but moderately unradiogenic $^{87}Sr/^{86}Sr$ and $^{143}Nd/^{144}Nd$ (Fig. 15). These characteristics are consistent with a derivation from an Afar plume – depleted mantle – Pan African lithosphere mix, though with a greater contribution from this depleted mantle component. Few datapoints exist for the Tirr Tirr Formation, and the extant data are quite scattered (Fig. 13). Isotopic data for Tirr Tirr Formation indicates a significant lithospheric component within the more evolved lavas (Fig. 13), though particularly radiogenic $^{143}Nd/^{144}Nd$ and $^{206}Pb/^{204}Pb$ suggest the contribution of a HIMU-like component (Fig. 15). It must be stressed that in many units a single datapoint is all that may exist, requiring significantly more research on this region in order to establish a firm origin for these rocks.

7.3.2 Geochemical Characteristics of the Turkana Shield Building Phase

There is limited available geochemical data for the shield building phase of activity in this region. In general terms the existing samples from Lenderit (north of Loiyangalani), the Kulal shield, and Lorikipi are evolved, while Logipi-Latarr and Huri Hills are more primitive. The undifferentiated samples tend to fall in between these two extremes. Unsurprisingly, given the wide geographic area from which these samples are derived, the magmas do not follow coherent fractionation pathways (Fig. 19): a subset of the Huri Hills samples and all the Logipi-Latarr samples have higher concentrations of TiO_2 and Zr at common values of MgO in comparison to the other units (noted as high Ti in the legend key). These same samples from both the Huri Hills and Latarr-Logipi exhibit broad incompatible trace element enrichment, consistent with low Zr/Nb and high

La/Yb (Fig. 19) and generally plot at higher chondrite normalized values (Fig. 20), though overlap is evident. Most all lavas from the Pliocene Shields exhibit a broad Type III lava pattern (Fig. 21), suggestive of a sub-lithospheric origin for these lavas. Logipi-Latarr exhibits a particularly well-developed correlation between decreasing MgO and less radiogenic $^{143}Nd/^{144}Nd$, suggestive of progressive crustal assimilation, though no clear correlation is observed for $^{87}Sr/^{86}Sr$ (Fig. 19). The evolved Lorikipi Basalts show no evidence of assimilation and plot at unradiogenic values of $^{87}Sr/^{86}Sr$ and radiogenic values of $^{143}Nd/^{144}Nd$, contrary to other evolved samples from this phase (Fig. 19). In Pb isotope space, samples lie along a linear array and require contributions from two endmembers – the radiogenic endmember is best developed at Kulal, while the less radiogenic endmember is best described at the Huri Hills (Fig. 19). In a general sense the isotopic behavior of the Pliocene shields mirrors that of the Quaternary samples from the same region (Furman et al., 2004, 2006b).

7.3.3 Geochemical Characteristics of the Stratoid Phase in the Main Ethiopian Rift

Little data exists for the Balchi Formation, but the three extant data points all plot at high SiO_2, within the rhyolite field (Fig. 8). Balchi Formation materials compositionally closely track the Wechacha Trachytes (Fig. 9) and are likely derived from the same origin (i.e. dominantly fractional crystallization with some limited crustal assimilation, however more data is needed to test this initial hypothesis. The Bofa Stratoid Series is typified by relatively low TiO_2 in comparison to the Gombe Stratoid Series to the south (Fig. 13) and typically overlaps the Mid-Miocene lavas erupted in Northern Ethiopia. Exceptions to this Mid-Miocene correlation are in lower CaO/Al_2O_3, FeO (not shown) and Nb in the Bofa Stratoid Series (Fig. 13). In comparison to the Mid-Miocene Resurgence Phase, the Bofa Stratoid Series exhibits REE patterns more similar to the Gombe Stratoid Series (Fig. 14), with a limited enrichment of the LREE. In contrast to the Gombe Stratoid Series, the Bofa Stratoid Series exhibits a much wider range in

compositions and has broadly less enriched MREE-HREE (Fig. 13). The Bofa Stratoid Series follow a clear Type III lava pattern (Fig. 14). Isotopically there is a notable difference between the Bofa Stratoid Series, which exhibit notably more radiogenic values of $^{87}Sr/^{86}Sr$ at all values of MgO (Fig. 13) in comparison with any other equivalent magma series (Fig. 15). These characteristics imply the contribution of a lithospheric component, consistent with the slight deviation towards more elevated $^{208}Pb/^{204}Pb$ with decreasing $^{206}Pb/^{204}Pb$ in comparison to the Mid-Miocene lavas in the same region and Gombe Stratoid Series (Fig. 16). These lavas have been described as originating from a plume-influenced upper mantle and interacting with lithospheric metasomes enroute the surface (Ayalew et al., 2018). It should also be noted that the asthenosphere beneath where the Bofa Stratoid Series was erupted has been probed by young volcanism that has shown that the upper mantle in this region is contaminated with lithospheric material (Rooney et al., 2012a).

7.3.4 Geochemical Characteristics of the Stratoid Phase on the Eastern and Western Ethiopian Plateaus

Small volume magmatism present on the western Ethiopian plateau and eastern Ethiopian plateau during the past ca. 4 Ma share many geochemical similarities with modern magmatic activity within the MER. Notably, the manifestation of these events as small cinder cones and associated dikes (e.g., Mohr and Potter, 1976; Ferrando et al., 2008; Rooney et al., 2014a; Chiasera et al., 2018) parallels that of the modern loci of extension within the rift. Note that some of these units are contemporaneous with the Axial phase described below, but are amalgamated here for discussion. Magmas on the eastern and western plateau exhibit broad differences in their major element characteristics. Lavas from the eastern plateau have enrichments in FeO (not shown) and TiO_2 in comparison those on the western plateau (Fig. 16). Such heterogeneities in the magma series appear to have been imparted by the primary

magmas given the parallel trends evident at equivalent high MgO contents (Fig. 16). Differences between the magma series are magnified by the increasing TiO_2 values evident within the eastern Plateau volcanics in comparison to the western plateau; while CaO/Al_2O_3 values overlap, units from Tepi and Injibara (western plateau) are displaced to lower values than the eastern plateau (Fig. 16), which may reflect the impact of deep clinopyroxene fractionation on lavas erupted on the western plateau, though the current evidence remains ambiguous. Tepi lavas exhibit further complexity with a group of lavas exhibiting a notable enrichment in LREE (Fig. 20), and a distinctive primitive mantle normalized pattern characterized by a Zr-Hf and Ti depletion in some samples (Fig. 21). Importantly, Pliocene lavas from the Bale Mountains area (Eastern Plateau) exhibit the same pattern with a distinctive negative Zr-Hf anomaly. The presence of a mild negative K anomaly in these Bale lavas has been interpreted as the influence of a metasomatic (amphibole-bearing) source in the origin of these lavas (Nelson et al., 2019). With time, this source became exhausted and quaternary volcanic rocks in this region exhibit a more typical Type III lava signature. The negative Zr-Hf signature evident at Tepi and in Pliocene Bale is also likely metasomatic in origin, however the similar Zr/Hf of these lavas in comparison to the less enriched lavas and only marginal differences in Ti/Eu are do not support a carbonatite-based metasomatic agent. Negative Zr-Hf anomalies are discussed in more detail in the subsequent synthesis volume on the Craton and are there interpreted as evidence for apatite in the source of such lavas (among other phases – see Nelson et al. 2019), consistent with slightly elevated P_2O_5 in these enriched samples at Tepi (0.63 to 0.89 wt. % vs 0.30 to 0.70 wt. %).

Isotopic data from these regions is somewhat limited. The trachyte plugs from Lake Tana would seem to be significantly contaminated in terms of $^{87}Sr/^{86}Sr$ (up to 0.73, and are not shown due to scale compression issues), however this contamination is not accompanied by a commensurate contamination in terms of $^{143}Nd/^{144}Nd$ (Fig. 16). The age of these plugs is

assumed to be Quaternary at present (Meshesha and Shinjo, 2007), but it should be noted that the high Rb/Sr (~22) of these samples could generate significant isotopic in-growth if these samples are older than currently assumed. The sparse existing isotopic data are consistent with an Afar Plume, Depleted Mantle, and Pan-African lithosphere model for the origin of these rocks (Fig. 16), though far more data is required to fully assess this and establish the influence of any potential metasomatic contribution (in particular from Tepi). One sample from Tepi plots towards unradiogenic values of $^{87}Sr/^{86}Sr$ that might suggest a contribution from a HIMU-like metasome – it is notable that this sample is also one that displays the negative Zr-Hf anomalies discussed above. On the Eastern Plateau, Pliocene Bale Mountains samples (interpreted to have a metasomatic influence) have isotopic characteristics that do not suggest a HIMU-like metasome, instead these samples isotopically resemble Type III lavas from the MER and may suggest a more recent metasomatic overprint associated with the Afar Plume (Nelson et al., 2019). Quaternary lavas from the Bale Mountains exhibit more plume-like isotopic compositions, suggestive of either derivation from the convecting upper mantle or anhydrous metasomes within the convecting upper mantle (Nelson et al., 2019)

7.4 Summary

The Stratoid Series Phase is characterized by an initial period of fissural basaltic activity that subsequently transitions to lower flux events such as shield volcanism in Turkana, or zones of focused magmatism in the Main Ethiopian Rift. The extant geochemical data for this period suggests that the primary origin of these events is through melting of the sub-lithospheric mantle and is interpreted in the context of a significant non-synchronous decompression melting event along the rift. For the Gombe Stratoid Series in particular, the homogeneity in erupted compositions suggest an efficient (and thus mature) magma hybridization system – consistent with a high magma flux event. The subsequent transition to a more diverse range of

incompatible trace element enriched lavas that comprise the later shields is suggestive of a decrease in magma flux.

Away from the rift axis, lavas on the Eastern and Western Ethiopian Plateaus exhibit signatures that indicate melting of geochemical reservoirs that are equivalent to those feeding magmatism within the rift. However, perturbation of the incompatible trace element ratios within these plateau lavas reflects melting and assimilation of metasomatic phases by these magmas as they traverse the lithosphere. While speculative, these observations could be interpreted as a lower volume of melt entering the lithosphere along the rift margins that may not have organized into lithosphere-traversing channels and may thus be more prone to assimilating metasomes within the lithospheric mantle.

In conclusion, the geochemical characteristics of lavas erupted during the Stratoid Series Phase appear to indicate that differences in magma flux into the lithosphere can significantly impact the composition of erupted lavas. Further detailed work is necessary to revolve crustal, lithospheric mantle, and sub-lithospheric mantle processes, but such studies will likely yield important insights into the relationship between extension and magma generation.

8. The Axial Phase (0.5 Ma to present)

Throughout the Kenya and Main Ethiopian Rift, the most recent phase of magmatic activity has manifested as small volume basaltic flows/cinder cone chains and larger central silicic volcanoes. This magmatic activity is typically restricted to axial or marginal grabens. As such, the modern magmatic system forms an interconnected chain of activity. To facilitate discussion of this phase of rift development, magmatic sectors have been named – typically after the large silicic volcano within that rift sector. This section is thus arranged in a discussion of the individual sectors throughout the eastern branch of the EARS.

8.1 Turkana and North Kenya Rift

Modern magmatism (ca. 0.5 Ma to present) in the region is focused in a series of narrow grabens that occur along the axis of the Kenya Rift, and in an array of fissure eruptions along the eastern margin (Fig. 22). Within the rift, basaltic eruptions form either as a late stage capping sequence on dominantly trachytic volcanoes, or as fissural eruptions along the volcano flanks and on the rift floor. Magma flow along the plumbing systems of the large silicic volcanoes during inflation and deflation events has been detected by INSAR (Biggs et al., 2009). Below I outline axial magmatic activity in discrete sectors as it occurs along the axis of the rift from south to north:

8.1.1 Korosi and Baringo

Volcanic activity at Korosi is predominantly comprised of peralkaline trachyte lavas that began at 0.380 Ma (± 0.007 $^{40}Ar/^{39}Ar$) (Dunkley et al., 1993). More recent dating has suggested a slightly different range of 0.364 Ma (± 0.021) to 0.092 Ma (+/ 0.005) (Clément et al., 2003). The early phase of activity is termed the 'Shield Formation', while the later phase is termed 'Faulting and Fissure Activity' (Dunkley et al., 1993). Contemporaneous with Korosi are eruptions on Ol Kokwe Island within Lake Baringo (0.175 Ma ± 0.008) (Clément et al., 2003). Young basalts erupted from scoria cones along fissures and also between Korosi and Paka.

8.1.2 Paka

Paka volcano is largely trachytic with some fissural basalt eruptions. Magmatic activity commenced at 0.390 Ma (± 0.006 $^{40}Ar/^{39}Ar$) (Clément et al., 2003) and is termed the 'Shield Phase', which was followed by a series of basalt and trachyte eruptions before the ca. 10 ka caldera event (Dunkley et al., 1993). The historical evolution of Paka is not well constrained, though its geothermal potential has raised some recent interest.

8.1.3 Silali

Silali is a large, dominantly peralkaline trachytic volcano, but also has fissural basaltic eruptions emanating from its flanks (Smith et al., 1995). The timing of the initiation of Silali is unknown but the earliest magmas examined were 0.230 Ma (± 0.005 $^{40}Ar/^{39}Ar$) (Smith et al., 1995), though activity could have begun as early as 0.4 Ma (Smith et al., 1995; Macdonald, 2012). These initial events correspond to the Shield Building Phase noted above in the discussion of Paka. Following faulting events further activity is recorded at 0.132 Ma (± 0.003 $^{40}Ar/^{39}Ar$) and 0.064 Ma (± 0.002) (Dunkley et al., 1993; Smith et al., 1995). A large caldera collapse (7.5 km x 5 km) occurred ca. 0.064 Ma (Smith et al., 1995). The most recent activity is the <10 ka post caldera lavas and small scoria cones, which are parasitic on Silali and appear recent (devoid of vegetation) (Dunkley et al., 1993).

8.1.4 Emuruangogolak

Emuruangogolak is dominantly comprised of peralkaline trachytes and subordinate younger basalts, with two phases of activity: an initial phase ca. 0.5 to 0.9 Ma; and a second phase commencing 0.205 Ma (±0.004 $^{40}Ar/^{39}Ar$) (Dunkley et al., 1993). Caldera formation occurred around 0.038 Ma and was followed by some modern trachyte and basalt lavas, including tuff and scoria cones (Dunkley et al., 1993).

8.1.5 Namarunu

Similar to the nearby Emuruangogolak, Namarunu is thought to have two phases of magmatic activity. Dunkley et al. (1993) noted that the majority of Namarunu was constructed during the Pliocene, but that after 0.871 Ma (± 0.01 $^{40}Ar/^{39}Ar$) a renewed phase of activity was coincident with rhyolite and trachyte lavas. This more evolved magmatic activity continued until a large-scale basaltic eruption after 0.509 Ma (± 0.005 Ma $^{40}Ar/^{39}Ar$). It is thus important to note that the lower portions of Namarunu are equivalent to the Lorikipi Basalts and are discussed in prior sections.

8.1.6 Barrier

The Barrier volcano is comprised of a composition of basalt-trachyte-phonolite (and other compositions), and is made up of 4 volcanic centers (Kalolenyang, Kakorinya, Likaiu West, Likaiu East) and two parasitic cinder cones (Andrew's and Teleki's) (Dunkley et al., 1993). The volcano is built upon the Logipi/Latarr basalts over which trachyte lavas began erupting ca. 1.37 Ma and continued to recent times (Dunkley et al., 1993). Trachytes associated with Likaiu East (1.37-1.34 Ma), are followed by mugearite, basalts, and trachytes associated with Kalolenyang at ca. 0.773 to 0.707 Ma. Likaiu West is dominated by basalts and trachytes, while Kakorinya is more recent, beginning at 0.221 Ma and continuing to today and erupting a wide range of compositions.

8.1.7 Turkana Islands and Highlands

Modern activity in Turkana is comprised of what have been termed 'axial' volcanic centers that continue from the Kenya rift through Lake Turkana, but also and fissural/cinder cone activity on the previously developed Pliocene Shields that dominate the eastern parts of the Turkana Depression. North of the Barrier complex (described previously) the volcanoes of South Island, Central Island, and North Island mark the most recent activity in the Lake Turkana region (Karson and Curtis, 1994). The composition of lavas within these volcanoes is variable and ranges from dominantly basaltic (South Island) to trachytic tuffs (North Island) (Brown and Carmichael, 1971). Modern volcanism continues into Southern Ethiopia but is no longer en-echelon with the alignment of the volcanoes of the Kenya Rift. The next volcanic region within the rift is the Korath field (Brown and Carmichael, 1969). This 'axial' volcanism thus appears to connect the MER and Kenya Rift (e.g., Corti et al., 2019), however the quaternary expression of magmatism in this region is more complex.

East of Lake Turkana, there is abundant volcanism that has developed as smaller, aligned monogenetic cones/maars and associated flows. This activity is well-developed on top of the previously described Pliocene Shield volcanoes that continue into Ethiopia. Cinder cones on the Huri Hills Shield volcano continue to the northeast as the Mega/Sidamo field in Ethiopia. Other monogenetic volcanic fields of similar age (e.g. Dukana, ~0.9 Ma) (Key and Watkins, 1988) may occur between the shield volcanoes. The existence of these diverse regions of Quaternary volcanism, whose surface expression mirrors the axial volcanism elsewhere in the rift, suggests a much wider zone of lithospheric instability. Indeed a model of a complex junction between the MER and northern Kenya Rift that occurs throughout the Northern Turkana basin (e.g., Ebinger et al., 2000) might be consistent with these observations. Further work is required to constrain the magmatic system and its relationship to the evolving strain field.

8.2 Geochemical variation of modern volcanism in the North Kenya Rift

For the Northern Kenya Rift there are sufficient data for each rift sector of the rift to warrant separate symbols and treatment in the data plots. No obvious latitudinal geochemical variation is evident within the modern axial lavas of the Northern Kenya Rift (Fig. 23). In terms of major and trace element variation versus MgO, lavas from the northern Kenya Rift largely overlap (Fig. 23). There is some minor variability between sectors – lavas at Silali and Emuruangogolak have elevated CaO/Al_2O_3 and TiO_2 in comparison to Baringo or Namarunu. Such variation is likely related to a greater role for titaniferous clinopyroxene in the latter group in comparison to the former. Distinct positive Eu anomalies are evident at Silali, which also exhibits the greatest degree of incompatible element enrichment (Fig. 24). Lava from other rift sectors largely exhibit the same slope and degree of enrichment (Fig. 24). Most lavas within the Kenya Rift exhibit a general Type III magma pattern in terms of primitive mantle normalized values. These patterns are particularly well-developed in Silali and Korosi (Fig. 25). There are, however, differences in

the degree of Ba and Nb-Ta enrichment within Namarunu, which exhibit marked enrichments in Nb-Ta but frequently occur without an equivalent enrichment in Ba as would be expected in a typical Type III magma (Fig. 25). This characteristic can be assigned to the Type IV lava category as described in more detail below in Turkana where this magma type is pervasive).

In a similar manner to the earlier lava series, lavas from the Northern Kenya Rift exhibit a correlation between the degree of magma evolution and more radiogenic $^{87}Sr/^{86}Sr$, with limited co-variation in $^{143}Nd/^{144}Nd$ (Fig. 26). This radiogenic Sr component is particularly well-developed within trachytic magmas erupted in the Silali region (Macdonald et al., 1995). This observation suggests continued involvement of a crustal assimilant with elevated $^{87}Sr/^{86}Sr$ in the Northern Kenya Rift. For more mafic samples, there is substantial overlap between the different rift sectors in the Northern Kenya Rift, caused in part by the limited range of $^{143}Nd/^{144}Nd$ values in comparison to the earlier time phase in this region. In terms of Pb isotopes, Korosi and Paka (in the southern most parts of the Northern Kenya Rift) exhibited the least radiogenic values of $^{208}Pb/^{204}Pb$-$^{206}Pb/^{204}Pb$, while more northerly sectors extend to much more radiogenic values (Fig. 26). Clément et al. (2003) suggest that the Baringo area lies at the boundary between the Pan-African Mobile Belt lithospheric domain and the Tanzania Craton Domain, and that the composition of lavas are strongly controlled by these lithospheric domains. These observations mirror the conclusions of Rogers et al. (2000) and MacDonald et al. (2001) who suggest the geochemical composition of erupted lavas is controlled by the interaction of asthenospheric melts with metasomatized lithospheric mantle. An alternative proposed mechanism is the incorporation of lithospheric material into the upper mantle and the subsequent melt generation in an upwelling and melting mantle (Rogers et al., 2006).

8.3 Geochemical variation of modern volcanism in Turkana

Lavas from Turkana fall into two categories – the typically incompatible trace element (e.g. Zr, Nb) and TiO_2 enriched varieties evident in the Huri Hills – Mega, and the less enriched varieties that are common to the Lake Turkana region (Fig. 23). Huri Hills – Mega samples tend to be more mafic while the less incompatible element enriched lavas from Lake Turkana span an array of compositions towards evolved endmembers. North Island exhibits only more evolved compositions (not divided in figures). Lavas from the Lake Turkana region display remarkable coherency in terms of enrichment, forming a linear array in Zr-Nb vs La/Yb, suggesting a derivation from the same source via different degrees of melting (Fig. 23). Lavas from the Huri Hills – Mega region of this figure do not lie along the linear extension of the Lake Turkana data. Moreover, the elevated Tb/Yb in these samples suggests a different source to the Lake Turkana samples (Fig. 23). These patterns are also evident in terms of chondrite normalized patterns that show a much steeper pattern in Huri Hills – Mega in comparison to Lake Turkana (Fig. 24). An exception are samples from Birds Nest vent (adjacent to Central Island in Lake Turkana), where lavas exhibit enrichments similar to the Huri Hills – Mega samples (Fig. 24, 25). Primitive mantle normalized figures show patterns that are similar between the different regions (Fig. 25). This pattern is unusual in having only a moderate Ba peak and a very pronounced positive Nb-Ta anomaly (Fig. 25). This lava pattern is observed elsewhere in the Eastern Branch of the East African Rift and is deserving of its own type category. I name this pattern Type IV – joining the existing three categories outlined in the first volume of this synthesis. Type IV lavas are likely the result of mixing of a Type II and Type III lava as the same pattern can be produced through simple mixing. Such an origin may explain the complex isotopic characteristics described below. Lavas from Barrier show a composition closer to Type III and have some negative Zr-Hf anomalies (Fig. 25).

It is unclear if there is an isotopic correlation between these magma types, however for more mafic lavas (>5 wt. % MgO), $^{206}Pb/^{204}Pb$ for Barrier and Birds Nest (both exhibiting some degree

of potential metasomatic influence given the negative Zr-Hf anomaly) exhibit more radiogenic values in comparison to Central Island. (Fig. 26). Lavas from Huri Hills – Mega also exhibit this radiogenic $^{206}Pb/^{204}Pb$. It should be noted that lavas from South Island, while below 5 wt. % MgO, occupy the same isotopic space as Barrier and thus any link between the magma types and isotopic characteristics remains ambiguous at present (Fig. 26). Such observations require further exploration of the sources of magmatism in this region.

8.4 Main Ethiopian Rift

This phase is also coincident with the formation of large silicic central volcanoes and basaltic cinder cone chains dominantly following magmatic-tectonic lineaments within the rift termed the 'Wonji Fault Belt' (Mohr, 1967) and Silti Debre Zeyit Fault Zone (WoldeGabriel et al., 1990). Note that the town of Debre Zeyit was until the late 1970s and again is now called Bishoftu, similarly with Adama and Nazret, however the intervening geologic names based on these locales have been retained. Rift development during this phase has been described in terms of the formation of 'magmatic segments' throughout the rift that connect to the axial system within the southern MER. Most modern studies refer to these regions of focused magmatic and tectonic activity as 'rift segments', however this nomenclature is potentially problematic as it evokes comparison with mid-ocean ridge systems where magma supply is an important factor controlling segmentation. The still thick continental crust in the Ethiopian Rift (ca. 35 km, and in much of Afar ca. 25 km) (Maguire et al., 2006) must play a significant role in the formation of 'segments'. The surface expression of these zones of focused magmatic intrusion differ from their oceanic cousins and the lack of parallelisms in the processes which form them require caution in how they are described. Similarly, zones of focused magmatic intrusion within the rift may sometime resemble oceanic spreading features, though are formed by different processes (Bridges et al., 2012; Rooney et al., 2014a). Furthermore, in some regions of the rift, where no

segments have been noted previously, the assignment of segments becomes problematic (Rooney et al., 2011). In this contribution I avoid the use of the term segment and instead speak of rift sectors.

Previous studies have noted en echelon magmatic sectors within the Main Ethiopian Rift (Gibson, 1969, 1974; Casey et al., 2006; Rooney et al., 2011) that extend from Arba Minch in the south to the Tendaho-Goba'ad discontinuity in the north, thus forming a semi-continuous chain of modern basaltic activity throughout the Eastern Branch of the East African Rift (Fig. 27) (Mohr and Wood, 1976). These en-echelon belts are offset towards the rift margins and are defined as the Wonji Fault Belt (WFB) and the Silti Debre Zeyit Fault Zone (SDFZ) (Rooney et al., 2005, 2007, 2011). The SDFZ is restricted to the central Main Ethiopian Rift, while the WFB continues in a rift-central orientation into Afar (Mohr, 1967; Ebinger and Casey, 2001; Ayalew et al., 2016). The primitive basaltic lavas erupting from scoria cones in the Wonji Fault Belt (Trua et al., 1999; Peccerillo et al., 2003; Rooney et al., 2007; Rooney, 2010; Ronga et al., 2010; Ayalew et al., 2016) and Silti Debre Zeyit Fault zone (WoldeGabriel et al., 1990; Gasparon et al., 1993; Rooney et al., 2005, 2012a, 2012b; Rooney, 2010) have provided important constraints on modern mantle conditions in the northern rift and conditions of melt ponding within the lithosphere (Mazzarini, 2004; Mazzarini et al., 2004, 2013). The silicic volcanic centers (which dominate the WFB and SDFZ) are typically peralkaline rhyolite to trachyte in composition, caldera-forming (5-15 km), and have a history of multiple explosive eruptive events (Fontijn et al., 2018). Volcanic centers along these lineaments show similar patterns of volcano growth, edifice collapse, and a later resurgence (Hutchison et al., 2016a). Critically, volcanic events between ca. 781 to 126 ka exhibit cyclic patterns of magmatic activity consistent with flare-up events between 320 and 170 ka, and are now in a post-caldera phase of magmatic activity (Mohr et al., 1980; Hutchison et al., 2016a). Siegburg et al. (2018) has provided new, very detailed, constraints on the Boset-Bericha Volcanic complex within the central Main

Ethiopian Rift and shows that the recent stratovolcano in that area develops only over the past 120 ka, and suggests a ca. 100 ka cyclicity in the silicic systems. These magmatic events within the rift floor have spread tephra to the adjacent plateaus where preliminary dates from 1.6 to 0.7 Ma have been reported (Resom et al., 2018).

8.4.1 Korath

Within the Southern Main Ethiopian Rift the Korath range is grouped with the Nakwa formation (Davidson, 1983), and is a dominantly basanite-tephrite composition (Brown and Carmichael, 1969). The abundant cinder cones are aligned with the border faults of the Turkana depression (Brown and Carmichael, 1969). Recent high precision dating of the range indicates an age of 0.091 Ma (± 0.015 $^{40}Ar/^{39}Ar$) (Jicha and Brown, 2014).

8.4.2 Arba Minch/Tosa Sucha

The most significant feature in this region is Mt. Bobem, a 0.68 Ma (± 0.03) trachybasalt volcano (Ebinger et al., 1993). The volcano has been dissected by faulting and has eruption of recent olivine basalts (Nech Sar Basalts)(George and Rogers, 1999). Basalts in this area show evidence of mixing with more evolved magmas (Rooney, 2010).

8.4.3 Diguna and Butajira

North of Arba Minch, the Diguna and Butajira sectors of the rift are characterized by chains of basaltic cinder cones, which are aligned with the north-northeast trending faults along the western margin of the rift. Within this sector are two silicic volcanoes: Diguna (Duguna) and Hobicha caldera. Fractionation of the basaltic lavas erupted in the Butajira sector is at deeper levels in the crust than that of the contemporaneous WFB (Rooney et al., 2005). These sectors are considered part of the Silti Debre Zeyit Fault Zone (SDFZ).

8.4.4 Debre Zeyit/Bishoftu

The Debre Zeyit (Bishoftu) volcanic field is comprised of aligned maars and cinder cones like the sections further south. Cinder cones at Debre Zeyit contain abundant megacrysts and also rare mantle xenoliths (Rooney et al., 2005). Along the Silti-Debre Zeyit Fault Zone (SDFZ), the primary silicic edifices are the rhyolitic Bede Gebabe, and trachytic Zikwala/ Ziqualla (Gasparon et al., 1993). Ziqualla has been dated to between to 1.28 Ma (± 0.15) and 0.85 Ma (± 0.05) (Morton et al., 1979).

8.4.5 Shala

This magmatic sector of the rift has only sparse basaltic volcanism (Rooney, 2010) and is instead dominated by calderas of Hawassa (Wilks et al., 2017), Corbetti (Di Paola, 1971; Mohr et al., 1980; Hutchison et al., 2016a) and Shala (also known as O'A) (Mohr et al., 1980; Hutchison et al., 2016a). Hawassa was the source a recent earthquake event but the caldera is older than most in this region and dates to 0.47 Ma (± 0.02) to 1.27 Ma (± 0.1) (WoldeGabriel et al., 1990). Corbetti has been active since at least 0.182 Ma (± 0.028 $^{40}Ar/^{39}Ar$) (Hutchison et al., 2016a) with an eruption in the past ca. 2300 years (Rapprich et al., 2016). Shala commenced activity at 0.280 Ma (± 0.01), while nearby basalts are dated to between 0.86 Ma (± 0.15) to 0.35 Ma (± 0.04) (Mohr et al., 1980).

8.4.6 Aluto-Gedemsa

This sector has a significantly greater volume of basaltic magmas, which are typically associated with cinder cones that are aligned along faults (Trua et al., 1999; Peccerillo et al., 2003; Furman et al., 2006a; Rooney, 2010). This rift sector contains the silicic centers of Gademotta (Morgan and Renne, 2008), Aluto (Trua et al., 1999; Biggs et al., 2011; Hutchison et al., 2015, 2016a, 2016b; Gleeson et al., 2017), Tullu Moye (Di Paola, 1972; Gouin, 1979; Trua et al., 1999), and Gedemsa (Peccerillo et al., 2003). Gademotta has been dated to 0.276 Ma (±

0.004 $^{40}Ar/^{39}Ar$) (Morgan and Renne, 2008). Gedemsa has been active from 0.319 Ma (± 0.02) to 0.265 Ma (± 0.02), while Aluto dates from 0.316 Ma (± 0.019 $^{40}Ar/^{39}Ar$) to ^{14}C dates in the past 400 years (Hutchison et al., 2016b, 2016a). Tullu Moye is a small recent edifice with multiple historic to subhistoric eruptions.

8.4.7 Boseti-Kone

This sector lies on northeast side of the Boru-Toru Structural High (Abebe et al., 1998), and thus is located within the northern Main Ethiopian Rift. This sector in particular has massive volumes of basalts erupted from aligned cinder cones. These basalts (and those of the Aluto-Gedemsa sector to the south), exhibit relatively shallow fractionation pathways in comparison to those from the Silti-Debre Zeyit fault zone (Rooney et al., 2007). The major silicic centers are: Boku (Boccaletti et al., 1999; Tadesse et al., 2018); Boset-Bericha (Boccaletti et al., 1995, 1998; Ronga et al., 2010; Macdonald, 2012; Siegburg et al., 2018), and Kone (Cole, 1969; Furman et al., 2006a; Rampey et al., 2010, 2014). The Boset-Bericha (also Berecha) edifice had originally been dated to 0.21 Ma (± 0.01)(Morton et al., 1979) from a nearby cone, though modern work constrains the twin volcanoes of Gudda and Bericha to have commenced their most recent stage of activity at 0.120 Ma (± 0.006 $^{40}Ar/^{39}Ar$) (Siegburg et al., 2018). It should be noted that this edifice has an older magmatic cycle that requires further examination (Siegburg et al., 2018).The Boset-Bericha volcanic center is unusual for this portion of the MER given it is comprised of a stratovolcano (and not calderas) (Siegburg et al., 2018). Fissure basalt eruption at Kone occurred as recently as 1810 CE, with radiogenic age constraints that come from obsidians at 0.391 Ma (± 0.01 $^{40}Ar/^{39}Ar$) to 0.395 Ma (± 0.008 $^{40}Ar/^{39}Ar$) (Vogel et al., 2006). Magmatic activity in the Boku edifice is constrained by the age of the derivative Boku Tede unit (Boccaletti et al., 1999), which is dated from 0.83 Ma (± 0.02) to 0.61 Ma (± 0.04) (Morton et al., 1979).

8.4.8 Fantale-Dofan

Within this sector, basaltic volcanism once again declines in volume, and where present near the silicic centers, can exhibit evidence of cumulate assimilation (Rooney et al., 2007). The major edifices are Dofan (Furman et al., 2006a; Ayalew et al., 2016), and Fantale (Gibson, 1974; Giordano et al., 2013). The age of Dofan remains unconstrained, though Fantale (also Fanta ‘Ale) is dated to ca. 0.168 Ma (± 0.038) using fission track methods (Williams et al., 2004).

8.4.9 Angelele-Hertali

This is an unusual sector of the rift given it appears to lack a large silicic center and instead, Hertali (which may be a basaltic shield volcano: Ayalew et al., 2016; Varet, 2017), dominates the landscape. Elsewhere in this sector, hyaloclastite and basaltic flows emanating from fissures are evident in satellite imagery (Varet, 2017). No geochronological controls are available for this region, though it is currently active (see Smithsonian Institution Global Volcano Database).

8.4.10 Adda’do

This sector is dominated by the twin volcanoes of Ayelu-Adwa (also Amoisa, and Abida) and Yangudi volcano. Varet (2017) suggest an age of 0.5 Ma for the base of Ayelu volcano, which is dominantly composed of rhyolitic flows. The younger volcano (Adwa) has had historic eruptions; pyroclastic deposits from these events blanket the area (Varet, 2017). Yangudi volcano is also a rhyolitic stratovolcano, though it has a range of compositions that extend to basalt (Varet, 2017). Scoria cones occur along the flanks of both volcanoes.

8.4.11 Gabillema

This sector of the rift could be subsumed into the Adda’do sector above given that it lies within the Adda’do graben. However, other papers have shown this region as a distinctive rift sector (e.g., Casey et al., 2006) and thus we retain such division here. This sector has until now been unnamed, and we thus adopt ‘the Gabillema’ sector after the silicic volcano located there.

Gabillema volcano is a rhyolite stratovolcano but it surrounded by recent basaltic lava fields. Rhyolite domes are also associated with this volcano (Varet, 2017). No geochronological constraints are available. The Gabillema sector intersects the Tendaho Goba'ad discontinuity in Afar, linking the East African Rift with the Red Sea and Gulf of Aden spreading axes. Further discussion of other rift sectors in Afar can be found in part IV of this synthesis.

8.5 Geochemical characteristics of MER sectors

Quaternary lavas erupted along the axis of the MER from Gabillema to Arba Minch display variations in their geochemical behavior consistent with heterogeneous melting characteristics, and different evolution pathways within the lithosphere. The wide spread in TiO_2 distribution with MgO, which is correlated with CaO/Al_2O_3, is evidence for the variable influence of clinopyroxene within the fractionation products of the rift lavas (Fig. 28). This phenomenon results in strong clinopyroxene control of the Debre Zeyit lavas, in contrast to the more olivine-plagioclase control on Fantale-Dofan lavas (Rooney et al., 2005, 2007). These heterogeneous differentiation pathways have been linked with deeper (cpx) versus shallower (ol-plag) depths of stalling within the continental crust (Rooney et al., 2005, 2011; Mazzarini et al., 2013). In regions of the rift where the magmatic plumbing system is well-developed, magmas rise rapidly and stall and shallow depths such as within the Boseti-Kone and Fantale-Kone sectors of the rift (Rooney et al., 2007). In contrast, where the magmatic system is less well-developed (e.g., SDFZ at Debre Zeyit), fractionation occurs at deeper levels within the crust (Mazzarini et al., 2013).

The degree to which the magmatic system has developed within any rift sector has implications for melt generation within the upper mantle. Given that adiabatic melting is occurring beneath the rift, well-developed sectors (where extension is focused) would naturally erupt lavas resulting from a greater degree of mantle melting. On the basis of this hypothesis,

trace element concentrations in erupted lavas should record sympathetic differences (assuming a similar source material). Inspection of incompatible trace element variation with MgO (e.g., Nb; Fig. 28) suggest differences in the primitive lavas parental to the various suites – an observation that is consistent with the fractionation evident in chondrite normalized diagrams (Fig. 29), and select trace element ratios (Fig. 28). Zr/Nb-La/Yb variation for lavas above 5 wt. % MgO shows a sample distribution whereby the most northerly samples of the MER (i.e those within the Afar Depression at Adda'do-Hertali) are the most depleted in terms of the more incompatible trace elements (Fig. 28; Fig. 30). Lavas erupted in the very south of the MER (i.e., those from Arba Minch and Korath) exhibit the greatest incompatible trace element enrichment (Fig. 28). All lavas erupted along the MER (with 1 exception) exhibit Type III lava characteristics (Fig. 31), suggesting a derivation from a potentially similar source. The exception is the Korath sector, where the extended trace element data needed for classification is absent. While the hypothesis of differential degree of melting based upon proximity to Afar is appealing, the isotopic observations are more complex.

Little evidence of crustal assimilation is evident in lavas that are > 5 wt. % MgO (Fig. 28), and we thus we focus our discussion on these less evolved lavas (Fig. 32). In a general sense, there is a correlation between the more radiogenic $^{206}Pb/^{204}Pb$ values in a lava and its proximity to Afar – lavas from Hertali-Adda'do plot at radiogenic values close to the Afar plume, while samples from Butajira and Aluto-Gedemsa (in the south) plot at less radiogenic values (Fig. 32). The endmember with less radiogenic $^{206}Pb/^{204}Pb$ isotopes is not simply Pan-African lithosphere, as samples from Butajira are deflected to lower $^{87}Sr/^{86}Sr$ than many samples to the north, and $^{143}Nd/^{144}Nd$-$^{176}Hf/^{177}Hf$ isotope values that overlap Fantale-Dofan (Fig. 32). These data are consistent with the existing model proposed in this region of ternary mixing of a plume, depleted mantle, and Pan-African lithosphere (Rooney et al., 2012a). In this model, the depleted upper mantle is variably contaminated with the Pan-African lithosphere component that may be mixed

in to the upper mantle due to lithospheric instabilities (Furman et al., 2016). Such a model explains the less radiogenic $^{206}Pb/^{204}Pb$ values in Butajira samples as reflecting a greater contribution from the depleted upper mantle. While a ternary mixing model effectively explains the isotopic characteristics of the rift sectors north from Butajira to Afar, data from Arba Minch is inconsistent with this melt generation process. For Arba Minch, extremely radiogenic values of $^{206}Pb/^{204}Pb$ are combined with unusually unradiogenic values of $^{87}Sr/^{86}Sr$ (Fig. 32) and suggest the involvement of a HIMU-like reservoir in the genesis of the magma suite that may be located in the lithospheric mantle (George and Rogers, 1999). The influence of such a reservoir is consistent with similar isotopic compositions evident in Quaternary magmas further south in the East African Rift (Class et al., 1994; Furman et al., 2004).

9. Conclusions

From ca. 20 Ma until today, extension within the African lithosphere has had a dominant impact on the distribution of magmatism within Northern Kenya Rift, the Main Ethiopian Rift, and Turkana Depression. Despite the geographic separation between the Northern Kenya Rift and Main Ethiopian Rift, the manifestation of magmatism within both has exhibited remarkable parallelism and hints at a plate-level control on rift evolution rather than stress fields within individual basins. When interpreted in unison, the extant data from this portion of East Africa reveals six dominant magmatic phases:

A) *The Samburu Phase (ca. 20 Ma – 16 Ma)*. This phase, which resulted in the widespread eruption of basalts throughout the Northern Kenya Rift, Southern Ethiopia, and parts of Turkana, may be contiguous with the previously identified Early Miocene Resurgence Phase (ca. 23 Ma), though further geochronology is necessary to test this hypothesis.

B) *The Flood Phonolite and Silicic Eruptives Phase (16 Ma – 12 Ma).* This phase represents a period of widespread evolved volcanism, consisting of phonolite flows in Northern Kenya, and explosive silicic eruptions in the Main Ethiopian Rift. While volcanism is evident in Turkana during this phase, it is significantly less pronounced than the activity further south within the nascent rift.

C) *The Mid-Miocene Resurgence Phase (12 Ma – 9 Ma).* This dominantly basaltic phase of activity appears centered on the Turkana Depression, and the northern termination of the MER near Afar. While this basaltic event has been previously recognized at individual locations, it is much more extensive than heretofore understood. This phase of activity appears linked with extension in both sectors.

D) *The Early Rift Development Phase (9 Ma to 4 Ma).* This phase of activity sees the return of bimodal activity, with basalts and trachytes erupting alongside large-scale silicic volcanism. Magmatic activity during this phase was centered on the Main Ethiopian Rift and Kenya Rift. During this phase there is a hiatus in volcanism in the Turkana Depression. The distribution of magmatic activity points towards a focusing of volcanism on the evolving rifts, and may suggest a parallel focusing of strain within these rifts during this phase.

E) *The Stratoid Phase (4 Ma – 0.5 Ma).* The volcanic maxima during this phase of activity is temporally heterogeneous throughout the region. The initial manifestation of this event is in Turkana/ southern Ethiopia with the eruption of the laterally extensive Gombe Group at about 4 Ma. Magmatism continued subsequently in Turkana with the building of extensive shield volcanoes. In the north Kenya Rift, fissural trachytic volcanism flooded the rift floor between ca. 2 Ma and 0.8 Ma. Similar activity during this interval is recorded in the Main Ethiopian Rift with the eruption of the extensive Bofa Stratoid series.

F) *The Axial Phase (0.5 Ma – Present).* This phase of activity produced silicic central volcanoes located within the axial grabens of the rift, in most cases with caldera-forming

eruptions. Subordinate basaltic volcanism is also evident as parasitic cinder cones and fissures located upon the silicic central volcanoes but also extending on the rift floor between these volcanoes. These cinder cones are frequently aligned in a linear en-echelon form, attesting to structural control on their distribution.

Phases of magmatic activity since 20 Ma in the Main Ethiopian Rift and the northern Kenya Rift have been synchronous, though in many instances with differing proportions of mafic and silicic volcanic products. Three major basaltic events occurred at ca. 20 Ma, 12-9 Ma, and 4-0.5 Ma, each followed by dominantly silicic events at 16-12 Ma, 9-4 Ma and 0.5 Ma-Present. The cyclic nature of this magmatism suggests that models of progressive rifting require accommodation to either discontinuous strain-rate, or to non-linear responses of the lithosphere to strain, or both. However, in the Turkana Basin that separates the rifts to north and south these phases occurred slightly earlier, until unification followed with the youngest basaltic and silicic phases. The temporal offsets in the older Turkana phases may have implications for the regional pattern of mantle melting. Within the evolving rifts there has been a progressive narrowing of the zone of volcanic emission.

Much more work is needed to constrain how each of these cycles initiate, evolve, and eventually transition into to the next phase of magmatic activity. This contribution should thus serve as the starting point for future work. In an effort at literary symmetry, I will end this synthesis with appeal for future studies though another quote from Dr. Suess - “Unless someone like you cares a whole awful lot, nothing is going to get better. It's not.”

REFERENCES CITED

Abbate, E., Bruni, P., Ferretti, M.P., Delmer, C., Laurenzi, M.A., Hagos, M., Bedri, O., Rook, L., Sagri, M., and Libsekal, Y., 2014, The East Africa Oligocene intertrappean beds: Regional distribution, depositional environments and Afro/Arabian mammal dispersals: Journal of African Earth Sciences, v. 99, p. 463–489.

Abbate, E., and Sagri, M., 1980, Volcanites of the Ethiopian and Somali Plateaus and Major Tectonic Lines: Accademia Nazionale dei Lincei: Geodynamic Evolution of the Afro-Arabian Rift System: Meeting, v. 47, p. 219–227.

Abebe, B., Acocella, V., Korme, T., and Ayalew, D., 2007, Quaternary faulting and volcanism in the main Ethiopian Rift: Journal of African Earth Sciences, v. 48, p. 115–124.

Abebe, T., Manetti, P., Bonini, M., Corti, G., Innocenti, F., Mazzarini, F., and Pecksay, Z., 2005, Geological map (scale 1:200,000) of the Northern Main Ethiopian Rift and its implications for the volcano-tectonic evolution of the rift: Geological Society of America.

Abebe, T., Mazzarini, F., Innocenti, F., and Manetti, P., 1998, The Yerer-Tullu Wellel volcanotectonic lineament; a transtensional structure in central Ethiopia and the associated magmatic activity: Journal of African Earth Sciences, v. 26, p. 135–150.

Asfaw, B., Beyene, Y., Semaw, S., Suwa, G., White, T., and WoldeGabriel, G., 1991, Fejej: a new paleoanthropological research area in Ethiopia: Journal of Human Evolution, v. 21, p. 137–143.

Ayalew, D., Jung, S., Romer, R.L., and Garbe-Schönberg, D., 2018, Trace element systematics and Nd, Sr and Pb isotopes of Pliocene flood basalt magmas (Ethiopian rift): A case for Afar plume-lithosphere interaction: Chemical Geology, v. 493, p. 172–188, doi:https://doi.org/10.1016/j.chemgeo.2018.05.037.

Ayalew, D., Jung, S., Romer, R.L., Kersten, F., Pfänder, J.A., and Garbe-Schönberg, D., 2016, Petrogenesis and origin of modern Ethiopian rift basalts: Constraints from isotope and trace element geochemistry: Lithos, v. 258, p. 1–14.

Ayalew, D., Marty, B., Barbey, P., Yirgu, G., and Ketefo, E., 2005, Sub-lithospheric source for Quaternary alkaline Tepi shield, southwest Ethiopia: Geochemical Journal-Japan-, v. 39, p. 1–10.

Baker, J., Chazot, G., Menzies, M., and Thirlwall, M., 1998, Metasomatism of the shallow mantle beneath Yemen by the Afar plume - Implications for mantle plumes, flood volcanism, and intraplate volcanism: Geology, v. 26, p. 431–434.

Baker, B.H., Mitchell, J.G., and Williams, L.A.J., 1988, Stratigraphy, geochronology and volcano-tectonic evolution of the Kedong–Naivasha–Kinangop region, Gregory Rift Valley, Kenya: Journal of the Geological Society, v. 145, p. 107–116.

Baker, B.H., Williams, L.A.J., Miller, J.A., and Fitch, F.J., 1971, Sequence and geochronology of the Kenya rift volcanics: Tectonophysics, v. 11, p. 191–215.

Beccaluva, L., Bianchini, G., Ellam, R.M., Natali, C., Santato, A., Siena, F., and Stuart, F.M., 2011, Peridotite xenoliths from Ethiopia: Inferences about mantle processes from plume to rift settings, *in* Luigi Beccaluva, Gianluca Bianchini, and Marjorie Wilson eds., Geological Society of America Special Papers, Boulder, CO, v. 478, p. 77–104.

Beccaluva, L., Bianchini, G., Natali, C., and Siena, F., 2009, Continental flood basalts and mantle plumes: a case study of the Northern Ethiopian Plateau: Journal of Petrology, v. 50, p. 1377–1403.

Bellieni, G., Brotzu, P., Morbidelli, L., Piccirillo, E.M., and Traversa, G., 1986, Petrology and Mineralogy of Miocene Fissural Volcanism of the East Kenya Plateau: Neues Jahrbuch Fur Mineralogie-Abhandlungen, v. 154, p. 153–178.

Berhe, S.M., Desta, B., Nicoletti, M., and Teferra, M., 1987, Geology, geochronology and geodynamic implications of the Cenozoic magmatic province in W and SE Ethiopia: Journal of the Geological Society, v. 144, p. 213–226.

Biggs, J., Anthony, E.Y., and Ebinger, C.J., 2009, Multiple inflation and deflation events at Kenyan volcanoes, East African Rift: Geology, v. 37, p. 979–982.

Biggs, J., Bastow, I.D., Keir, D., and Lewi, E., 2011, Pulses of deformation reveal frequently recurring shallow magmatic activity beneath the Main Ethiopian Rift: Geochemistry, Geophysics, Geosystems, v. 12, p. doi:10.1029/2011GC003662, doi:doi:10.1029/2011GC003662.

Boccaletti, M., Bonini, M., Mazzuoli, R., Abebe, B., Piccardi, L., and Tortorici, L., 1998, Quaternary oblique extensional tectonics in the Ethiopian Rift (Horn of Africa): Tectonophysics, v. 287, p. 97–116.

Boccaletti, M., Bonini, M., Mazzuoli, R., and Trua, T., 1999, Pliocene-Quaternary volcanism and faulting in the northern Main Ethiopian Rift (with two geological maps at scale 1:50,000): Giardini Editore Pisa Italy (ITA) colored geologic maps.

Boccaletti, M., Getaneh, A., Mazzuoli, R., Tortorici, L., and Trua, T., 1995, Chemical variations in a bimodal magma system; the Plio-Quaternary volcanism in the Dera Nazret area (Main Ethiopian Rift, Ethiopia): Africa Geoscience Review, v. 2, p. 37–60.

Bonini, M., Corti, G., Innocenti, F., Manetti, P., Mazzarini, F., Abebe, T., and Pecskay, Z., 2005, Evolution of the Main Ethiopian Rift in the frame of Afar and Kenya rifts propagation: Tectonics, v. 24, p. TC1007, doi: 10.1029/2004TC00168.

Boschetto, H.B., Brown, F.H., and McDougall, I., 1992, Stratigraphy of the Lothidok Range, northern Kenya, and K/Ar ages of its Miocene primates: Journal of Human Evolution, v. 22, p. 47–71.

Boynton, W.V., 1984, Cosmochemistry of the rare earth elements: meteorite studies, *in* Henderson, P. ed., Rare earth element geochemistry, Amsterdam, Elsevier, p. 63–114.

Bridges, D.L., Mickus, K., Gao, S.S., Abdelsalam, M.G., and Alemu, A., 2012, Magnetic stripes of a transitional continental rift in Afar: Geology, v. 40, p. 203–206, doi:10.1130/g32697.1.

Brotzu, P., Morbidelli, L., Nicoletti, M., Piccirillo, E.M., and Traversa, G., 1984, Miocene to Quaternary volcanism in eastern Kenya: sequence and geochronology: Tectonophysics, v. 101, p. 75–86.

Brown, F.H., and Carmichael, I.S.E., 1969, Quaternary volcanoes of the lake Rudolf Region: 1. The basanite-tephrite series of the Korath range: Lithos, v. 2, p. 239–260, doi:https://doi.org/10.1016/S0024-4937(69)80018-6.

Brown, F.H., and Carmichael, I.S.E., 1971, Quaternary volcanoes of the Lake Rudolf region: II. The lavas of North Island, South Island and the Barrier: Lithos, v. 4, p. 305–323.

Brown, F.H., Jicha, B.R., and Leakey, R.E., 2016, An age for Kajong, a Miocene fossil site east of Lake Turkana, Kenya: Journal of African Earth Sciences, v. 114, p. 74–77.

Brown, F.H., and McDougall, I., 2011, Geochronology of the Turkana depression of northern Kenya and southern Ethiopia: Evolutionary Anthropology: Issues, News, and Reviews, v. 20, p. 217–227.

Brown, F.H., and Nash, W.P., 1976, Radiometric dating and tuff mineralogy of Omo Group deposits: Earliest man and environments in the Lake Rudolf Basin, p. 50–63.

Brune, S., Williams, S.E., and Müller, R.D., 2017, Potential links between continental rifting, CO2 degassing and climate change through time: Nature Geoscience, v. 10, p. 941–946, doi:10.1038/s41561-017-0003-6.

Casey, M., Ebinger, C., Keir, D., Gloaguen, R., and Mohamed, F., 2006, Strain accomodation in transitional rifts: Extension by magma intrusion and faulting in Ethiopian rift magmatic segments, *in* Yirgu, G., Ebinger, C., and Maguire, P. eds., The Afar Volcanic Province within the East African Rift System, London, Geological Society, London, v. 259, p. 143–164.

Chapman, G.R., and Brook, M., 1978, Chronostratigraphy of the Baringo basin, Kenya: Geological Society, London, Special Publications, v. 6, p. 207–223.

Chapman, G.R., Lippard, S.J., and Martyn, J.E., 1978, The stratigraphy and structure of the Kamasia range, Kenya Rift Valley: Journal of the Geological Society, v. 135, p. 265–281.

Chauvel, C., Lewin, E., Carpentier, M., Arndt, N.T., and Marini, J.-C., 2008, Role of recycled oceanic basalt and sediment in generating the Hf–Nd mantle array: Nature geoscience, v. 1, p. 64.

Chernet, T., Hart, W.K., Aronson, J.L., and Walter, R.C., 1998, New age constraints on the timing of volcanism and tectonism in the northern Main Ethiopian Rift-southern Afar transition zone (Ethiopia): Journal of Volcanology and Geothermal Research, v. 80, p. 267–280.

Chiasera, B., Rooney, T.O., Girard, G., Yirgu, G., Grosfils, E.B., Ayalew, D., Mohr, P., and Zimbelman, M.R.R., 2018, Magmatically assisted off-rift extension—The case for broadly distributed strain accommodation: Geosphere, v. 14, p. 1544–1563, doi:10.1130/ges01615.1.

Chorowicz, J., Collet, B., Bonavia, F.F., Mohr, P., Parrot, J.F., and Korme, T., 1998, The Tana basin, Ethiopia: intra-plateau uplift, rifting and subsidence: Tectonophysics, v. 295, p. 351–367.

Class, C., Altherr, R., Volker, F., Eberz, G., and Mcculloch, M.T., 1994, Geochemistry of Pliocene to Quaternary alkali basalts from the Huri Hills, Northern Kenya: Chemical Geology, v. 113, p. 1–22.

Clément, J.-P., Caroff, M., Hémond, C., Tiercelin, J.-J., Bollinger, C., Guillou, H., and Cotton, J., 2003, Pleistocene magmatism in a lithospheric transition area: petrogenesis of alkaline and peralkaline lavas from the Baringo-Bogoria Basin, central Kenya Rift: Canadian Journal of Earth Sciences, v. 40, p. 1239–1257.

Cole, J.W., 1969, Gariboldi Volcanic Complex, Ethiopia: Bulletin Volcanologique, v. 33, p. 566–578.

Conticelli, S., Sintoni, M.F., Abebe, T., Mazzarini, F., and Manetti, P., 1999, Petrology and geochemistry of ultramafic xenoliths and host lavas from the Ethiopian Volcanic Province; an insight into the upper mantle under eastern Africa: Acta Vulcanologica, v. 11, p. 143–159.

Corti, G. et al., 2019, Aborted propagation of the Ethiopian rift caused by linkage with the Kenyan rift: Nature Communications, v. 10, p. 1309, doi:10.1038/s41467-019-09335-2.

Corti, G., Sani, F., Agostini, S., Philippon, M., Sokoutis, D., and Willingshofer, E., 2018, Off-axis volcano-tectonic activity during continental rifting: Insights from the transversal Goba-Bonga lineament, Main Ethiopian Rift (East Africa): Tectonophysics, v. 728–729, p. 75–91, doi:https://doi.org/10.1016/j.tecto.2018.02.011.

Davidson, A., 1983, The Omo River Project: Reconnaissance geology and geochemistry of parts of Illubabor, Kefa, Gemu Gofa, and Sidamo: Ethiopian Institute Geological Surveys Bulletin, v. 2, p. 1–89.

Davidson, A., and Rex, D.C., 1980, Age of Volcanism and Rifting in Southwestern Ethiopia: Nature, v. 283, p. 657–658.

Deino, A.L., and McBrearty, S., 2002, 40Ar/39Ar dating of the Kapthurin Formation, Baringo, Kenya: Journal of Human Evolution, v. 42, p. 185–210, doi:10.1006/jhev.2001.0517.

Deino, A.L., Tauxe, L., Monaghan, M., and Hill, A., 2002, 40Ar/39Ar geochronology and paleomagnetic stratigraphy of the Lukeino and lower Chemeron Formations at Tabarin and Kapcheberek, Tugen Hills, Kenya: Journal of Human Evolution, v. 42, p. 117–140.

Di Paola, G.M., 1971, Geology of the Corbetti Caldera area (Main Ethiopian Rift Valley): Bulletin Volcanologique, v. 35, p. 497–506.

Di Paola, G.M., 1972, The Ethiopian Rift Valley (between 7 00′ and 8 40′ lat. north): Bulletin Volcanologique, v. 36, p. 517–560.

Dunkley, P.N., Smith, M., Allen, D.J., and Darling, W.G., 1993, The geothermal activity and geology of the northern sector of the Kenya Rift Valley:

Ebinger, C.J., and Casey, M., 2001, Continental breakup in magmatic provinces: An Ethiopian example: Geology, v. 29, p. 527–530.

Ebinger, C.J., Yemane, T., Harding, D.J., Tesfaye, S., Kelley, S., and Rex, D.C., 2000, Rift deflection, migration, and propagation: Linkage of the Ethiopian and Eastern rifts, Africa: Geological Society of America Bulletin, v. 112, p. 163–176.

Ebinger, C.J., Yemane, T., WoldeGabriel, G., Aronson, J.L., and Walter, R.C., 1993, Late Eocene-Recent volcanism and faulting in the southern main Ethiopian Rift: Journal of the Geological Society of London, v. 150, p. 99–108.

Erbello, A., and Kidane, T., 2018, Timing of volcanism and initiation of rifting in the Omo-Turkana depression, southwest Ethiopia: Evidence from paleomagnetism: Journal of African Earth Sciences, v. 139, p. 319–329.

Ferrando, S., Frezzotti, M.L., Neumann, E.R., De Astis, G., Peccerillo, A., Dereje, A., Gezahegn, Y., and Teklewold, A., 2008, Composition and thermal structure of the lithosphere beneath the Ethiopian plateau: evidence from mantle xenoliths in basanites, Injibara, Lake Tana Province: Mineralogy and Petrology, v. 93, p. 47–78, doi:10.1007/s00710-007-0219-z.

Foley, S.F., Link, K., Tiberindwa, J.V., and Barifaijo, E., 2012, Patterns and origin of igneous activity around the Tanzanian craton: Journal of African Earth Sciences, v. 62, p. 1–18.

Fontijn, K., McNamara, K., Tadesse, A.Z., Pyle, D.M., Dessalegn, F., Hutchison, W., Mather, T.A., and Yirgu, G., 2018, Contrasting styles of post-caldera volcanism along the Main Ethiopian Rift: Implications for contemporary volcanic hazards: Journal of Volcanology and Geothermal Research, v. 356, p. 90–113.

Frezzotti, M.L., Ferrando, S., Peccerillo, A., Petrelli, M., Tecce, F., and Perucchi, A., 2010, Chlorine-rich metasomatic H2O–CO2 fluids in amphibole-bearing peridotites from Injibara (Lake Tana region, Ethiopian plateau): Nature and evolution of volatiles in the mantle of a region of continental flood basalts: Geochimica Et Cosmochimica Acta, v. 74, p. 3023–3039.

Furman, T., Bryce, J.G., Karson, J., and Iotti, A., 2004, East African Rift System (EARS) plume structure: Insights from quaternary mafic lavas of Turkana, Kenya: Journal of Petrology, v. 45, p. 1069–1088.

Furman, T., Bryce, J.G., Rooney, T., Hanan, B.B., Yirgu, G., and Ayalew, D., 2006a, Heads and tails: 30 million years of the Afar plume, *in* Yirgu, G., Ebinger, C., and Maguire, P. eds., The Afar Volcanic Province within the East African Rift System, Special Publication of the Geological Society, London, v. 259, p. 95–120.

Furman, T., Kaleta, K.M., Bryce, J.G., and Hanan, B.B., 2006b, Tertiary mafic lavas of Turkana, Kenya: Constraints on East African plume structure and the occurrence of high-mu volcanism in Africa: Journal of Petrology, v. 47, p. 1221–1244.

Furman, T., Nelson, W.R., and Elkins-Tanton, L.T., 2016, Evolution of the East African rift: Drip magmatism, lithospheric thinning and mafic volcanism: Geochimica Et Cosmochimica Acta, v. 185, p. 418–434.

Gasparon, M., Innocenti, F., Manetti, P., Peccerillo, A., and Tsegaye, A., 1993, Genesis of the Pliocene to Recent bimodal mafic-felsic volcanism in the Debre Zeyt area, central Ethiopia; volcanological and geochemical constraints: Journal of African Earth Sciences, v. 17, p. 145–165.

Gathogo, P.N., Brown, F.H., and McDougall, I., 2008, Stratigraphy of the Koobi Fora Formation (Pliocene and Pleistocene) in the Loiyangalani region of northern Kenya: Journal of African Earth Sciences, v. 51, p. 277–297.

George, R.M.M., 1997, Thermal and tectonic controls on magmatism in the Ethiopian province: The Open University.

George, R., and Rogers, N., 1999, The petrogenesis of Plio-Pleistocene alkaline volcanic rocks from the Tosa Sucha region, Arba Minch, southern Main Ethiopian Rift: Acta Vulcanologica, v. 11, p. 121–130.

George, R., Rogers, N., and Kelley, S., 1998, Earliest magmatism in Ethiopia: Evidence for two mantle plumes in one flood basalt province: Geology, v. 26, p. 923–926.

Gibson, I.L., 1974, A review of the geology, petrology and geochemistry of the volcano Fantale: Bulletin Volcanologique, v. 38, p. 791–802.

Gibson, I.L., 1969, The structure and volcanic geology of an axial portion of the Main Ethiopian Rift: Tectonophysics, v. 8, p. 561–565.

Giordano, F., D'Antonio, M., Civetta, L., Tonarini, S., Orsi, G., Ayalew, D., Yirgu, G., Dell'Erba, F., Di Vito, M.A., and Isaia, R., 2013, Genesis and evolution of mafic and felsic magmas at Quaternary volcanoes within the Main Ethiopian Rift: Insights from Gedemsa and Fanta 'Ale complexes (In Press): Lithos, p. doi:10.1016/j.lithos.2013.08.008, doi:http://dx.doi.org/10.1016/j.lithos.2013.08.008.

Gleeson, M.L.M., Stock, M.J., Pyle, D.M., Mather, T.A., Hutchison, W., Yirgu, G., and Wade, J., 2017, Constraining magma storage conditions at a restless volcano in the Main Ethiopian Rift using phase equilibria models: Journal of Volcanology and Geothermal Research, v. 337, p. 44–61, doi:https://doi.org/10.1016/j.jvolgeores.2017.02.026.

Golden, M., 1978, The Geology of the area east of silale, rift valley province, Kenya.: Royal Holloway, University of London.

Gouin, P., 1979, Earthquake history of Ethiopia and the Horn of Africa: IDRC, Ottawa, ON, CA.

Gregory, J., 1896, The Great Rift Valley: London, John Murray, 405 p.

Griffiths, P.S., and Gibson, I.L., 1980, The geology and petrology of the Hannington Trachyphonolite formation, Kenya Rift Valley: Lithos, v. 13, p. 43–53, doi:https://doi.org/10.1016/0024-4937(80)90060-2.

Guth, A.L., 2013, Spatial and Temporal Evolution of the Volcanics and Sediments of the Kenya Rift: Michigan Technological University.

Hackman, B.D., 1988, Geology of the Baringo-Laikipia area: degree sheet 35 with coloured 1: 250,000 geological map and results of geochemical exploration: Ministry of Environment and Natural Resources, Mines and Geological Deptartment.

Hackman, B.D., Charsley, T.J., Key, R.M., and Wilkinson, A.F., 1990, The development of the East African Rift system in north-central Kenya: Tectonophysics, v. 184, p. 189–211.

Hagos, M., Koeberl, C., Kabeto, K., and Koller, F., 2010, GEOCHEMICAL CHARACTERISTICS OF THE ALKALINE BASALTS AND THE PHONOLITE-TRACHYTE PLUGS OF THE AXUM AREA, NORTHERN ETHIOPIA.: Austrian Journal of Earth Sciences, v. 103.

Haileab, B., Brown, F.H., McDOUGALL, I.A.N., and Gathogo, P.N., 2004, Gombe Group basalts and initiation of Pliocene deposition in the Turkana depression, northern Kenya and southern Ethiopia: Geological Magazine, v. 141, p. 41–53.

Hautot, S., Tarits, P., Whaler, K., Le Gall, B., Tiercelin, J.-J., and Le Turdu, C., 2000, Deep structure of the Baringo Rift Basin (central Kenya) from three-dimensional magnetotelluric imaging: Implications for rift evolution: Journal of Geophysical Research: Solid Earth, v. 105, p. 23493–23518.

Hautot, S., Whaler, K., Gebru, W., and Desissa, M., 2006, The structure of a Mesozoic basin beneath the Lake Tana area, Ethiopia, revealed by magnetotelluric imaging: Journal of African Earth Sciences, v. 44, p. 331–338.

Hill, A., Curtis, G., and Drake, R., 1986, Sedimentary stratigraphy of the Tugen Hills, Baringo, Kenya: Geological Society, London, Special Publications, v. 25, p. 285–295.

Hilton, D.R., Halldórsson, S.A., Barry, P.H., Fischer, T.P., de Moor, J.M., Ramirez, C.J., Mangasini, F., and Scarsi, P., 2011, Helium isotopes at Rungwe Volcanic Province, Tanzania, and the origin of East African Plateaux: Geophysical Research Letters, v. 38, p. doi:10.1029/2011GL049589.

Hutchison, W. et al., 2016a, A pulse of mid-Pleistocene rift volcanism in Ethiopia at the dawn of modern humans: Nature Communications, v. 7, p. 13192, doi:10.1038/ncomms13192 https://www.nature.com/articles/ncomms13192#supplementary-information.

Hutchison, W., Mather, T.A., Pyle, D.M., Biggs, J., and Yirgu, G., 2015, Structural controls on fluid pathways in an active rift system: A case study of the Aluto volcanic complex: Geosphere, v. 11, p. 542–562.

Hutchison, W., Pyle, D.M., Mather, T.A., Yirgu, G., Biggs, J., Cohen, B.E., Barfod, D.N., and Lewi, E., 2016b, The eruptive history and magmatic evolution of Aluto volcano: new insights into silicic peralkaline volcanism in the Ethiopian rift: Journal of Volcanology and Geothermal Research, v. 328, p. 9–33.

Itaya, T., and Sawada, Y., 1987, K-Ar ages of volcanic rocks in the Samburu Hills area, northern Kenya:

Jicha, B.R., and Brown, F.H., 2014, An age for the Korath Range, Ethiopia and the viability of 40Ar/39Ar dating of kaersutite in Late Pleistocene volcanics: Quaternary Geochronology, v. 21, p. 53–57.

Juch, D., 1978, Geologic des Athiopischen Sudost-Escarpments 39° und 42° ostlicher Lange: Clausthaler Geo. Abh., v. 29, p. 139pp.

Justin-Visentin, E., and Zanettin, B., 1974, Dike swarms, volcanism and tectonics of the Western Afar margin along the Kombolcha-Eloa traverse (Ethiopia): Bulletin of Volcanology, v. 38, p. 187–205.

Kabeto, K., Sawada, Y., Iizumi, S., and Wakatsuki, T., 2001, Mantle sources and magma–crust interactions in volcanic rocks from the northern Kenya rift: geochemical evidence: Lithos, v. 56, p. 111–139, doi:https://doi.org/10.1016/S0024-4937(00)00063-3.

Kabeto, K., Sawada, Y., and Roser, B., 2009, Compositional Differences between Felsic Volcanic Rocks from the Margin and Center of the Northern Main Ethiopian Rift: Momona Ethiopian Journal of Science, v. 1.

Karson, J.A., and Curtis, P.C., 1994, Quaternary volcanic centres of the Turkana Rift, Kenya: Journal of African Earth Sciences, v. 18, p. 15–35, doi:http://dx.doi.org/10.1016/0899-5362(94)90051-5.

Kazmin, V., Berhe, S.M., and Wondm-Agennehu, B., 1981, Geological map of the Ethiopian Rift: The Ethiopian Government - Ministry of Mines, Energy and Water Resources.

Kazmin, V., Seife, M.B., Nicoletti, M., and Petrucciani, C., 1980, Evolution of the northern part of the Ethiopian Rift: Atti Convegni Lincei, v. 47, p. 275–292.

Keranen, K.M., Klemperer, S.L., Julia, J., Lawrence, J.F., and Nyblade, A.A., 2009, Low lower crustal velocity across Ethiopia: Is the Main Ethiopian Rift a narrow rift in a hot craton? Geochemistry Geophysics Geosystems, v. 10, p. doi:10.1029/2008gc002293, doi:Artn Q0ab01 Doi 10.1029/2008gc002293.

Key, R.M., Rop, B.P., and Rundle, C.C., 1987, The development of the late Cenozoic alkali basaltic Marsabit Shield-Volcano, Northern Kenya: Journal of African Earth Sciences, v. 6, p. 475–491.

Key, R.M., and Watkins, R.T., 1988, Geology of the Sabarei area: Republic of Kenya Ministry of Environment and Natural Resources, Mines and Geological Department Report, v. 111.

Kieffer, B. et al., 2004, Flood and shield basalts from Ethiopia: Magmas from the African superswell: Journal of Petrology, v. 45, p. 793–834.

Kingston, J.D., Jacobs, B.F., Hill, A., and Deino, A., 2002, Stratigraphy, age and environments of the late Miocene Mpesida Beds, Tugen Hills, Kenya: Journal of Human Evolution, v. 42, p. 95–116.

Le Maitre, R.W., 2002, Igneous Rocks - A classification and glossary of terms: Cambridge, U.K., Cambridge University Press, 236 p.

Lippard, S.J., 1973, The petrology of phonolites from the Kenya Rift: Lithos, v. 6, p. 217–234.

Macdonald, R., 2012, Evolution of peralkaline silicic complexes: Lessons from the extrusive rocks: Peralkaline Rocks and Carbonatites with Special Reference to the East African Rift, v. 152, p. 11–22, doi:10.1016/j.lithos.2012.01.014.

Macdonald, R., Davies, G.R., Upton, B.G.J., Dunkley, P.N., Smith, M., and Leat, P.T., 1995, Petrogenesis of Silali volcano, Gregory Rift, Kenya: Journal of the Geological Society, v. 152, p. 703–720.

MacDonald, R., Rogers, N.W., Fitton, J.G., Black, S., and Smith, M., 2001, Plume-lithosphere interactions in the generation of the basalts of the Kenya Rift, East Africa: Journal of Petrology, v. 42, p. 877–900.

Macgregor, D., 2015, History of the development of the East African Rift System: A series of interpreted maps through time: Journal of African Earth Sciences, v. 101, p. 232–252.

Maguire, P. et al., 2006, Crustal structure of the Northern Main Ethiopian Rift from the EAGLE controlled source survey; a snapshot of incipient lithospheric break-up, *in* Yirgu, G., Ebinger, C., and Maguire, P. eds., The Afar Volcanic Province within the East African Rift System, Special Publication of the Geological Society, London, v. 259, p. 269–292.

Martyn, J.E., 1969, Geological history of the country between Lake Baringo and the Kerio river, Baringo district, Kenya: Royal Holloway, University of London.

Mazzarini, F., 2004, Volcanic vent self-similar clustering and crustal thickness in the northern Main Ethiopian Rift: Geophysical Research Letters, v. 31, p. L04604, doi:10.1029/2003gl018574.

Mazzarini, F., Corti, G., Manetti, P., and Innocenti, F., 2004, Strain rate and bimodal volcanism in the continental rift: Debre Zeyt volcanic field, northern MER, Ethiopia: Journal of African Earth Sciences, v. 39, p. 415–420, doi:DOI 10.1016/j.jafrearsci.2004.07.025.

Mazzarini, F., Rooney, T.O., and Isola, I., 2013, The intimate relationship between strain and magmatism: A numerical treatment of clustered monogenetic fields in the Main Ethiopian Rift: Tectonics,.

McDougall, I., and Feibel, C.S., 1999, Numerical age control for the Miocene-Pliocene succession at Lothagam, a hominoid-bearing sequence in the northern Kenya Rift: Journal of the Geological Society, v. 156, p. 731–745, doi:10.1144/gsjgs.156.4.0731.

McDougall, I., and Watkins, R.T., 1985, Age of hominoid-bearing sequence at Buluk, northern Kenya: Nature, v. 318, p. 175.

McDougall, I., and Watkins, R.T., 2006, Geochronology of the Nabwal Hills: a record of earliest magmatism in the northern Kenyan Rift Valley: Geological Magazine, v. 143, p. 25–39.

McDougall, I., and Watkins, R.T., 1988, Potassium–argon ages of volcanic rocks from northeast of Lake Turkana, northern Kenya: Geological Magazine, v. 125, p. 15–23.

McKenzie, D., and Bickle, M.J., 1988, The volume and composition of melt generated by extension of the lithosphere: Journal of Petrology, v. 29, p. 625–679.

Mège, D., Purcell, P., Bézos, A., Jourdan, F., and La, C., 2016, A major dyke swarm in the Ogaden region south of Afar and the early evolution of the Afar triple junction: Geological Society, London, Special Publications, v. 420, p. 221–248.

Meshesha, D., and Shinjo, R., 2007, Crustal contamination and diversity of magma sources in the northwestern Ethiopian volcanic province: Journal of Mineralogical and Petrological Sciences, v. 102, p. 272–290, doi:10.2465/jmps.061129.

Meshesha, D., and Shinjo, R., 2010, Hafnium isotope variations in Bure volcanic rocks from the northwestern Ethiopian volcanic province: a new insight for mantle source diversity: Journal of Mineralogical and Petrological Sciences, v. 105, p. 101–111, doi:Doi 10.2465/Jmps.090427a.

Mohr, P., 2009, Africa Beckoning: Explorers of Eastern Africa, Its Rift Valleys and Geology, in the Late 19th and Early 20th Centuries : Two Essays and Bibliographies: Millbrook Nova Press, 192 p.

Mohr, P., 1983, Ethiopian flood basalt province: Nature, v. 303, p. 577–584.

Mohr, P.A., 1967, Major volcano-tectonic lineament in the Ethiopian rift system: Nature, v. 213, p. 664–665.

Mohr, P., Mitchell, D.G., and Raynolds, 1980, Quaternary volcanism and faulting at O'A caldera, Central Ethiopian Rift: Bulletin of Volcanology, v. 43, p. 173–189.

Mohr, P.A., and Potter, E.C., 1976, Sagatu Ridge Dike Swarm, Ethiopian Rift Margin: Journal of Volcanology and Geothermal Research, v. 1, p. 55–71.

Mohr, P.A., and Wood, C.A., 1976, Volcano Spacings and Lithospheric Attenuation in Eastern Rift of Africa: Earth and Planetary Science Letters, v. 33, p. 126–144.

Mohr, P., and Zanettin, B., 1988, The Ethiopian flood basalt province, *in* MacDougall, J.D. ed., Continental Flood Basalts, Dordrecht, Kluwer Academic, p. 63–110.

Morgan, L.E., and Renne, P.R., 2008, Diachronous dawn of Africa's Middle Stone Age: new 40Ar/39Ar ages from the Ethiopian Rift: Geology, v. 36, p. 967–970.

Morley, C.K., Wescott, W.A., Stone, D.M., Harper, R.M., Wigger, S.T., and Karanja, F.M., 1992, Tectonic evolution of the Northern Kenyan rift: Journal of the Geological Society, v. 149, p. 333–348.

Morton, W.H., Rex, D.C., Mitchell, J.G., and Mohr, P., 1979, Riftward younging of volcanic units in the Addis Ababa region, Ethiopian Rift valley: Nature, v. 280, p. 284–288.

Mugisha, F., Ebinger, C.J., Strecker, M., and Pope, D., 1997, Two-stage rifting in the Kenya rift: implications for half-graben models: Tectonophysics, v. 278, p. 63–81.

Natali, C., Beccaluva, L., Bianchini, G., and Siena, F., 2013, The Axum–Adwa basalt–trachyte complex: a late magmatic activity at the periphery of the Afar plume: Contributions to Mineralogy and Petrology, v. 166, p. 351–370, doi:10.1007/s00410-013-0879-0.

Nelson, W.R., Hanan, B.B., Graham, D.W., Shirey, S.B., Yirgu, G., Ayalew, D., and Furman, T., 2019, Distinguishing Plume and Metasomatized Lithospheric Mantle Contributions to Post-Flood Basalt Volcanism on the Southeastern Ethiopian Plateau: Journal of Petrology, v. 60, p. 1063–1094, doi:10.1093/petrology/egz024.

Ochieng, J.O., Wilkinson, A.F., Kenya. Ministry of Environment, and Natural Resources, 1988, Geology of the Loiyangalani Area: Degree: Ministry of Environment and Natural Resources.

Peccerillo, A., Barberio, M.R., Yirgu, G., Ayalew, D., Barbieri, M., and Wu, T.W., 2003, Relationships between mafic and peralkaline silicic magmatism in continental rift settings: A petrological, geochemical and isotopic study of the Gedemsa volcano, central Ethiopian rift: Journal of Petrology, v. 44, p. 2003–2032.

Purcell, P.G., 2018, Re-imagining and re-imaging the development of the East African Rift: Petroleum Geoscience, v. 24, p. 21–40.

Rampey, M.L., Oppenheimer, C., Pyle, D.G., and Yirgu, G., 2010, Caldera-forming eruptions of the Quaternary Kone Volcanic Complex, Ethiopia: Journal of African Earth Sciences, v. 58, p. 51–66.

Rampey, M.L., Oppenheimer, C., Pyle, D.M., and Yirgu, G., 2014, Physical volcanology of the Gubisa Formation, Kone Volcanic Complex, Ethiopia: Journal of African Earth Sciences, v. 96, p. 212–219, doi:https://doi.org/10.1016/j.jafrearsci.2014.04.009.

Rapprich, V., Žáček, V., Verner, K., Erban, V., Goslar, T., Bekele, Y., Legesa, F., Hroch, T., and Hejtmánková, P., 2016, Wendo Koshe Pumice: The latest Holocene silicic explosive eruption product of the Corbetti volcanic system (southern Ethiopia): Journal of Volcanology and Geothermal Research, v. 310, p. 159–171.

Resom, A., Asrat, A., Gossa, T., and Hovers, E., 2018, Petrogenesis and depositional history of felsic pyroclastic rocks from the Melka Wakena archaeological site-complex in South central Ethiopia: Journal of African Earth Sciences, v. 142, p. 93–111.

Rogers, N., Macdonald, R., Fitton, J.G., George, R., Smith, M., and Barreiro, B., 2000, Two mantle plumes beneath the East African Rift system; Sr, Nd and Pb isotope evidence from Kenya Rift basalts: Earth and Planetary Science Letters, v. 176, p. 387–400.

Rogers, N.W., Thomas, L.E., Macdonald, R., Hawkesworth, C.J., and Mokadem, F., 2006, U-238-Th-230 disequilibrium in recent basalts and dynamic melting beneath the Kenya rift: Chemical Geology, v. 234, p. 148–168, doi:DOI 10.1016/j.chemgeo.2006.05.002.

Ronga, F., Lustrino, M., Marzoli, A., and Melluso, L., 2010, Petrogenesis of a basalt-comendite-pantellerite rock suite: the Boseti Volcanic Complex (Main Ethiopian Rift): Mineralogy and Petrology, v. 98, p. 227–243, doi:DOI 10.1007/s00710-009-0064-3.

Rooney, T.O., 2010, Geochemical evidence of lithospheric thinning in the southern Main Ethiopian Rift: Lithos, v. 117, p. 33–48, doi:doi:10.1016/j.lithos.2010.02.002.

Rooney, T.O., 2017, The Cenozoic magmatism of East-Africa: Part I–Flood basalts and pulsed magmatism: Lithos, v. 286, p. 264–301.

Rooney, T.O., Bastow, I.D., and Keir, D., 2011, Insights into extensional processes during magma assisted rifting: Evidence from aligned scoria cones: Journal of Volcanology and Geothermal Research, v. 201, p. 83–96.

Rooney, T.O., Bastow, I.D., Keir, D., Mazzarini, F., Movsesian, E., Grosfils, E.B., Zimbelman, J.R., Ramsey, M.S., Ayalew, D., and Yirgu, G., 2014a, The protracted development of focused magmatic intrusion during continental rifting: Tectonics, v. 33, p. 875–897, doi:DOI: 10.1002/2013TC003514.

Rooney, T., Furman, T., Bastow, I.D., Ayalew, D., and Gezahegn, Y., 2007, Lithospheric modification during crustal extension in the Main Ethiopian Rift: Journal of Geophysical Research, B, Solid Earth and Planets, v. 112, p. B10201, doi:10.1029/2006JB004916.

Rooney, T., Furman, T., Yirgu, G., and Ayalew, D., 2005, Structure of the Ethiopian lithosphere: Xenolith evidence in the Main Ethiopian Rift: Geochimica Et Cosmochimica Acta, v. 69, p. 3889–3910.

Rooney, T.O., Hanan, B.B., Graham, D.W., Furman, T., Blichert-Toft, J., and Schilling, J.-G., 2012a, Upper Mantle Pollution during Afar Plume–Continental Rift Interaction: Journal of Petrology, v. 53, p. 365–389, doi:10.1093/petrology/egr065.

Rooney, T.O., Hart, W.K., Hall, C.M., Ayalew, D., Ghiorso, M.S., Hidalgo, P., and Yirgu, G., 2012b, Peralkaline magma evolution and the tephra record in the Ethiopian Rift: Contributions to Mineralogy and Petrology, v. 164, p. 407–426, doi:DOI: 10.1007/s00410-012-0744-6.

Rooney, T.O., Herzberg, C., and Bastow, I.D., 2012c, Elevated mantle temperature beneath East Africa: Geology, v. 40, p. 27–30, doi:10.1130/g32382.1.

Rooney, T.O., Nelson, W.R., Ayalew, D., Hanan, B., Yirgu, G., and Kappelman, J., 2017, Melting the lithosphere: Metasomes as a source for mantle-derived magmas: Earth and Planetary Science Letters, v. 461, p. 105–118, doi:http://dx.doi.org/10.1016/j.epsl.2016.12.010.

Rooney, T.O., Nelson, W.R., Dosso, L., Furman, T., and Hanan, B., 2014b, The role of continental lithosphere metasomes in the production of HIMU-like magmatism on the northeast African and Arabian plates: Geology, v. 42, p. 419–422, doi:10.1130/g35216.1.

Savage, R.J., and Williamson, P.G., 1978, The early history of the Turkana Depression: Geological Society, London, Special Publications, v. 6, p. 375–394.

Sawada, Y., Pickford, M., Itaya, T., Makinouchi, T., Tateishi, M., Kabeto, K., Ishida, S., and Ishida, H., 1998, K-Ar ages of Miocene Hominoidea (Kenyapithecus and Samburupithecus) from Samburu Hills, northern Kenya: Comptes Rendus de l'Académie des Sciences-Series IIA-Earth and Planetary Science, v. 326, p. 445–451.

Sawada, Y., Pickford, M., Senut, B., Itaya, T., Hyodo, M., Miura, T., Kashine, C., Chujo, T., and Fujii, H., 2002, The age of Orrorin tugenensis, an early hominid from the Tugen Hills, Kenya: Comptes Rendus Palevol, v. 1, p. 293–303.

Shinjo, R., Chekol, T., Meshesha, D., Itaya, T., and Tatsumi, Y., 2011, Geochemistry and geochronology of the mafic lavas from the southeastern Ethiopian rift (the East African Rift System): assessment of models on magma sources, plume–lithosphere interaction and plume evolution: Contributions to Mineralogy and Petrology, v. 162, p. 209–230.

Siegburg, M., Gernon, T.M., Bull, J.M., Keir, D., Barfod, D.N., Taylor, R.N., Abebe, B., and Ayele, A., 2018, Geological evolution of the Boset-Bericha Volcanic Complex, Main Ethiopian Rift: 40Ar/39Ar evidence for episodic Pleistocene to Holocene volcanism: Journal of Volcanology and Geothermal Research, v. 351, p. 115–133, doi:https://doi.org/10.1016/j.jvolgeores.2017.12.014.

Smith, M., 1994, Stratigraphic and structural constraints on mechanisms of active rifting in the Gregory Rift, Kenya: Tectonophysics, v. 236, p. 3–22.

Smith, M., Dunkley, P.N., Deino, A., Williams, L.A.J., and McCall, G.J.H., 1995, Geochronology, stratigraphy and structural evolution of Silali volcano, Gregory Rift, Kenya: Journal of the Geological Society, v. 152, p. 297–310, doi:10.1144/gsjgs.152.2.0297.

Sueß, E., 1891, Die Brüche des östlichen Afrika: Tempsky.

Sun, S. -s, and McDonough, W.F., 1989, Chemical and isotopic systematics of oceanic basalts: implications for mantle composition and processes: Geological Society, London, Special Publications, v. 42, p. 313–345, doi:10.1144/gsl.sp.1989.042.01.19.

Suwa, G., Beyene, Y., Nakaya, H., Bernor, R.L., Boisserie, J.-R., Bibi, F., Ambrose, S.H., Sano, K., Katoh, S., and Asfaw, B., 2015, Newly discovered cercopithecid, equid and other mammalian fossils from the Chorora Formation, Ethiopia: Anthropological Science, p. 150206.

Tadesse, A.Z., Ayalew, D., Pik, R., Yirgu, G., and Fontijn, K., 2018, Magmatic evolution of the Boku Volcanic Complex, Main Ethiopian Rift: Journal of African Earth Sciences, doi:https://doi.org/10.1016/j.jafrearsci.2018.08.003.

Tatsumi, Y., and Kimura, N., 1991, Secular variation of basalt chemistry in the Kenya Rift: evidence for the pulsing of asthenospheric upwelling: Earth and Planetary Science Letters, v. 104, p. 99–113.

Teklemariam, M., Battaglia, S., Gianelli, G., and Ruggieri, G., 1996, Hydrothermal alteration in the Aluto-Langano geothermal field, Ethiopia: Geothermics, v. 25, p. 679–702.

Tommasini, S., Manetti, P., Innocenti, F., Abebe, T., Sintoni, M., and Conticelli, S., 2005, The Ethiopian subcontinental mantle domains: geochemical evidence from Cenozoic mafic lavas: Mineralogy and Petrology, v. 84, p. 259–281, doi:10.1007/s00710-005-0081-9.

Trua, T., Deniel, C., and Mazzuoli, R., 1999, Crustal control in the genesis of Plio-Quaternary bimodal magmatism of the Main Ethiopian Rift (MER); geochemical and isotopic (Sr, Nd, Pb) evidence: Chemical Geology, v. 155, p. 201–231.

Truckle, P.H., 1977, The geology of the area to the south of Lokori, South Turkana, Kenya.:

Ukstins, I.A., Renne, P.R., Wolfenden, E., Baker, J., Ayalew, D., and Menzies, M., 2002, Matching conjugate volcanic rifted margins; 40Ar/39Ar chrono-stratigraphy of pre- and syn-rift bimodal flood volcanism in Ethiopia and Yemen: Earth and Planetary Science Letters, v. 198, p. 289–306.

Varet, J., 2017, Geology of Afar (East Africa): Springer.

Vogel, N., Nomade, S., Negash, A., and Renne, P.R., 2006, Forensic 40Ar/39Ar dating: a provenance study of Middle Stone Age obsidian artifacts from Ethiopia: Journal of Archaeological Science, v. 33, p. 1749–1765.

Walsh, J., 1969, Geology of the Eldama Ravine-Kabarnet area: Rep. Geol. Surv. Kenya, v. 83, p. 1–48.

Webb, P.K., and Weaver, S.D., 1975, Trachyte shield volcanoes: a new volcanic form from South Turkana, Kenya: Bulletin Volcanologique, v. 39, p. 294–312, doi:10.1007/bf02597833.

White, J.C., Espejel-García, V.V., Anthony, E.Y., and Omenda, P., 2012, Open System evolution of peralkaline trachyte and phonolite from the Suswa volcano, Kenya rift: Lithos, v. 152, p. 84–104, doi:https://doi.org/10.1016/j.lithos.2012.01.023.

Wilkinson, A.F., 1988, Geology of the Allia Bay area: Report of the Mines and Geology Department, Kenya, p. 54.

Wilks, M., Ayele, A., Kendall, J.-M., and Wookey, J., 2017, The 24th January 2016 Hawassa earthquake: Implications for seismic hazard in the Main Ethiopian rift: Journal of African Earth Sciences, v. 125, p. 118–125.

Williams, F.M., Williams, M.A.J., and Aumento, F., 2004, Tensional fissures and crustal extension rates in the northern part of the Main Ethiopian Rift: Journal of African Earth Sciences, v. 38, p. 183–197.

Williams, M.A.J., Williams, F.M., Gasse, F., Curtis, G.H., and Adamson, D.A., 1979, Plio–Pleistocene environments at Gadeb prehistoric site, Ethiopia: Nature, v. 282, p. 29, doi:10.1038/282029a0.

Williamson, P.G., and Savage, R.J., 1986, Early rift sedimentation in the Turkana basin, northern Kenya: Geological Society, London, Special Publications, v. 25, p. 267–283.

Wolde, B., and Widenfalk, L., 1994, Petrochemical and geochemical constraints on Cenozoic magmatism in Ethiopia: Africa Geoscience Review, v. 1, p. 475–494.

Woldegabriel, G., and Aronson, J.L., 1987, Chow Bahir Rift - a Failed Rift in Southern Ethiopia: Geology, v. 15, p. 430–433.

WoldeGabriel, G., Aronson, J.L., and Walter, R.C., 1990, Geology, geochronology, and rift basin development in the central sector of the Main Ethiopia Rift: Geological Society of America Bulletin, v. 102, p. 439–458.

WoldeGabriel, G., Hart, W.K., Katoh, S., Beyene, Y., and Suwa, G., 2005, Correlation of Plio-Pleistocene Tephra in Ethiopian and Kenyan rift basins: Temporal calibration of geological features and hominid fossil records: Journal of Volcanology and Geothermal Research, v. 147, p. 81–108, doi:DOI 10.1016/j.jvolgeores.2005.03.008.

WoldeGabriel, G., Walter, R.C., Hart, W.K., Mertzman, S.A., and Aronson, J.L., 1999, Temporal relations and geochemical features of felsic volcanism in the central sector of the Main Ethiopian Rift: Acta Vulcanologica, v. 11, p. 53–67.

Woldegabriel, G., Yemane, T., Suwa, G., White, T., and Asfaw, B., 1991, Age of Volcanism and Rifting in the Burji-Soyoma Area, Amaro Horst, Southern Main Ethiopian Rift -

Geochronological and Biochronologic Data: Journal of African Earth Sciences, v. 13, p. 437–447.

Wolfenden, E., Ebinger, C., Yirgu, G., Deino, A., and Ayalew, D., 2004, Evolution of the northern Main Ethiopian rift: birth of a triple junction: Earth and Planetary Science Letters, v. 224, p. 213–228.

Wolfenden, E., Ebinger, C., Yirgu, G., Renne, P.R., and Kelley, S.P., 2005, Evolution of a volcanic rifted margin: Southern Red Sea, Ethiopia: Geological Society of America Bulletin, v. 117, p. 846–864.

Zanettin, B., 1992, Evolution of the Ethiopian Volcanic Province: Memorie Lincee Scienze Fisiche e Naturali, v. 1, p. 155–181.

Acknowledgements

I would like to thank all the authors I contacted who provided more details and answers to my queries on their work – there were many and I am not able to mention them all here. This work is a synthesis of all the hard work put in by the persons cited herein and the contributions from these persons should be acknowledged. Peter Purcell is thanked for providing the digital files for the rift maps used in the accompanying maps. Alex Steiner is given thanks for his assistance in collating the Turkana materials, discussions on the GIS aspects of the project, and insights into Turkana volcanism. Thanks is provided to the MSU Library and in particular Kathleen Weessies at the Map Library and the interlibrary loans group – they tried to obtain the requests I placed, and most always succeeded. I am indebted to the persons who read and provided feedback on this work prior to publication: Chris Svoboda. Andrew Kerr is thanked for his tireless efforts in editing this synthesis series. I am grateful for the formal peer reviews by Francesco Mazzarini and Paul Mohr, which significantly improved the manuscript. This work was supported by US National Science Foundation Grants: EAR 1551872 and EAR 1850606. Lastly, I acknowledge the NSF GeoPRISMS program which was part of the motivation for undertaking this synthesis.

Figure Captions

Figure 1: Map showing the generalized distribution of Precambrian rocks in East Africa, the distribution of Cenozoic volcanism, and the footprints of Cretaceous and Cenozoic rifting. In a general sense rifting occurs along the boundary of the between Neoproterozoic rocks and Mesoproterozoic and older rocks, however the Western Branch of the East African Rift does transit these rocks and generally follows the boundary of the craton (white shaded overlay). Outcrop shapes are derived from the USGS Surficial Geology of Africa (geo7_2ag), rifts are from Purcell (2018), the extent of the craton is taken from Foley et al. (2012).

Figure 2: $^{87}Sr/^{86}Sr$ vs $^{143}Nd/^{144}Nd$ isotopic data for Quaternary rocks located throughout the East African Rift System. Cool colors are assigned to lavas erupted near the craton, warmer colors are those erupted through the mobile belt. Large symbols are for samples > 5 wt. MgO; small symbols are < 5wt. % MgO or no major element data is available.

Figure 3: Map showing the distribution of lavas erupted during the Samburu/Getra Kele events throughout East Africa. Note that this map shows distribution both on the craton and mobile belt. Units are derived from Guth (2013), the Geological Map of Ethiopia, Mège et al. (2016) and the Smithsonian Volcano database. Units include: Samburu Formation (20-16 Ma), consisting of: (Nachola, Kapcherat, Chembalao, Samburu) – Kenya Rift, (Lower Kalakol, lower Irile Member, Nakoret, Muruanasigar) - Turkana, (Teltele, Surma Basalts, Getra-Kele).

Figure 4: XY plots for various elements and isotopes vs MgO (A though F). Element and isotope ratio plots also shown (G, H). Data are for the Samburu Basalts, Getra Basalts, Early Miocene Resurgence Phase, Flood Phonolite Phase, Simien-Axum event, and Early Rift Development Phase.

Figure 5: Chondrite normalized diagram (Boynton, 1984) for more mafic samples (MgO > 5 wt. %). Shown are Samburu Basalts, Getra Basalts, Early Miocene Resurgence Phase, Flood

Phonolite Phase, Simien-Axum event, and Early Rift Development Phase. Background field is the data extremes for the dataset presented in this figure.

Figure 6: Primitive mantle normalized diagram (Sun and McDonough, 1989) for more mafic samples (MgO > 5 wt. %). Shown are Samburu Basalts, Getra Basalts, Early Miocene Resurgence Phase, Flood Phonolite Phase, Simien-Axum event, and Early Rift Development Phase. Background field is the data extremes for the dataset presented in this figure.

Figure 7: Map showing the distribution of lavas erupted during the Flood Phonolite Phase throughout East Africa. Note that this map shows distribution both on the craton and mobile belt. Units are derived from Guth (2013), the Geological Map of Ethiopia, and the Smithsonian Volcano database. Consists of: (Flood Phonolites, upper Nachola, Aka Aiteputh, Elgeyo Formation, Chof phonolite, Sidekh phonolite, Uasin Gishu phonolite, Tiim phonolite, Rumuruti phonolites). (Jarigole Volcanics) – Turkana, S. Ethiopia (Weyto, Mimo Trachytes/Phonolites, Sabarei Volcanics, Gum Dura). (Shebele Trachytes, Damole/Cawa ignimbrite and flood trachyte) Ethiopia. (Simien Shield top, Axum complex – NW Ethiopian Plateau).

Figure 8: Total Alkali Silica diagram displaying the more silicic samples from the region (Le Maitre, 2002). Balchi, Wechacha, Shebele, and Axum are from the Ethiopian sector of the province; the Flood Phonolites are from the Kenya sector of the province.

Figure 9: Compositional data for the more silicic samples from the region. Balchi, Wechacha, Shebele, and Axum are from the Ethiopian sector of the province; the Flood Phonolites are from the Kenya sector of the province. Panels A through G are plotted against SiO_2 and log scales are used all elements on the Y axes. Panel G shows the isotopic variation of these same units.

Figure 10: Chondrite normalized diagram (Boynton, 1984) for the more silicic samples from the region. Wechacha, Shebele, and Axum are from the Ethiopian sector of the province. No data is available for Balchi or the Flood Phonolites.

Figure 11: Primitive mantle normalized diagram (Sun and McDonough, 1989) for >55 wt. % SiO_2 samples from the Axum-Adwa region. Two different magma types are illustrated: (A) A high Ti magma type and (B) A lower 'other' magma type. These two varieties reflect magma evolution towards phonolite composition via fractional crystallization.

Figure 12: Map showing the distribution of lavas erupted during the Mid-Miocene Resurgence Phase throughout East Africa. Note that this map shows distribution both on the craton and mobile belt. Units are derived from Guth (2013), the Geological Map of Ethiopia, and the Smithsonian Volcano database. Note that some units in the vicinity of the Dida Galgalu plateau and Laisamis area have been reassigned from the classification of Guth (2013) on the basis of work reported by Bellieni et al. (1986). The Mid-Miocene Resurgence Phase (12-9 Ma) in Kenya and S. Ethiopia consists of: upper Nakwele formation basalts, Tatesa Hill basalts, The Loperi basalts, the Lakhapelinyang Basalt, Laisamis area basalts, Kele basalts, The Aiteputh formation, Lomujal basalts, and the Chencha basalts). In Ethiopia this phase consists of: Tarmaber, Megezez, Weti, Mt. Arba Gugu, and Abuna Josef volcanoes, Jebel Saddle, a basaltic shield volcano in the vicinity of Asebe Teferi, Guraghe-Anchar basalts, The Upper Trap Series, lower Kessem Formation, The Lower aphyric basalts and Upper Basalts from western Ethiopia, The Reira Basalts, the Astit Formation, and the Guna Shield.

Figure 13: XY plots for various elements and isotopes vs MgO (A though F). Element ratio plots also shown (G, H). Data are for the Ethiopian and Kenyan Mid-Miocene Resurgence Phase, and the contemporaneous and Kele Basalts and Mid Miocene activity along the YTVL. Also shown are the Stratoid basalts from the Pliocene (Gombe Stratoid Series, Tirr Tirr, and Bofa Stratoid Series).

Figure 14: Chondrite normalized diagram (Boynton, 1984) for more mafic samples (MgO > 5 wt. %). Data are for the Ethiopian and Kenyan Mid-Miocene Resurgence Phase, and the contemporaneous and Kele Basalts and Mid Miocene activity along the YTVL. Also shown are the Stratoid basalts from the Pliocene (Gombe Stratoid Series, Tirr Tirr, and Bofa Stratoid Series).

Figure 15: Primitive Mantle normalized diagram (Sun and McDonough, 1989) for more mafic samples (MgO > 5 wt. %). Data are for the Ethiopian and Kenyan Mid-Miocene Resurgence Phase, and the contemporaneous and Kele Basalts and Mid Miocene activity along the YTVL. Also shown are the Stratoid basalts from the Pliocene (Gombe Stratoid Series, Tirr Tirr, and Bofa Stratoid Series).

Figure 16: Isotopic variation plots for Sr, Nd and Pb isotopes. Data are for the Ethiopian and Kenyan Mid-Miocene Resurgence Phase, and the contemporaneous and Kele Basalts and Mid Miocene activity along the YTVL. Also shown are the Stratoid basalts from the Pliocene (Gombe Stratoid Series, Tirr Tirr, and Bofa Stratoid Series).

Figure 17: Map showing the distribution of lavas erupted during the Early Rift Development Phase throughout East Africa. Note that this map shows distribution both on the craton and mobile belt. Units are derived from Guth (2013), the Geological Map of Ethiopia, and the Smithsonian Volcano database. Mt. Kenya, Ol Esayeti, and Olorgesailie are shown but not discussed in this volume (see volume III). YTVL = Yerer Tullu Wellel volcanic tectonic lineament (Abebe et al., 1998).

Figure 18: Map showing the distribution of lavas erupted during the Stratoid Phase throughout East Africa. Units are derived from Guth (2013), the Geological Map of Ethiopia, and the Smithsonian Volcano database. The distribution of Gombe Stratoid Series lavas is based upon the maps of Haileab et al. (2004) and Erbello & Kidane (2018). The Bofa Stratoid Series is

poorly defined in modern maps and is largely buried beneath the thick volcanoclastic pile that has developed in the MER over the past 2 Ma and is not split from other Stratoid basalts in Ethiopia. Shields in Turkana are also shown in this representation in addition to the rift filling units of Northern Kenya. In addition, Plio-Quaternary basalts of the Ethiopian Plateaus are shown.

Figure 19: XY plots for various elements and isotopes vs MgO (A though F). Element and Isotope ratio plots also shown (G, H). Data are for the Pliocene Shields of Turkana (Balo Basalt, Gus Basalt, Kankam Basalt, Kulal Shield, Lenderit, Lowasera-Gus Rd. Basalt, Mega-Huri Hills Shield, Lorikipi Basalt). High Ti Pliocene are some samples from Mega-Huri Hills and also Logipi-Latarr shield. Samples from the Eastern Ethiopian Plateau are from: Chilalo and the Galema Range. Samples from the Western Ethiopian Plateau are: Injibara, Tepi, YTVL, and Akaki. Samples from the Bale Mountains (also Eastern Plateau) are Pliocene and Quaternary lavas.

Figure 20: Chondrite normalized diagram (Boynton, 1984) for more mafic samples (MgO > 5 wt. %). Data are for the Pliocene Shields of Turkana (Balo Basalt, Gus Basalt, Kankam Basalt, Kulal Shield, Lenderit, Lowasera-Gus Rd. Basalt, Mega-Huri Hills Shield, Lorikipi Basalt). High Ti Pliocene are some samples from Mega-Huri Hills and also Logipi-Latarr shield. Samples from the Eastern Ethiopian Plateau are from: Chilalo and the Galema Range. Samples from the Western Ethiopian Plateau are: Injibara, Tepi, YTVL, and Akaki. Samples from the Bale Mountains (also Eastern Plateau) are Pliocene and Quaternary lavas.

Figure 21: Primitive Mantle normalized diagram (Sun and McDonough, 1989) for more mafic samples (MgO > 5 wt. %). Data are for the Pliocene Shields of Turkana (Balo Basalt, Gus Basalt, Kankam Basalt, Kulal Shield, Lenderit, Lowasera-Gus Rd. Basalt, Mega-Huri Hills Shield, Lorikipi Basalt). High Ti Pliocene are some samples from Mega-Huri Hills and also Logipi-Latarr shield. Samples from the Eastern Ethiopian Plateau are from: Chilalo and the

Galema Range. Samples from the Western Ethiopian Plateau are: Injibara, Tepi, YTVL, and Akaki. Samples from the Bale Mountains (also Eastern Plateau) are Pliocene and Quaternary lavas.

Figure 22: Map showing the distribution of lavas erupted during the Axial Phase within the Kenya Rift and Turkana (including Korath from Ethiopia). Units are derived from Guth (2013), the Geological Map of Ethiopia (Kazmin et al., 1981), and the Smithsonian Volcano database.

Figure 23: XY plots for various elements and isotopes vs MgO (A though F). Element ratio plots also shown (G, H). Data are for Turkana Islands (North Island, Central Island and Birds Nest, and South Island), recent activity in the Huri Hills and Mega, and the axial centers of the northern Kenya Rift (Barrier, Namarunu, Emuruangogolak, Silali, Paka, Korosi, Baringo).

Figure 24: Chondrite normalized diagram (Boynton, 1984) for more mafic samples (MgO > 5 wt. %). Data are for Turkana Islands (North Island, Central Island and Birds Nest, and South Island), recent activity in the Huri Hills and Mega, and the axial centers of the northern Kenya Rift (Barrier, Namarunu, Emuruangogolak, Silali, Paka, Korosi, Baringo).

Figure 25: Primitive Mantle normalized diagram (Sun and McDonough, 1989) for more mafic samples (MgO > 5 wt. %). Data are for Turkana Islands (North Island, Central Island and Birds Nest, and South Island), recent activity in the Huri Hills and Mega, and the axial centers of the northern Kenya Rift (Barrier, Namarunu, Emuruangogolak, Silali, Paka, Korosi, Baringo).

Figure 26: Isotopic variation plots for Sr, Nd and Pb isotopes. Data are for Turkana Islands (North Island, Central Island and Birds Nest, and South Island), recent activity in the Huri Hills and Mega, and the axial centers of the northern Kenya Rift (Barrier, Namarunu, Emuruangogolak, Silali, Paka, Korosi, Baringo).

Figure 27: Map showing the distribution of lavas erupted during the Axial Phase within the Ethiopian Rift (excluding Korath). Units are derived the Geological Map of Ethiopia (Kazmin et al., 1981), and the Smithsonian Volcano database. BTSH = Boru-Toru Structural High

Figure 28: XY plots for various elements and isotopes vs MgO (A though F). Element ratio plots also shown (G, H). Data are for most sectors of the Ethiopian Rift from south to north (Korath, Arba Minch/Tosa Sucha, Diguna/Butajira, Debre Zeyit, Shala, Aluto-Gedemsa, Boseti-Kone, Fantale-Dofan. Limited data is available for the Adda'do and Angelele-Hertali sectors and so they are merged. No data exists for the Gabillema sector.

Figure 29: Chondrite normalized diagram (Boynton, 1984) for more mafic samples (MgO > 5 wt. %). Data are for most sectors of the Ethiopian Rift from south to north (Korath, Arba Minch/Tosa Sucha, Diguna/Butajira, Debre Zeyit, Shala, Aluto-Gedemsa, Boseti-Kone, Fantale-Dofan. Limited data is available for the Adda'do and Angelele-Hertali sectors and so they are merged. No data exists for the Gabillema sector.

Figure 30: Geochemical variation by latitude for samples >5 wt. % MgO from the Main Ethiopian Rift. The latitude of the central point of each rift sector has been assigned to all samples from that rift sector (current location information is imprecise for many samples in the rift). The central point of the rift sector is represented by a grey line and is labelled.

Figure 31: Primitive Mantle normalized diagram (Sun and McDonough, 1989) for more mafic samples (MgO > 5 wt. %). Data are for most sectors of the Ethiopian Rift from south to north (Korath, Arba Minch/Tosa Sucha, Diguna/Butajira, Debre Zeyit, Shala, Aluto-Gedemsa, Boseti-Kone, Fantale-Dofan. Limited data is available for the Adda'do and Angelele-Hertali sectors and so they are merged. No data exists for the Gabillema sector.

Figure 32: Isotopic variation plots for Sr, Nd, Hf, and Pb isotopes. Data are for most sectors of the Ethiopian Rift from south to north (Korath, Arba Minch/Tosa Sucha, Diguna/Butajira, Debre

Zeyit, Shala, Aluto-Gedemsa, Boseti-Kone, Fantale-Dofan. Limited data is available for the Adda'do and Angelele-Hertali sectors and so they are merged. No data exists for the Gabillema sector. The Mantle Array is that of Chauvel et al. (2008).